# Geomechanical Studies on Fluid Flow Behaviour Influencing Rock Deformation Mechanisms of Mudstones and Sandstones( Dissertation_全文 )

AUTHOR(S):

Puttiwongrak, Avirut

# Geomechanical Studies on Fluid Flow Behaviour Influencing Rock Deformation Mechanisms of Mudstones and Sandstones

2013

Puttiwongrak Avirut

# Geomechanical Studies on Fluid Flow Behaviour Influencing Rock Deformation Mechanisms of Mudstones and Sandstones

by

Puttiwongrak Avirut

A dissertation submitted in partial fulfillment of the requirements for the degree of Doctor of Engineering

Nationality: Thai

Previous Degree: Master degree of Engineering in Geotechnical and Geoenvironmental Engineering,
Asian Institute of Technology, Thailand

Department of Urban Management,
Graduate School of Engineering,
Kyoto University
Japan

2013

# ACKNOWLEDGEMENT

Firstly, I would like to express my profound appreciation and deepest gratitude to my supervisor, Prof. Toshifumi Matsuoka, for his supports and guidance throughout my study. I also would like to thank for kindness and friendliness to me and giving me several good opportunities to have great experiences in study and living in Japan.

Grateful acknowledgement is due to the committee members, Prof. Hiroyasu Ohtsu and Associate Prof. Sumihiko Murata, for their valuation time for their scientific suggestions.

I would like to give special thanks to Mr. Hiromi Honda for his valuable information, collaborations and important advices including encouragement in regard to challenging research. Without his guidance and kind helps, this dissertation would not have been completed.

Similarly, I specially thank Prof. Ziqiu Xue and Mr. Yuki Horiuchi for good collaborations and helpful discussions on my research works.

In addition, I sincerely express to thank my advisors in the past: Associate Prof. Pham Huy Giao (Asian Institute of Technology, AIT) and Associate Prof. Piti Sukontasukkul (King Mongkut's University of Technology North Bangkok, KMUT'NB) for valuable knowledge, good suggestions, and encouraging me to continue study.

My deep thank is to Japanese Government and Kyoto University for giving me the great opportunity with a scholarship to study in the doctoral program here.

Unforgettably, I would like to give many thanks to Associate Prof. Yasuhiro Yamada, Associate Prof. Takashi Tsuji, Assistant Prof. Yunfeng Liang, and all of my laboratory members in Environment and Resource System Engineering laboratory, *i.e.* Dr. Ayumu Miyakawa, Dr. Jongwook Kim, Dr. Makoto Kunieda, Dr. Mokhamad Yusup Nur Khakim, Dr. Mia Ledyastuti, Dr. Ryu Seung Youl, Mr. Dai Makimura, Mr. Hiroki Miyamoto, Mr. Tatsuya Yamada, Mr. Reona Masui, Mr. Hiroaki Kadono, Mr. Kazuya Ishitsuka, Mr. Hirotatsu Yamabe, Mr. Shinya Tsuji, Mr. Masashi Nakatsukasa, Mr. Yuki Horiuchi, Mr. Yohei Mikami, Mr. Hiroto Nakagiri, Mr. Satoshi Iwasaki, Mr. Kazuya Kobayashi, Mr. Yasuto Shigei, Mr. Jun Shibanuma, Mr. Mao Charithyrouth, Mr. Takanori Imaizumi, Mr. Tatsuya Dotare, Mr. Nobuhito Yoshitani, Ms. Kanako Tagami, Ms. Yumi Katasho, Mr. Kazuki Umeda, Mr. Itsuki Kondo, Mr. Yunosuke Sawa, Mr. Katsuya Shiraishi and Mr. Ryutaro Hibi to be friendly and sharing experiences in our laboratory. Especially, sincere thanks are contributed to Dr. Shohei Minato and Mr. Tatsunori Ikeda, who was my tutors during I was a first year student, for kind helps and recommendations about student's life in Japan.

I also greatly thank Mrs. Kana Kurosaka and Ms. Hiroko Inoue, the laboratory's secretary, for supporting and helping me everything about official documents.

Finally, my success in this dissertation and everything in my life are devoted to my beloved family for giving my life and educating with their warmest care and love.

# ABSTRACT

Geomechanics have occupied a central, common position among civil, mining and petroleum engineerings. Its importance is increasing; the main principles of geomechanics are common among these disciplines as mechanics treating rocks and porous media for fluid flow and storage. Subjects to be stressed in each discipline are different from each other; civil engineering emphasizes safety factor concepts, design conservatism and empiricism; mining and tunnel engineerings emphasize safety during excavation, and put more weight on practice than on analysis (Dusseault, 2011). Petroleum geomechanics normally more fundamentally discuss physics, data analysis, empirical models, field observations and laboratory testing of samples because it is younger discipline that others. It prefers discussions of methods of observations on geomechanical responses to depict subsurface geomechanical changes and to rack fluid movements. Consequently when carbon dioxide capture and storage (CCS) was urgent subject of research in the late 1990s, geomechanics was paid much attention.

Due to the Renewable Energy Industry Institute (IWR), a German renewable energy institute in Muenster, has reported that world carbon emissions reached a new record in 2011 at 34 billion tonnes. Likewise, CCS has drawn increasing consideration as a promising method to mitigate the adverse impacts of climate change (Holloway, 1996; Gale, 2004; IPCC, 2005; Hepple and Benson, 2005). Rock deformation mechanisms are critically important for geomechanics; the major rock types in petroleum, are mudstones (*e.g.* shale) and sandstones that perform as trapping or sealing rock and storage reservoir, respectively, should be understood their deformation mechanisms induced by geomechanical changes.

Fluid flow behavior in porous media caused by extraction and injection alters the pressure in the injection or extraction zones and surrounding areas, and it also affects the state of stress. Therefore, pressure and stress changes result in rock deformation. Understanding the rock deformations of mudstones and sandstones relate to seal integrity and being considered as $CO_2$ sequestration site is necessary for developing the appropriate injection strategy and estimating injection potential.

From such view points, this study paid attention on the fluid flow behaviors in mudstones and sandstones; the fluid expulsion from mudstones is well known mudstone compaction and the fluid injection into sandstones usually generates reservoir expansion, eventually surface rising problem. The main purpose of this research was to better understanding on deformation mechanisms caused by fluid expulsion from mudstones and $CO_2$ injection into sandstones. The properties of mudstones, *e.g.* porosity, depth, etc., were studied in term of compaction mechanism with respect to understanding of caprock properties before $CO_2$ injection. On the other hands, the deformations of the sandstones were studied as reservoir deformations after $CO_2$ injection regarding to surface uplift problem in CCS sites. The geomechanical processes, namely rock deformation, affect rock permeability, porosity, and bulk modulus. The theories of hydrostatic and poroelastic are used to obtain dependencies of rock permeability, porosity, and bulk volume on pore pressure and effective stress (Winterfeld and Wu, 2011). Chemical

reactions with minerals require a much longer time scale than the other mechanisms, therefore, are not considered in this research. In the case of the mudstone compaction, the fluid expulsion is focused by compaction trend in porosity-burial depth curves. Observed data from published researched were used for analysis. In contrast, the injection of fluid into sandstones, the laboratory results were used to constrain fluid flow model in simulation in order to analyze rock deformations (strain changing).

Although mudstone compaction has been studied for many years, there are still no unique compaction curve and mathematic equation up to now. The compilation curves for mudstones have also showed wide variations and scattered data, especially at the shallow depth where is dominated by mechanical compaction. The factors, *i.e.* basin type, lithology, thickness, time and compaction factors, are classified and analyzed to influence on mudstone compactions. Based on Terzaghi (1925, 1943) and Fowler and Yang (1998), time factor was revealed to be an important factor influencing on mudstone compactions. The results also show that mechanical process is the main among factors controlling the compaction, and is controlled mainly by overburden (*i.e.*, burial depths), effective stress and pore pressure. The mechanical compaction (or burial depths) is certainly one of the main controlling factors of compaction of mudstones, but it cannot be a single factor to explain the relationship between porosity of mudstones and burial depths in a form of a compaction curve. In addition, pore-pressure ($P_p$) prediction is based on compaction of mudstones. Early recognition of abnormally high pore pressures (AHPR) before and during drilling operations can substantially reduce drilling costs and troubles. The most world-widely used methods to estimate pore pressure in shale and to detect AHPR are Eaton method, Equivalent depth method, Ratios Method, Bower method; all of those are based on compaction concept of mudstones. According to effect of time to compaction of mudstones was demonstrated as an important factor that can explain variations of compaction curves as well as effect of burial depths. Likewise, it leads us to time-effect-adjusted $P_p$ prediction based on compaction concept method.

Based on effect of time on mudstone compactions, a compaction curve of Paleozoic mudstone showed a steeper slope than young mudstones and the curve was shifted to the direction of high porosity reduction at any present depth. However, the Paleozoic data of mudstones are very scanty, the porosity data used in this study, which are valuable and quantitative, in Paleozoic ages of mudstones are Athy (1930)'s data. They were taken from several fields at Oklahoma basin, USA. Those data were reported that they located at areas where had been occurred by uplift and erosion. Therefore, thickness of sedimentary rocks, which had been removed and disappeared by erosion, was estimated in order to correct and re-construct a compaction curve of Paleozoic mudstone. The result showed that, after corrections, the Paleozoic mudstone compaction curve seems to be consistent with mudstone compaction curve considering with time of Paleozoic age. Consequently, the compaction curve of the Paleozoic mudstone could be proposed.

Adding temperature effect combined with time effect, the correction and re-construction of mudstone compaction curves toward an establishment of a standard curve of mudstone compactions, especially during mechanical compaction, was proposed in this work. The

standard curve of compaction for mudstones will be very useful to apply for prediction and detection of overpressures and basin modeling works.

In study of fluid injection behavior, deformation results of sandstone core samples from laboratory experiments were analyzed and re-produced using geomechanical simulation. The experiment was setup to emulate a surface uplift problem caused by $CO_2$ injection in CCS site. Strain changing of core sample in laboratory testing can be implied to reservoir deformation in field observation.

Berea sandstone was selected to be a homogenous and isotropic rock representing a storage formation for $CO_2$ injection of CCS project. Deformations of Berea sandstone lead to understand more on a simple knowledge of deformations in formation caused by $CO_2$ injection. In addition, more complex deformations of heterogeneous and anisotropic rock were focused on experiments and simulations; that is Tako sandstone. Different layers, *i.e.* coarse-grain and fine-grain parts, were separated clearly in Tako sandstone, and thus the deformations of Tako sandstone could be inferred as multi-sequence (shale-sandstone) layers as seal-reservoir rocks. Finally, the simulations can help us to understand the deformations of sandstones from laboratory testing, especially in the case of $CO_2$ injection in which relates to CCS project, and the results also showed that properties of $CO_2$ in supercritical phase are a crucial parameter influencing deformations of sandstones induced by $CO_2$ injection.

# TABLE OF CONTENTS

# LIST OF FIGURES

# LIST OF TABLE

# CHAPTER 1

# INTRODUCTION

## 1.1 Research background

Available data and special reports indicate that the concentration of $CO_2$ in the atmosphere has drastically increased since 1900 as shown in Figure 1.1. Noticeably, the Renewable Energy Institute (IWR), a German renewable energy institute in Muenster, has reported that world $CO_2$ emissions reached a new record in 2011 at 34 billion tonnes, more $CO_2$ from fossil energy being blown into the atmosphere than ever before. At present, the world concentration of $CO_2$ in the atmosphere is increasing. If recent trends in world $CO_2$ emissions continue, the world will not be on a path towards stabilization of greenhouse gas concentrations. Due to $CO_2$ is the greenhouse gas that makes the largest contribution from human activities. It is released into the atmosphere and influences on the trends in global average temperatures and sea level are projected to rise during the 21st century (IPCC, 2001). Likewise, $CO_2$ capture and storage (CCS) is considered an option in the portfolio of mitigation actions for stabilization of atmospheric greenhouse gas concentrations.

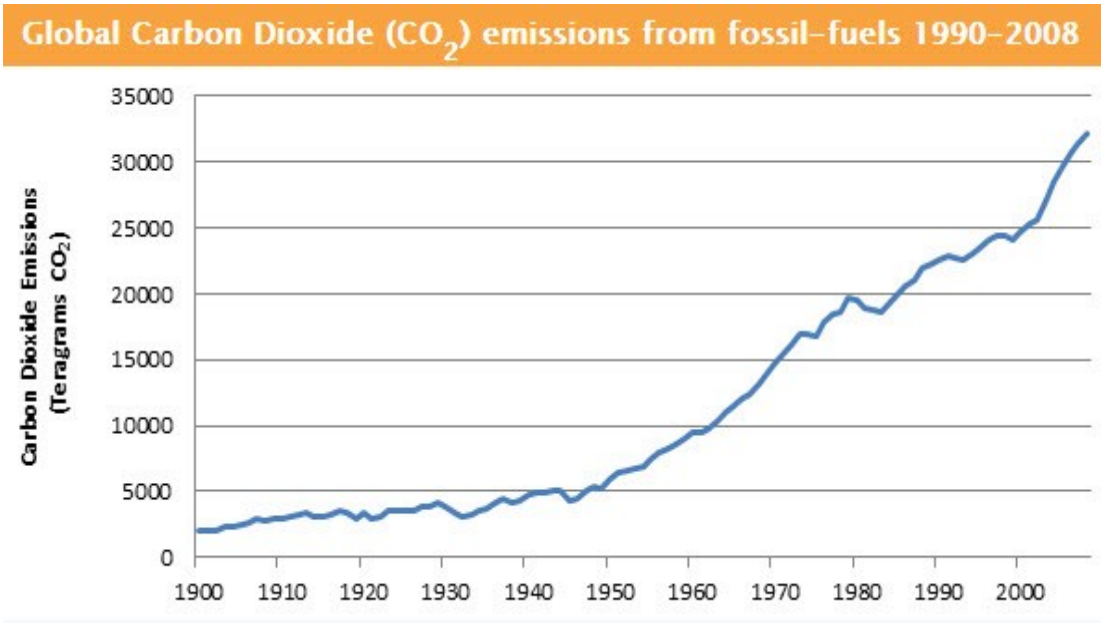


**Figure 1.1 World $CO_2$ emissions increased by over 16 times between 1900 and 2008 and by about 1.5 times between 1990 and 2008 (Boden *et al.*, 2010)**

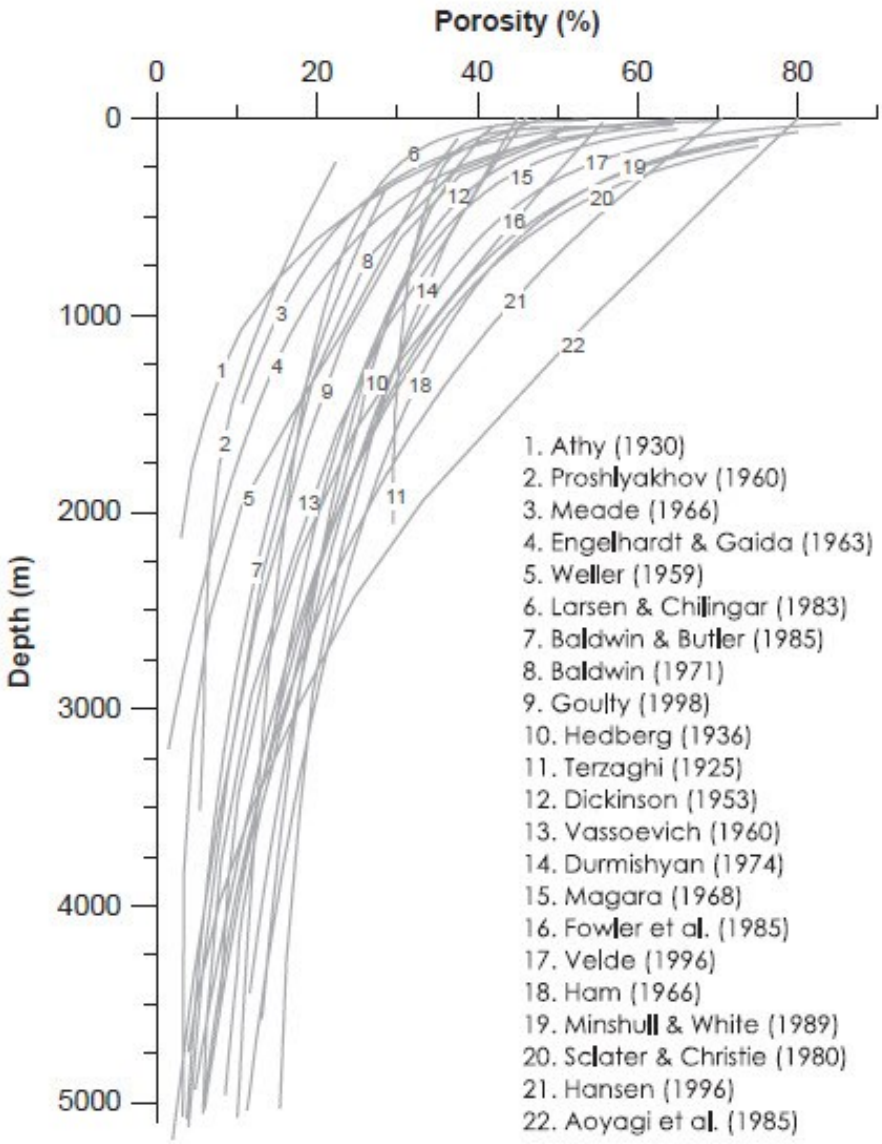


**Figure 1.2 Compilation curves of mudstone compactions from Fig. 1 in Mondol *et al.* (2007)**

Geomechanical study is an efficient tool and plays a prominent role in the assessment of the impact of CCS project. Deformation and rock property measurements are critically important for geomechanics. Tracking fluid movements and monitoring of geomechanical responses are emphasized in the geomechanics and has become more widely conducted in CCS project. The two major lithology types are mainly dominant in oil and gas field around the world; those are mudstones and sandstones. Mudstones are normally known as a caprock which has good sealing or trapping capacity, while sandstones are the most reservoir rock in oil and gas fields and are suitable storage formation which can occur in both onshore and offshore sedimentary basins. Oil and gas reservoirs are promising candidates for $CO_2$ sequestration due to the availability of field experiences on $CO_2$ injection, aimed to increase the recovery of residual oil.

Properties of mudstones can be observed and studied in term of fluid expulsion as well known mudstone compactions. Compaction plays a major role in hydrocarbon production (Alam *et al.*, 2010), and the geomechanical aspect has started to gain momentum with the interest in predicting subsidence resulting from fluid expulsion operation (Settari and Walters, 2001). However, mudstone compactions corresponding porosity will typically decrease with depth as overlying sediments compress the underlying material. Models of mudstone compaction process have become increasingly sophisticated, shifting from vague empiricisms to numerical codes, but the fundamental behavior underlying changes in mudstone porosity is still obscure. Therefore, variations and scattered data of mudstone compactions are still arguments.

Figure 1.2 shows the compilation of compaction curves which have been published by Mondol *et al.* (2007) which revealed the discrepancies among the cited data from several basins. The variations are mostly showed at the shallow part (0-2000 m) in which mechanical compaction is dominant. Due to the most world-widely used methods to estimate pore pressure in mudstone to detect abnormally high pore pressure are Eaton method, Equivalent depth method, Ratios Method, Bower method; all of those are based on compaction concept of mudstones and, in basin modeling works, reconstruction of basin geometries normally use default compaction curves and default thermal properties, the parameters which influence on compaction curves, *i.e.* time and temperature, are normally not considered in basin analysis.

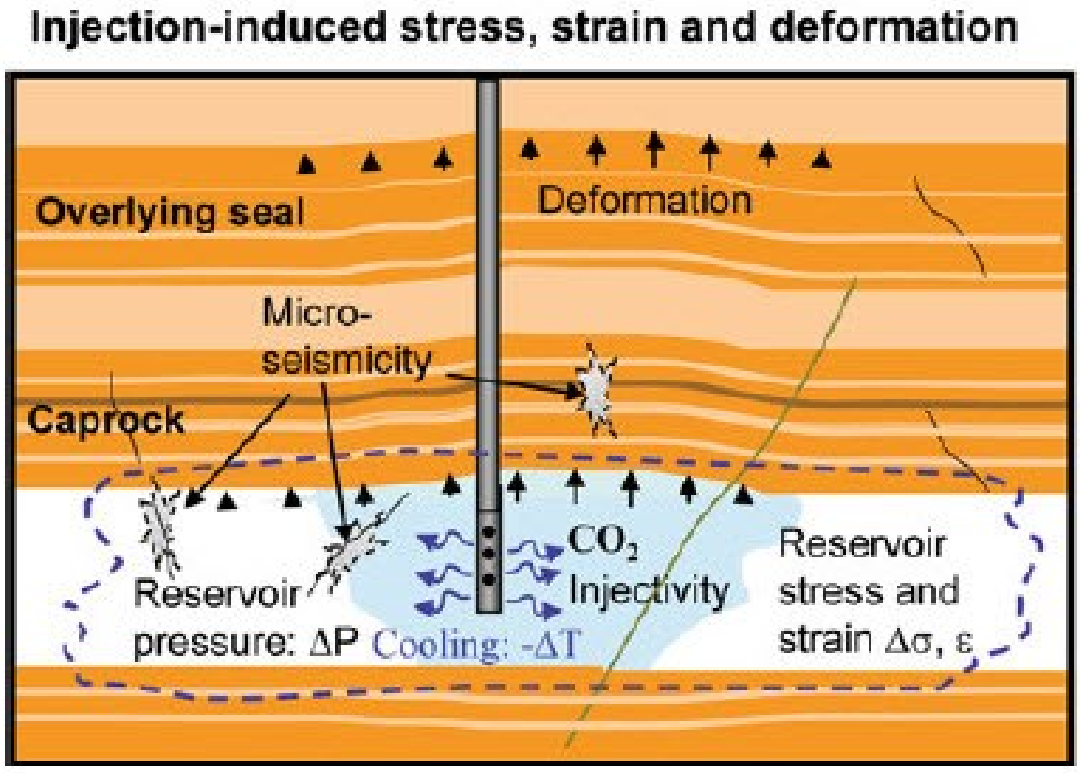


**Figure 1.3 Geomechanic processes in storage formation. $CO_2$ plum influencing formation pressure and creating geomechanic problems in a multilayered system (Rutqvist, 2012)**

To give an answer and the better understanding on variations and scattered data of mudstone compactions will help us to improve the accurate pore pressure prediction before drilling operations in order to reduce borehole trouble time and avoid drilling accidents. In addition, it is possible to establish a standard curve of compaction for mudstones which will be very useful to apply for petroleum works, hopefully CCS project.

Similarly, changing of geomechanical processes caused by $CO_2$ injection in formation pressure will induce some stress and strain changes in and around the injection zone. This may result in detectable ground surface deformations. Moreover, if formation pressure becomes sufficiently high, more substantial, irreversible mechanical changes could occur, *e.g.*, creating new fractures, straining the well assembly, or re-activing larger faults, in the caprock (Rutqvist, 2012) as shown in Figure1.3.

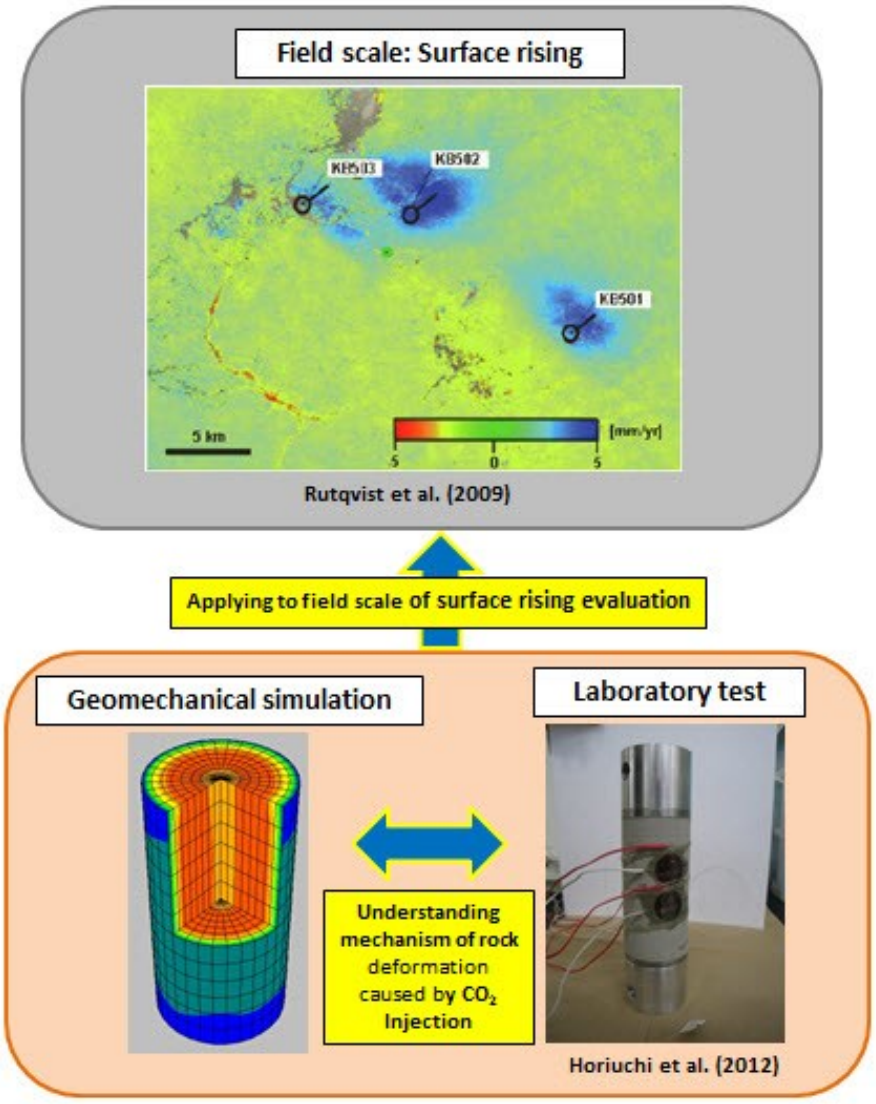


**Figure 1.4 Schematic of geomechanic simulation incorporate with laboratory testing applying for surface uplift problem in the field scale**

Consequently, geomechanical simulation was used to analyze and re-produce laboratory results of core sample in term of deformations. Strain changes of core sample in laboratory testing can be inferred to reservoir deformation relating to a surface uplift in field observation. The surface uplift evaluation is normally calculated before injection of fluid or steaming that it is important for the design of safe operations compatible with the environment.

Figure 1.4 is a schematic of relationship of geomechanical simulation and laboratory testing applying for surface uplift problem in the field scale. Because laboratory core tests are the best source using for study on gemechanical model. Using geomechanical simulation corresponding with laboratory testing studying on core sample deformations based on steps of experiments leads us to understand $CO_2$, which becomes less viscous and dense (Supercritical phase), movements inside core sample generated rock deformations because $CO_2$ in the supercritical state is highly sensitive to pressure change (Shukla *et al.*, 2010).

This study paid attention on the rock deformation mechanism relating to fluid flow behavior. Rock contraction is due to overburden stress increasing and/or pore pressure decreasing as well known compaction process, the fluid is expelled from the formation. On the other hands, the pressurization caused by fluid injection induces vertical expansion of the formation and changes in the stress field.

## 1.2 Research objective

The main objective of this study was to understand geomechanical processes of rock deformations based on both fluid expulsion and injection from the system. This research was separated to two main topics, *i.e.* mudstone compaction and simulation of $CO_2$ injection into sandstones, so the main proposes of each topic are to study of caprock properties before $CO_2$ injection, and study of reservoir deformations after $CO_2$ injection, repectively. The better understanding in these topics can develop and contribute petroleum industry such as overpressure prediction, reconstruction of basin modeling, surface uplift evaluation, etc.

The specific purposes are:

1. To analyze and reconstruct the variations and scattered data of mudstone compactions, especially mechanical compaction, from several basins.

2. To determine on effect of time on mudstone compactions and give an answer variations and scattered data of mudstone compaction are due to time effect.

3. To try an adjustment of compaction concept method based on effect of time on mudstone compactions in order to improve the accuracy of pore pressure and overpressure predictions.

4. To reveal effect of erosion on mudstone compaction and show a compaction curve of Paleozoic mudstone after correction due to unloading mechanism.

5. To try corrections data of mudstone compactions and establish a standard curve of mudstone compactions.

6. To re-produce and analyze deformations of a core sample of sandstones from laboratory experiment using geomechanical simulation.

7. To simulate and study on a motion of supercritical $CO_2$ in a core sample influencing on rock deformations.

## 1.3 Scope of research study

The overall framework and scope of research study of rock deformations caused by fluid flow behaviors, *i.e.* fluid expulsion from mudstones (mudstone compactions) based on observed data analysis and fluid injection into sandstone based on simulations of laboratory testing data, are presented in Figure 1.5. The dissertation consists of eight chapters and overall contents are introduced as followed:

Chapter 1: gave a brief introduction of the study, including research background, research objectives and scopes of the study.

Chapter 2: reviewed the literatures relating to this research study, including mechanism of mudstone compactions and the knowledge of supercritical $CO_2$ injection into storage formations.

Chapter 3: demonstrated the effect of time on mudstone compactions and set up the mathematic equation for time effect and adjusted the compaction concept method based on effect of time on mudstone compaction for developing in pore pressure prediction in mudstones.

Chapter 4: revealed effect of erosion on mudstone compactions and correct compaction data of Paleozoic mudstone due to unloading mechanism.

Chapter 5: tried the establishment of standard curve of mudstone compactions.

Chapter 6: re-produced and understood rock deformation caused by supercritical $CO_2$ injection into Berea sandstone from laboratory testing using geomechanical simulation.

Chapter 7: re-produced and understood rock deformation caused by supercritical $CO_2$ injection into Tako sandstone from laboratory testing using geomechanical simulation.

Chapter 8: gave conclusions of the research study and recommendations for further research.

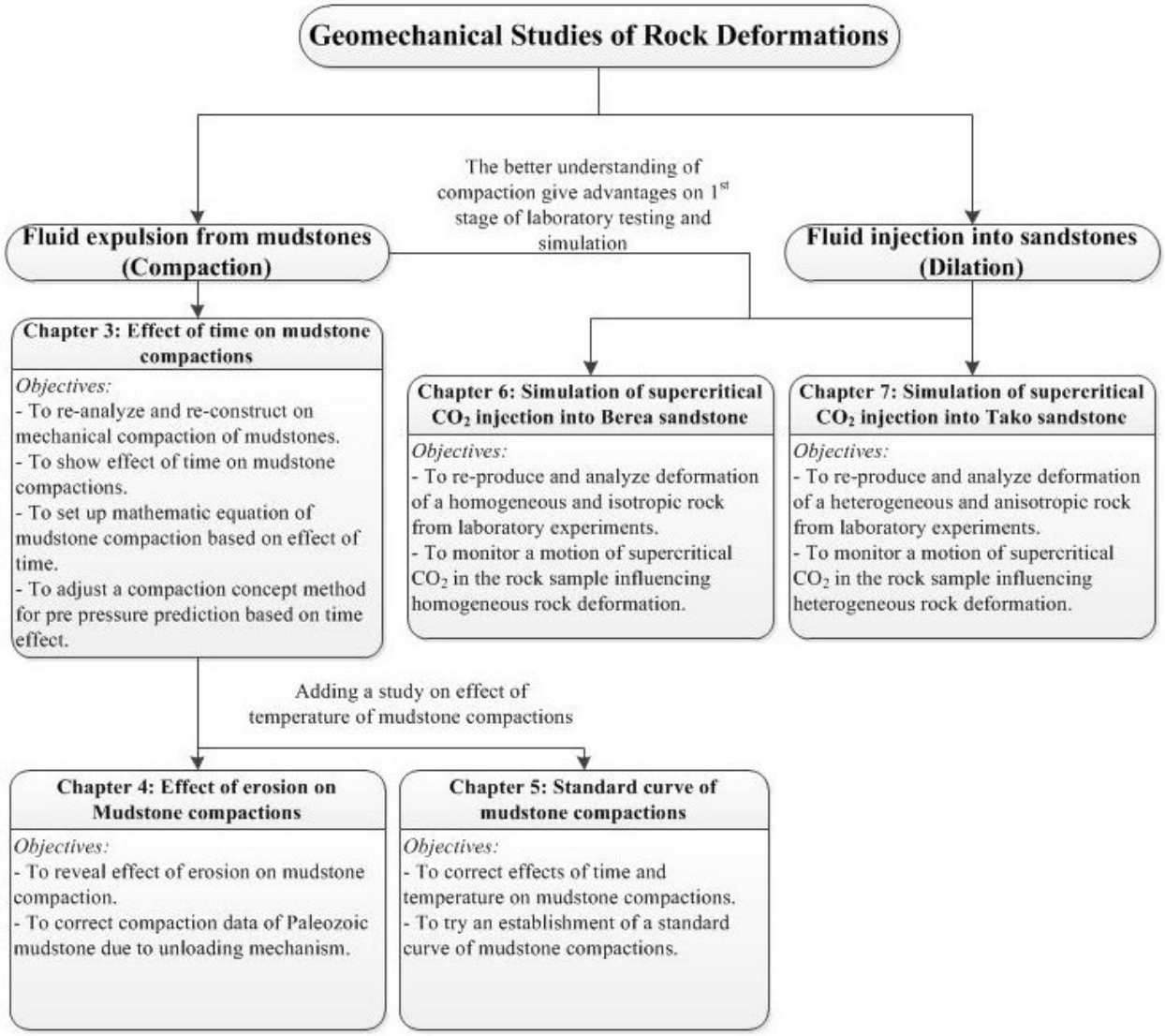


**Figure 1.5 Frame work and scope of the study**

# CHAPTER 2

# LITERATURE REVIEW

## 2.1 Fluid expulsion from mudstones (mudstone compaction)

### 2.1.1 History of mudstone compactions

Compaction of sediments has been studied for long times ago. Compaction of mudstones is simply described in a burial diagenetic process to reduce porosity of the mudstones; through this process, mud (sediment of particle-size of clay) changes from loose mud (soupy clay, loose fluidal clayey sediments) into plastic clay mass and finally into mudstones and slate. The person who studied on sediment compactions is H.C. Sorby in 1908. He showed that considerable shrinkage occurs in finely divided clay sediments on drying and it has been found that within certain limits the diminution of volume is equal to the volume of water lost in the process. Afterward, the idea that compaction of sediments might have played a part in the origin of oil field structures seem to have been conceived largely during the period 1915-1920. The information on compaction has come from two directions, *i.e.* field observations and experimental investigations.

For field observations, Hedberg (1926) attempted a quantitative evaluation of the compaction of sediments. He stated that sediments are compacted under the influence of their own weight has long been a commonplace. Rubey (1927) used data as the basis for a suggestion and published the void-ratio of a mudstone is inversely proportional to the original depth of burial. The most widespread model of mudstone compactions was proposed by L.F. Athy in 1930. He assembled determinations of density and porosity of some specimens from various depths in oil wells in Oklahoma and Texas. Then, in 1936, Hedberg reviewed the process of compaction and put on record a series of porosity-depth determinations of certain wells in the Venezuela. He believed that the effect of gravitational pressure on the compaction of sediments is principally concerned with relation of rock overburden to the porosity of clays and mudstones. In addition, since 1965 several papers (Hottman and Johnson, 1965; Wallace, 1965) on the presence of an empirical relationship between mudstone compaction and its pore pressure were published, which drew the attention of many geologists and engineers in the oil industry. Magara (1966, 1968, 1971, 1974 and 1978) continued compaction research in Japan, using well-log and other geological data. He showed studies on mudstone compactions relating to overpressure mechanism, primary hydrocarbon migration, aquathermal effect on fluid pressure, erosion and structural timing. The conversion of seismic velocity changes to porosity for study on mudstone compaction in the Makran accretionary prism, Gulf of Oman, was conducted by Fowler *et al.* (1985). They concluded that the movement of pore waters and the consolidation of the accreting sediments play an important role in the deformational process taking place in the prism. Velde (1996) assembled porosity data for clay-rich deep sea sediments. The data included different sites, ages and bottom

depths. The assembled data of Velde showed accordingly match with exponential model of mudstone compactions of Athy (1930).

While, the experimental investigations were mainly inspired by Terzaghi (1925 and 1943), who gave the results of theoretical and experimental studies on the consolidation of sediments. Furthermore, Skempton (1944) assembled some samples of various kinds of muds and clays. Within the limits of pressure, all these material reveal a similar behavior, which is expressed by a formula suggested by Terzaghi. In 1963, Engelhardt and Gaida (1963) studied concentration changes of pore solution during the compaction of clay sediments. They found that there is no concentration change of pore solutions in the course of all the experiments with kaolinitic clays, but definite changes with montmorillonitic clays. Meade (1966) determined factors influencing the compaction of clays, especially the early stages of compaction, based on several data of laboratory experiments. He concluded that particle sizes, rates of deposition, geochemical factors, re-arrangement of clay particles, organic matter and temperature are all of factors which influence on early stage of clay compactions. Recently, Mondol *et al.* (2007) studied on changes in physical properties of mudstones during burial. They did experiments of clay compaction of smectite and kaolinite mixtures, and then they measured changes on physical properties during mechanical compaction, *i.e.* acoustic velocities. They stated that the variations of mudstone compaction curves may be due to differences in lithology, pore pressure and diagenetic history.

## 2.1.2 Mechanical compaction

Mechanical compaction is a type of the diagenetic processes in the compaction. The mechanical compaction can be described as a function of porosity, and controlled by overburden (*i.e.*, burial depths), effective stress and pore pressure. The function has been proposed in term of porosity and burial depth based on both field observations and experimental studies. Modol *et al.* (2007) have defined mechanical compaction of mudstones that mechanical compaction is a function of effective stress and dominates in the shallow parts of the basin down to 2-4 km depth (80-100 °C) depending on the geothermal gradient, while chemical compaction, including dissolution and precipitation of minerals, dominates in the deeper parts of the basin at higher temperatures (> 80-100 °C), where time, temperature and mineralogy are the principle controls on compactions. An empirical equation of compaction is practically expressed as an exponential function with a negative coefficient (Athy, 1930), and has been widely used for exploring the relationship of compaction of mudrock sediments as shown in Figure 2.1. The porosity ($\phi$) is expressed as a function of burial depth ($z$) as shown in Eq. 2.1. This model was derived from viewpoints of statistical physics by Korvin (1984).

$$\phi = \phi_0 e^{-az} \tag{2.1}$$

Where $a$ is the constant number representing localism environments of basins, and $\phi_0$ is the initial porosity at a datum depth.

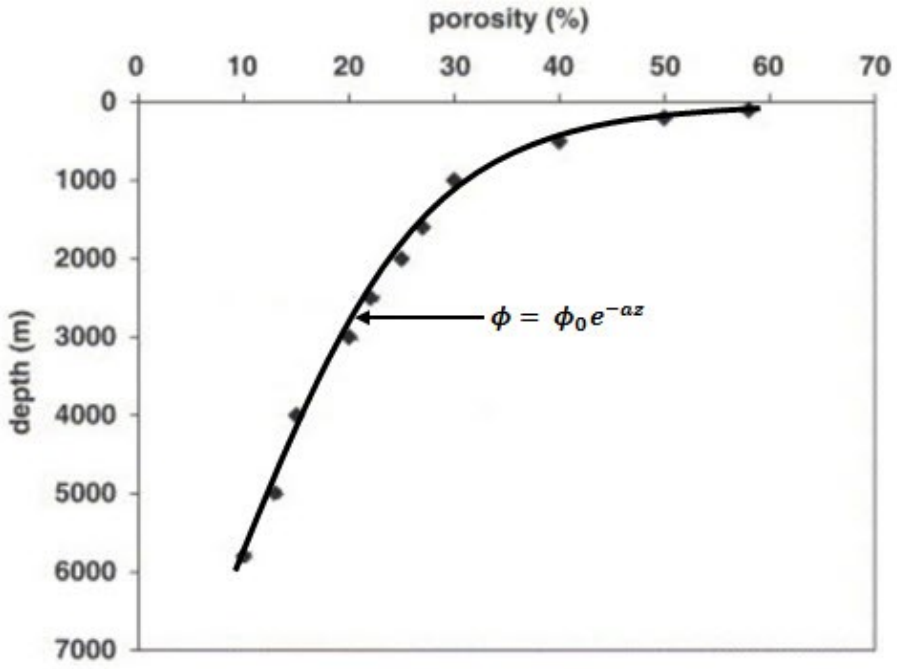


**Figure 2.1 Mudstone compaction curve represented by Athy's model**

Nevertheless, porosity of mudstones at a depth is also determined by effective stress ($\sigma_e$). The same relationships of porosity and effective stress (Dutta, 2002; Flemings *et al.*, 2002; Peng and Zhang, 2007, Zhang, 2011) can be established:

$$\phi = \phi_0 e^{-a\sigma_e} \tag{2.2}$$

The effective stress can be determined by total stress ($\sigma_v$) and pore pressure ($P_p$) that satisfy a famous equation as called Terzaghi's model. Following relationship (Terzaghi, 1925; Rubey and Hubbert, 1959):

$$P_p = \sigma_v - \sigma_e \tag{2.3}$$

where Biot coefficient ($\alpha$) is normally assumed to be 1 (*i.e.*, rock framework-grains are incompressible) and $\sigma_v$ is normally known the overburden stress (total stress; here horizontal stress, normally of tectonic origin, is neglected). This has been done extensively in soil mechanics but only for stresses equivalent to loads corresponding to depths of a few tens of meters below the earth's surface.

Therefore, Rubey and Hubbert (1959) explained that, in geology, the problem involves the compaction of clays deposited as sediments in geosynclinals basins under loads that have increased from zero up to the weight of several kilometers of superposed sediments. A related problem involves compaction of clays in response to a tectonically applied compressive stress. The magnitude of the stresses involved, and the degree of compaction produced, is thus in a range far beyond the limits for which laboratory data are available.

As stratum becomes buried under an ever increasing load of sediments, it will be subjected to vertical total compressive stress of magnitude:

$$\sigma_v = \rho_{bw} g z \tag{2.4}$$

Where $\rho_{bw}$ is the mean value of the saturated water of bulk density in the overlying sediments, $g$ is the acceleration of gravity, and $z$ is the depth.

Rubey and Hubbert (1959) introduced a useful parameter, $\lambda$, which is the ratio of pore-fluid pressure to total overburden pressure:

$$\lambda = \frac{P_p}{\sigma_v} \tag{2.5}$$

Hence, the final state of equilibrium to which the pressure in the sediments tends is essentially the state of normal pressure referred to earlier, and all pressure states occurring prior to the terminal state must have been characterized by pressure higher than normal, and by of values of $\lambda > P_p/\sigma_v$.

Consequently, the relationship between effective stress and depth at normal compaction can be expressed:

$$\sigma_e = (1 - \lambda)\rho_{bw} g z \tag{2.6}$$

A schematic of mechanical compaction of mudstones can be represented by Figure 2.2. At conditions for stage A, $\lambda$ has a value of 1; the system is overpressured.

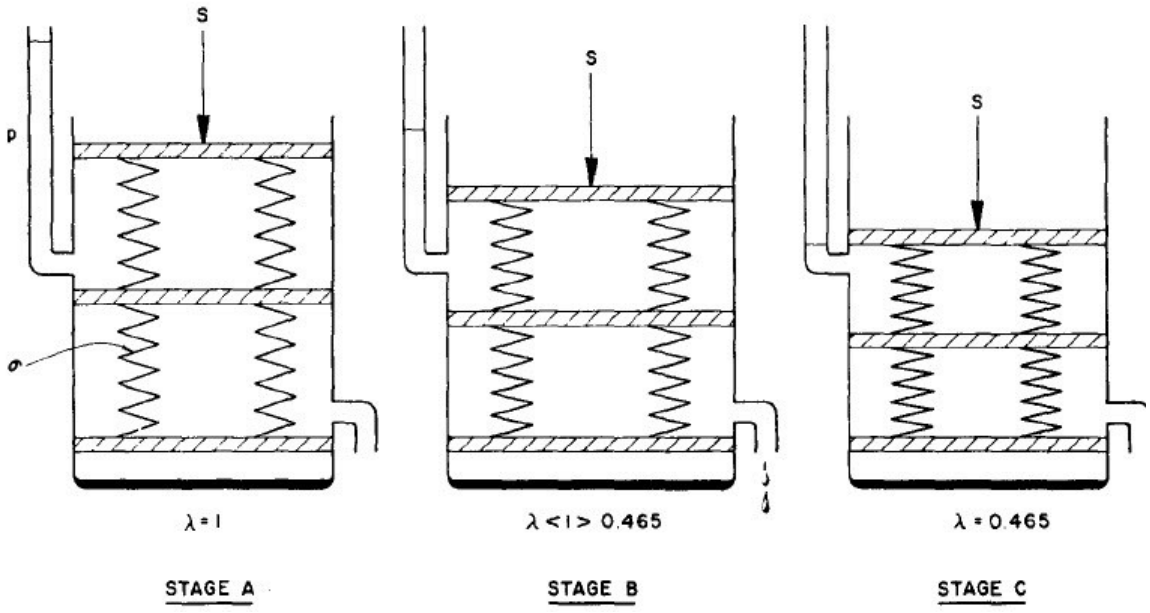


**Figure 2.2 Schematic representing mechanical mudstone compactions**

As water is allowed to escape from the system, the plates move downward slightly (compaction system), and the springs ($\sigma$) carry part of the applied load ($S$). As more and more water is allowed to expel from the system, the springs carry a greater share of the load, and $\lambda$ has value less than 1. Finally, sufficient water is expelled from the system for the springs to attain their compaction equilibrium. At this stage, terminal compaction equilibrium, the load is supported jointly by the springs and the water pressure ($p$), which is simply hydrostatic. The value of $\lambda$ is approximately 0.465.

### 2.1.3 Time effect

Effect of time or geologic age has been studied to be an important factor to influence on mudrock compactions for a very long time (Terzaghi, 1925, 1943; Versluys, 1927; McCoy and Keyte, 1934; Weatherby and Faust, 1935; Van Olphen, 1963; Burst, 1969, Dzevanshir *et al.*, 1986). Terzaghi (1925) discussed the primitive expression of his compaction equation. He considered compaction in term of excess pore pressure of soils and relaxation of the excess pressure in time. Versluys (1927) discussed effective processes in compaction of clay, calculated compaction pressure, and he stated that time factor relates to the escape of water, which was also considered by Terzaghi. McCoy and Keyte (1934) studied on the expulsion of enormous quantities of water from compacting muds and raise doubts to the existence of a definite relation between overburden and density of mudstones. They confirmed that geologic age may also be an important factor in controlling density.

An evidence of seismograph work, it is known that, in argillaceous sediments, the velocity of seismic waves in general increases with rock density. Increasing water content, on the other hands, tends to diminish velocity. Both of these factors are usually dependent on degree of compaction. Weatherby and Faust (1935) have supplied data on the increase of seismic velocities with geologic age. However, they ignored effects of uplift and erosions. Van Olphen (1963) studied on clay mineral dehydration and concluded that many clay lattices in Paleozoic and older Tertiary sediments appear to have been dehydrated completely under normal compaction. In contrast, partial dehydration has also been observed in relatively young sediments. Because of the paucity of fully swelling clay material in Paleozoic and older Tertiary rocks and its abundance in young sediments, clay hydration state is a function of geologic age.

Burst (1969) is a pioneer to study effect of time on compaction processes quantitatively. He demonstrated his plots (Figure 2.3) between porosity and geologic time based on Manger (1963)'s data of mudstones (Manger reported only data without physical discussion).

Burst (1969) suggested that the porosity of mudstones tend to decline as a function of increasing time. However, his plot was not clear because he only plotted ranges of porosities with times, and depths (or age range of sample) were not specified. Furthermore, Dzevanshir *et al.* (1986) proposed a mathematic equation of shale with consideration of time and

lithology (ratio of mudstones to total thickness), but their test was based on scanty quantities and was still not clear.

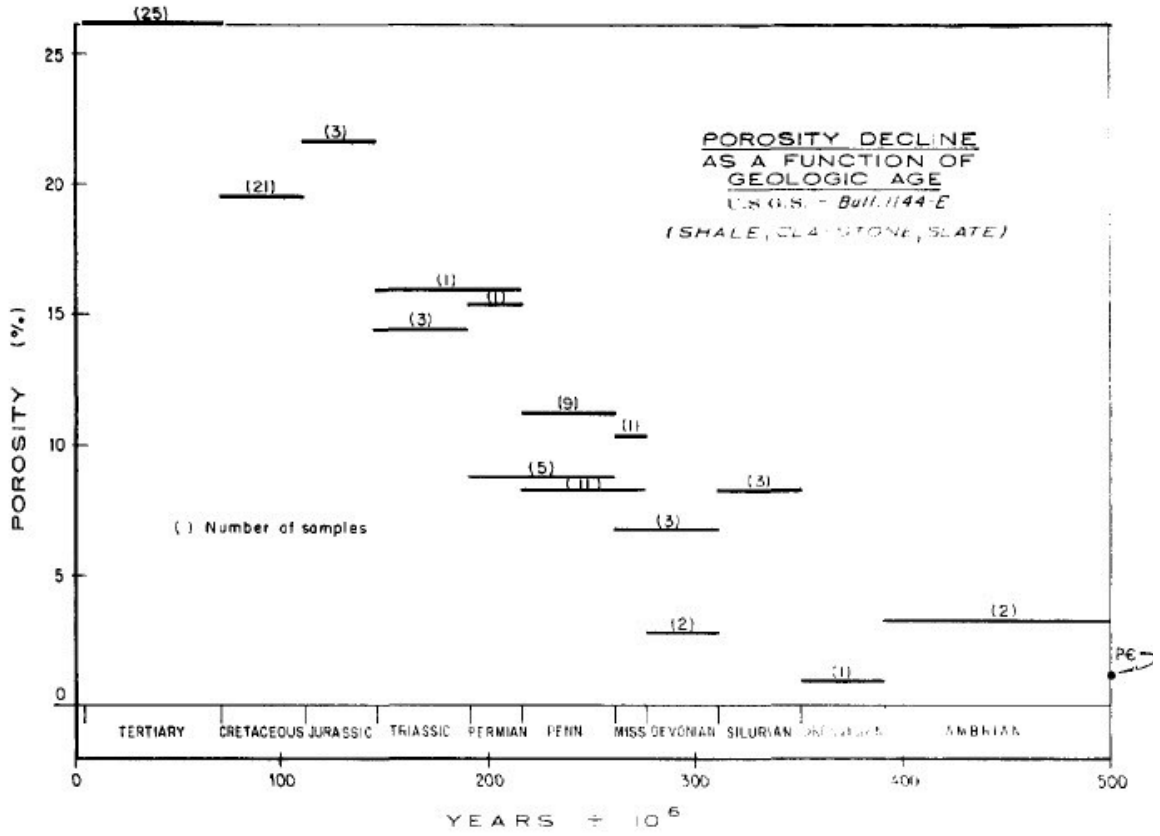


**Figure 2.3 Porosity of mudstones decline as function of geologic time based on Manger (1963)'s data created by Burst (1969)**

## 2.1.4 Pore pressure measurement in formation

Pore pressure is simply the pressure of the fluid in the voids or pores between the individual grains comprising a rock's matrix. The most pore pressure measurements are available only on porous and permeable formations, *e.g.* sandstones, and are obtained after the well is drilled, while the measurements are not applicable to the surrounding, largely impermeable, mudstone sections where the majority of the overpressure is developed. Likewise, the effectiveness of geophysics and petrophysics methods for estimation and calculating of pore pressure from mud logging, wireline, and drilling data, as known indirect measurements, are restricted to the impermeable formations such as mudstones.

Two main measurements are the Repeat Formation Test (RFT) and Drill Stem Test are an open hole wireline instrument primarily used for measuring vertical pressure distribution in reservoir, as well as for recovering formation fluid samples. In addition, nowadays a modern tool has been developed as multi-tester tool in order to measure both RFT and DST by using only one tool as shown in Figure 2.4.

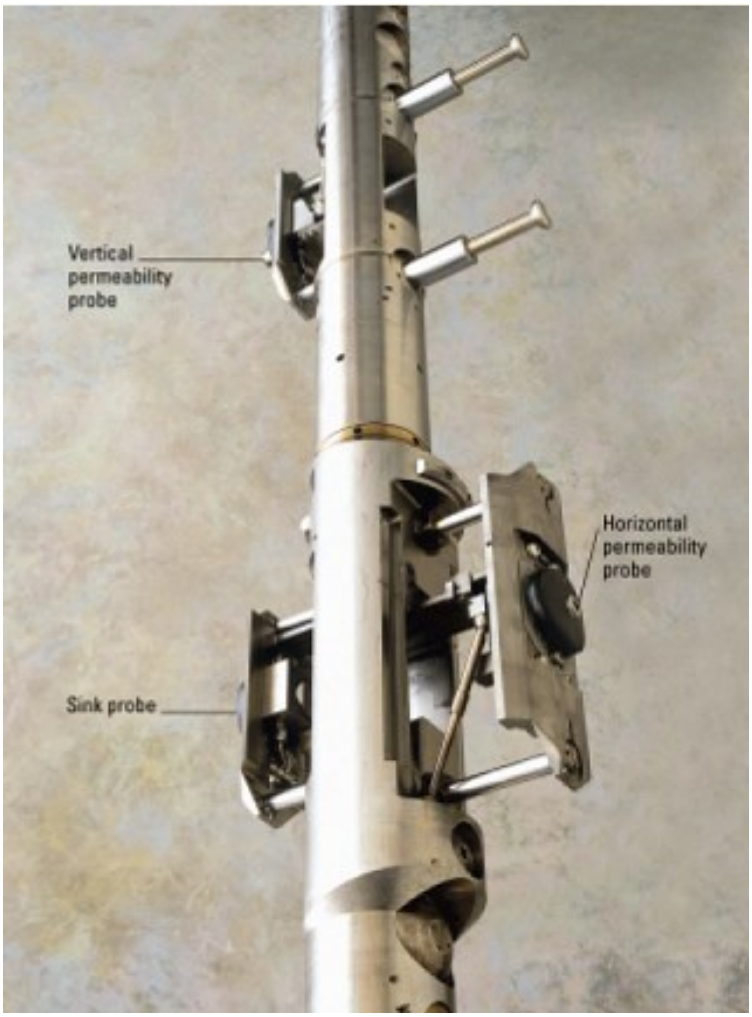


**Figure 2.4 Modern Multi-Tester tool (RFT, DST, etc.) from Schlumberger (Source: NETL, 2013)**

### 2.1.4.1 RFT tool

The RFT tool has been designed for measuring formation test and collecting reservoir fluid samples. When the tool is set, the pressure rises slightly because of the compression of mud cake by the packer. Probe piston retracts and the pressure drops due to the resulting flow line volume expansion and communication with the formation. When the piston stops, the pressure build up again because the packer is still continuing to compress the mud cake until tool is fully set. When both pressure chambers are full, the pressure chambers build up towards a final pressure.

The running time used for pressure analyses of the build-up curve may yield permeability and reservoir pressure as with conventional drill stem and production pressure tests. Finally, after the tool is retracted, the mud column pressure is again measured (Soufi, 2009). Figure 2.5 shows a typical pressure recording which shows both analog and digital pressure curves as standard log penetration.

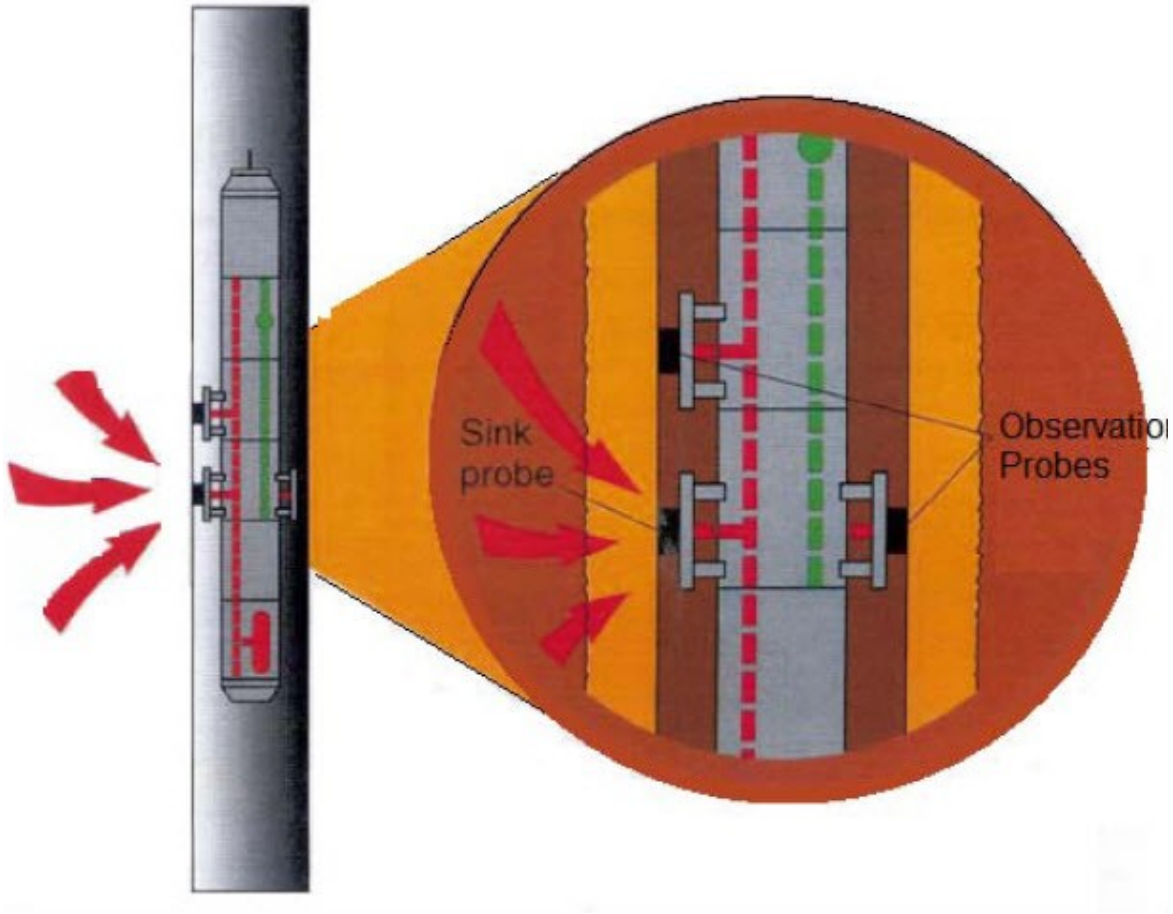


**Figure 2.5 RFT tool (Soufi, 2009)**

### 2.1.4.2 DST tool

DST is a method of the testing formation pressure and fluid. A drill stem with a packer is run and set just above the zone to be tested. The packer is set and a DST valve is opened to allow the reservoir to communicate with the inside of the drillstem which is run either empty or with a small calculated cushion.

The drill stem is run with several pressure gauges. The purpose of the pressure gauges is to record the down-hole pressure during the sequence of flow and shut in periods that comprise the DST. The pressure recorded during the test is used to calculate reservoir characteristics, *e.g.* formation pressure, permeability, skin damage and productivity index. Analysis of the pressure build up from shut in leads to accurate determination of the formation pore pressure. The second shut-in period is used for determining the final shut-in reservoir pressure. The actual static reservoir pressure is determined from Horner analyses of the DST pressure data.

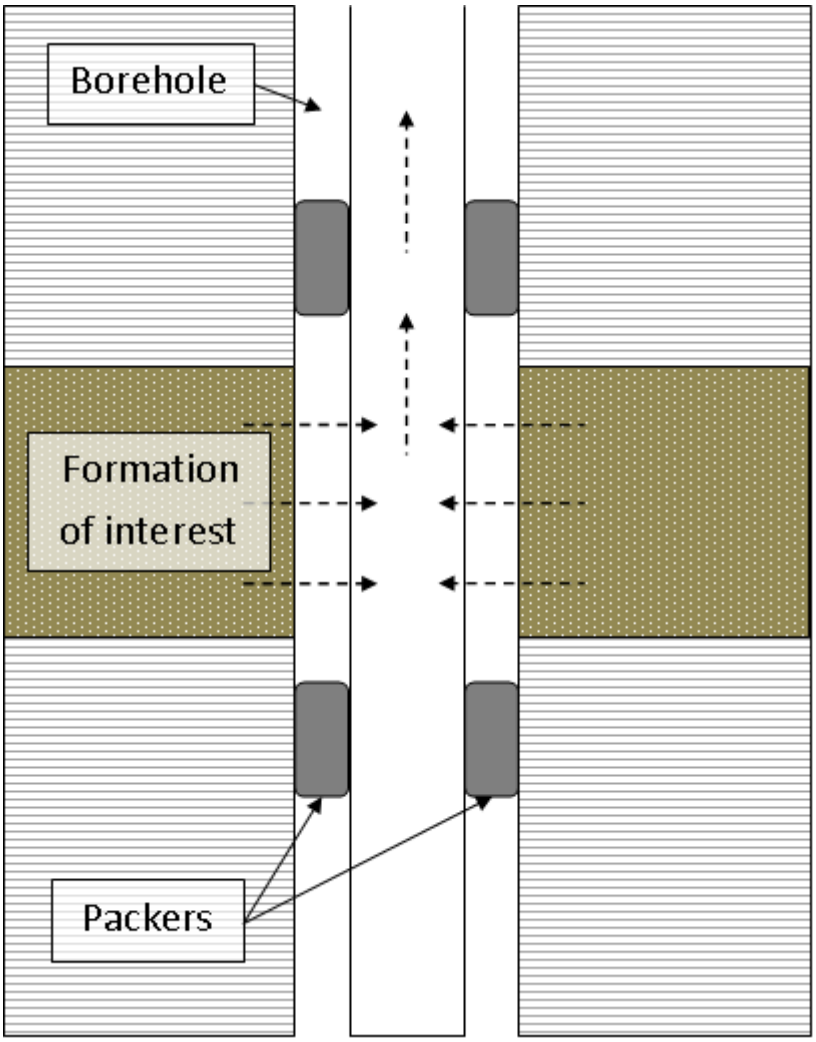


**Figure 2.6 DST tool (Source: Wikipedia, 2013)**

### 2.1.5 Phenomenon of overpressure relating mudstone compaction

There are still arguments in mechanisms of overpressure generations, but the main ones, which are widely believed to be a cause of overpressure, are increase in stress and in-situ fluid generating mechanisms. All of mechanisms have been discussed the subjects of numerous publications are summarized as follows.

- *Rapid overburden loading*

  Rapid overburden loading results in an increase of the pore fluid pressure, *i.e.* if a layer of low-permeability, *e.g.* clay or mudstones, prevents the escape of pore fluids at rates sufficient to keep up with the rate of increase in vertical stress (overburden), the pore fluid begins to carry a large part of the load and pore pressure increase. This process is referred to as under-compaction or compaction disequilibrium (Rubey and Hubbert, 1959).

- *Aquathermal pressuring*

  The pressure of water heated in a closed system will rise due to thermal expansion. The rock matrix constrains the increased volume of the pore fluid; therefore the pore spaces of a formation can result by fluid expansion mechanism. This process has been proposed by Baker (1972) and Magara (1974) as an overpressuring mechanism. Aquathermal pressuring is related to the geothermal gradient.

- *Diagenesis of clay dehydration*

  The rates of clay dehydration are a function of subsurface temperature, pressure and pore water chemistry. The conversion of montmorillonite (smectite) to illite layers results removing interlayer water into bulk system. The amount of released water can reach up by volume, eventually pore pressure increasing.

- *Hydrocarbon generation*

  Most high pressures in this mechanism are believed to be caused by present-day or recently active oil and gas generation in low permeability, oil mature, source rocks and reservoirs. Evidence of gas generation as an overpressuring mechanism is inferred from the occurrences of highly geopressure reservoirs at moderate depth in some basins. This mechanism has been firstly proposed by Spencer, 1987.

- *Lateral transfer*

  This mechanism could happen when migration of fluid along faults takes place or if a high-permeability pathway such as a reservoir, or a connected network of reservoirs and faults allows transmission of pore fluid from a deeper trap to a shallower one, a process termed later transfer (Chopra and Huffman, 2006).

- *Structural uplift (Erosion)*

  Uplift of sediments alone will not cause unloading if the overburden load is not changed, but when the overburden is reduced during uplift either by syn-depositional tectonic processes or by erosion, the accompanying reduction in overburden results in the original in-situ pore pressure being contained by a much lower overburden, which results in a reduction of the effective stress, and unloading (Chopra and Huffman, 2006).

### 2.1.6 Pore pressure and overpressure predictions in mudstones

In drilling operations, it is necessary to determine formation pressure of various formations penetrated by the borehole. This enables the driller take extra precautions while penetrating abnormally high pressure zones in order to avoid damages, including accidents due to blow outs. Such abnormal pressures are called geopressure and the formations where they occur are known as overpressure zones (NFOR *et al.*, 2011). The mistake of assuming there is immediacy between the pressure in the sand and the sandwiching mudstone leads to serious drilling problems (Shaker, 2002).

Techniques for detection, evaluation and prediction of pore pressure and overpressure in low-permeability rocks are based on relationships between porosity and effective stress in mudstones. The possible existence of this relationship in low-permeability rocks, *e.g.* mudstones, cannot be tested by laboratory experiments, because the pore pressure of such tight rocks cannot be experimentally controlled, and thus the pressure in low-permeability rocks can be inferred from indirect measurements. Pioneers in geopressure analysis used rock mechanic effective stress in relation to the change of petrophysical properties to establish several empirical pore pressure calculation methods, *i.e.* sonic, resistivity and porosity are used during and post drilling estimate pore pressure prediction.

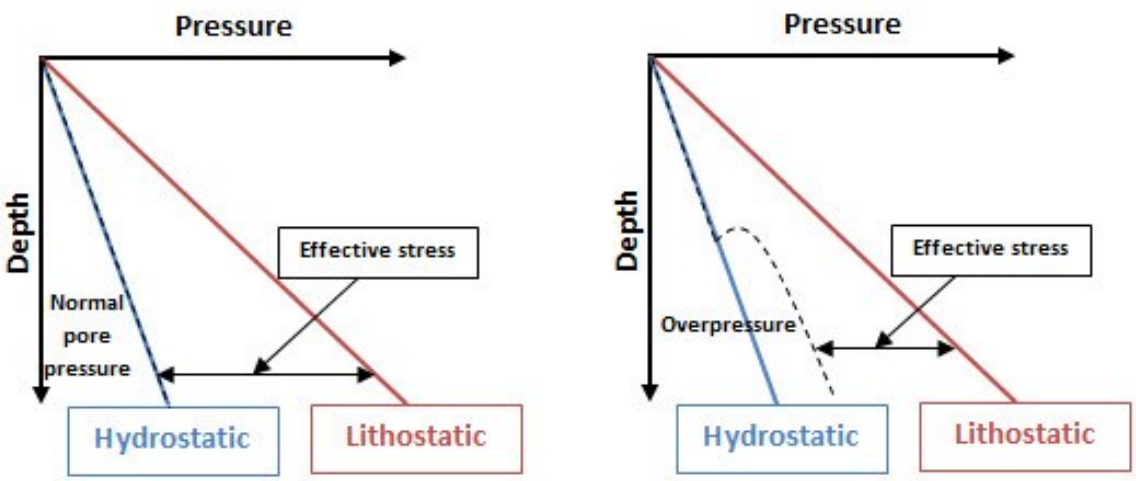


**Figure 2.7 Plots of pressure and depth demonstrating normal pressure and overpressure based on the relationship between total stress (vertical or lithostatic stress), pore pressure and effective stress**

Most of the techniques are linked to porosity and assume that the porosity is controlled by the effective stress the sediment has experienced. Many practitioners use effective stress (difference between pore pressure and total vertical stress (overburden or lithostatic pressure). Hence, there is a tendency to use effective stress in pore pressure prediction. Figure 2.7 shows a difference of pore pressure between areas of normal compaction and overpressured zone. Left panel demonstrates the pore pressure is on the hydrostatic pressure gradient indicating a normal pressure. The normal effective stress is the difference between the total (vertical or lithostatic stress) and the pore pressure. Whilst, right panel shows the pore

pressure is above hydrostatic and therefore overpressured. The effective stress is smaller than if the sediment was normally pressured, either due to under-compaction or a secondary fluid expansion process.

Zhang (2011) has listed up methods of pore pressure and overpressure prediction based on mudstone properties derived from well log data (acoustic travel time/velocity, resistivity and porosity). The details of all methods are summarized as discussed below.

### 2.1.6.1 Resistivity approach

In young sedimentary basins where under-compaction is the major cause of overpressure, the well log based resistivity method (Figure 2.8) can fairly predict pore pressure. Eaton (1972, 1975) proposed the following equation to predict pore pressure gradient in mudstones using resistivity log. Eaton's resistivity method is applicable in pore pressure prediction, particularly for young sedimentary basins, if the normal mudstone resistivity is properly determined.

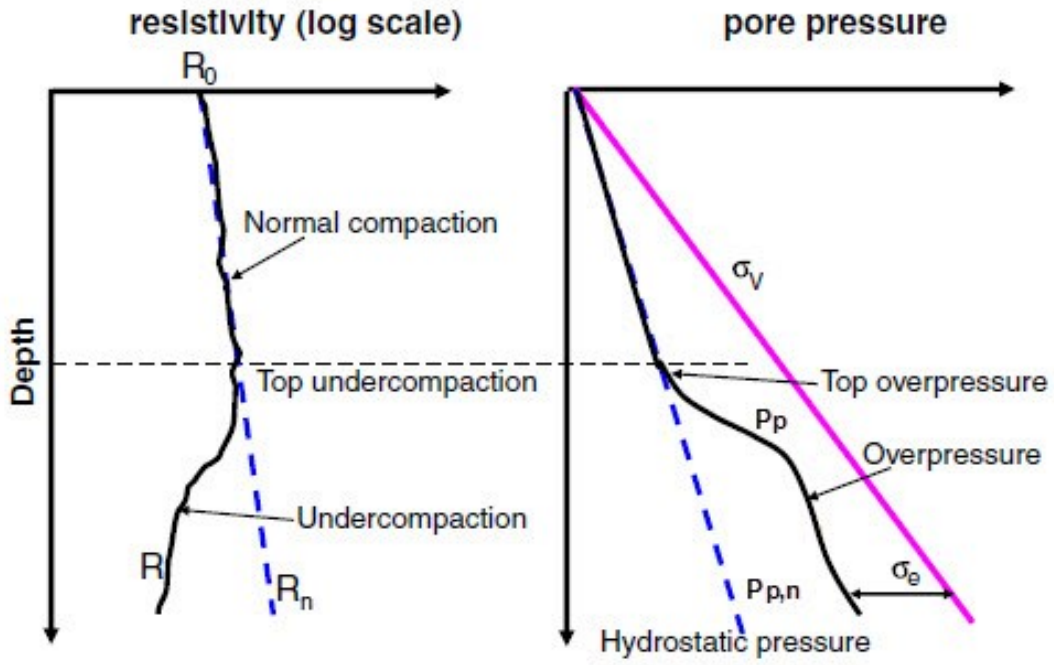


**Figure 2.8 Schematic mudstone resistivity and pore pressure demonstrating the relationship for pore pressure prediction (Zhang, 2011)**

### 2.1.6.2 Transit time approach

Eaton (1975) presented the following empirical equation for pore pressure gradient prediction from sonic compressional transit time (Figure 2.9). This method is applicable in some

petroleum basins, but it does not consider unloading effects. This limits its application in geologically complicated area.
Afterwards, Bowers (1995) developed this approach by calculating the effective stress from measured pore pressure data of mudstone and overburden stresses. He analyzed the corresponded sonic interval velocities from well logging data in the Gulf of Mexico slope. The effective stress and compressional velocity do not follow the loading curve if formation uplift or unloading occurs, and a higher than the velocity in the loading curve appears at the same effective stress. Hence, Bower's method is applicable to many petroleum basins. However, this method overestimated pore pressure when shallow is poorly or unconsolidated, because the velocity in such a formation is very slow.

Next developed methods are Miller's method and Tau's model. Miller's method and Tau's model are similar to Bowers's method. The advantage of Miller's method and Tau's model is that both the effects of the matrix and mudline velocities are considered on pore pressure prediction.

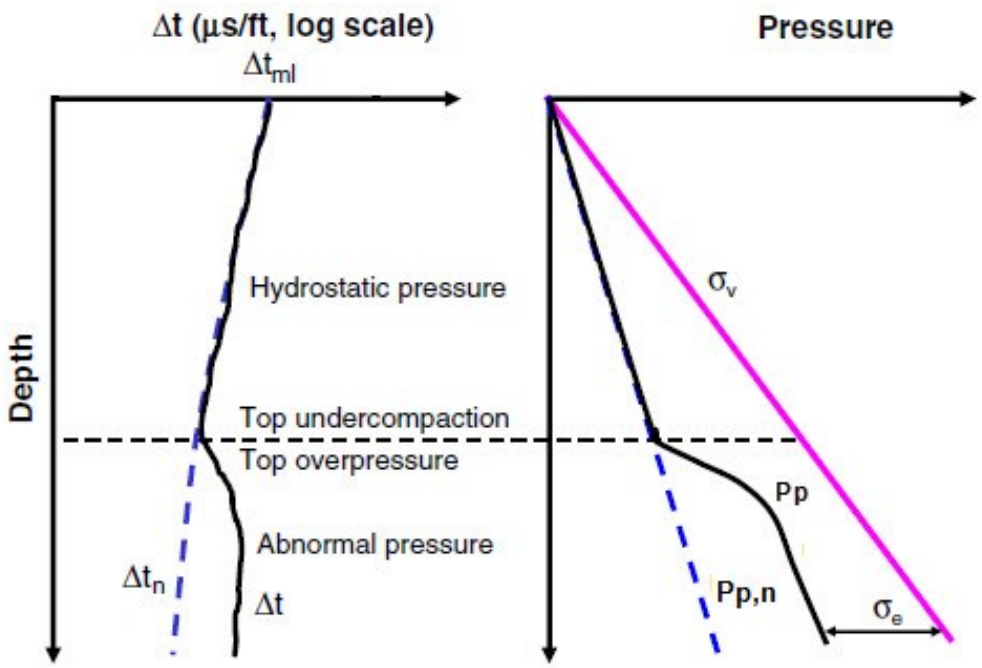


**Figure 2.9 Schematic mudstone transit time and pore pressure demonstrating the relationship for pore pressure prediction (Zhang, 2011)**

In addition, sonic transit time can be converted by seismic velocity. Slotnick (1936) recognized that the compressional velocity is a function of depth. Therefore, the normal compaction trend-line of travel time should be a function of depth. Sayers *et al.* (2002) used this relationship as the normally pressured velocity for pore pressure prediction. A normal compaction trend for mudstone acoustic travel time with depth in the Canarvon Basin was established by fitting an exponential relationship to averaged acoustic travel time.

### 2.1.6.3 Porosity approach

Porosity is a major criterion in determining a good reservoir hence lending credence to its usefulness as an overpressure indicator (Figure 2.10). Therefore, it is strongly recommended that porosity is used as an alternative for overpressure indicator. This method is more precise and can be easily applied, and thus it is even more economical than other methods (NFOR *et al.*, 2011).

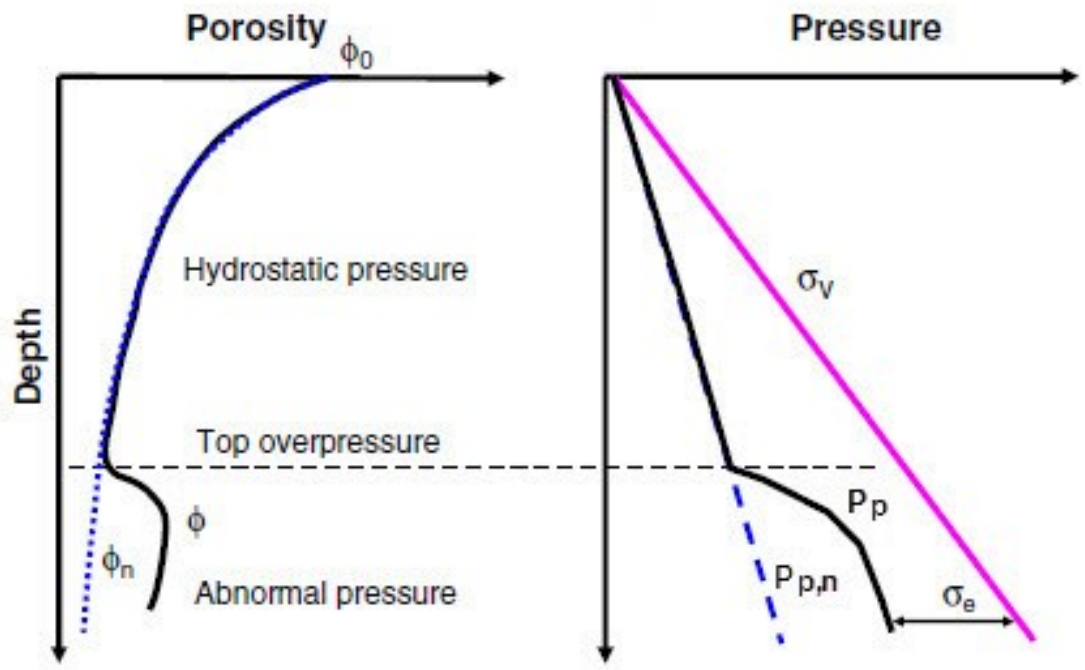


**Figure 2.10 Schematic mudstone porosity and pore pressure demonstrating the relationship for pore pressure prediction (Zhang, 2011)**

## 2.1.7 Compaction concept method for pore pressure prediction based on porosity approach

Because indicators of under-compaction (overpressued zones) are higher pore pressure and larger formation porosity than other geophysics parameters, *e.g.* formation resistivity and formation sonic transit time, in the normal compaction condition, and porosity is an indicator (a function) of effective stress and pore pressure. Hence, pore pressure can be predicted from formation porosity.

The evidences that try to use porosity data for prediction pore pressure in mudstone, for example Holbrook *et al.* (2005). They presented porosity-dependent effective stress for pore pressure prediction. Heppard *et al.* (1998) used an empirical porosity equation similar to Eaton's sonic method to predict pore pressure using mudstone porosity data. Fleming *et al.*

(2002) and Schneider *et al.* (2009) also applied porosity-stress relationships to predict overpressures in mudstones.

Zhang (2011) demonstrated an equation for pore pressure prediction from porosity according to normal compaction of porosity trend. The pore pressure gradient can be calculated from the following equation:

$$P_{pg} = OBG - \left(OBG - P_{p,ng}\right)\frac{ln\,\phi_0 - ln\,\phi}{az} \tag{2.7}$$

where $\phi$ is the porosity in mudstones at depth of $z$, $\phi_0$ is the porosity in the mud-line (in the ground surface or sea floor), $z$ is the depth below the mud-line, a can be obtained from the normal compaction porosity trend-line in Eq. 2.1, $OBG$ is the overburden pressure gradient, $P_{p,ng}$ is the normal (hydrostatic) pressure gradient and $P_p$ is the pore pressure gradient.

Based on Eq. 2.2, the effective stress can be obtained:

$$\sigma_e = \frac{1}{a} ln \frac{\phi_0}{\phi} \tag{2.8}$$

Similarly, the effective stress at normal pressure condition ($\sigma_n$) can also be obtained from Eq. 2.8, when the porosity is the normal porosity ($\phi_n$) as expressed:

$$\sigma_n = \frac{1}{a} ln \frac{\phi_0}{\phi_n} \tag{2.9}$$

Combining Eq. 2.8 and 2.9, one has:

$$\sigma_e = \sigma_n \frac{ln\,\phi_0 - ln\,\phi}{ln\,\phi_0 - ln\,\phi_n} \tag{2.10}$$

Substituting Eq. 2.10 into 2.3 and remarking $\sigma_n = \sigma_v - P_{p,n}$, so from Eq. 2.7, the pore pressure, overburden pressure and porosity have the following relationship:

$$P_p = \sigma_v - (\sigma_v - P_{p,n})\frac{ln\,\phi_0 - ln\,\phi}{az} \tag{2.11}$$

This equation proposed by Zhang (2011) is deferent with other existing pore pressure-porosity equations (Heppard *et al.*, 1998; Fleming *et al.*, 2002; Holbrook *et al.*, 2005; Schneider *et al.*, 2009) is that the pressure calculated from Eq. 2.11 are dependent on depths. In addition, the normal compaction trendline of porosity is not a constant, but a function of depth.

## 2.1.8 Erosion effect

Structure uplift of sediments alone will not cause the compaction changing if the overburden load is not changed. As uplift accompanying erosion processes result a reduction of an effective stress as known unloading mechanism. Although compaction is an irreversible elastoplastic process in which sediments can only move down the normal compaction curve, never move up it. However, the area where has experienced a significant uplift and erosion, the normal compaction trend is shifted to the direction of increased compaction at any present depth, in comparison with the trend in an area of no erosion. Erosion and uplift can be expected to decrease pore pressure, so that most of the overpressure may have disappeared in such area. In addition, grains of mudstones are usually weaker and more sensitive to the changes of overburden load, estimation of erosion from mudstones data seems to be much more reliable than sandstones. Figure 2.11 explains 3 stages of geologic cycles, *i.e.* uplift, erosion and deposition processes.

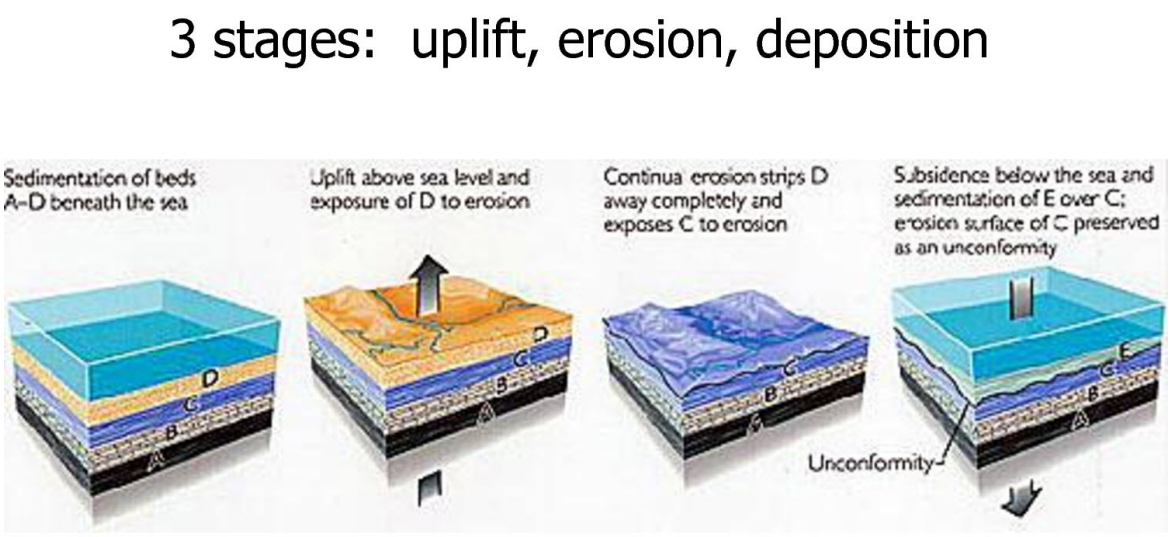


**Figure 2.11 Geologic cycles of uplift, erosion and deposition processes**

## 2.1.6.1 Estimation of eroded thickness

Porosity-depth trend in well data can be used to estimate the amount of missing sedimentary section in areas that have undergone significant erosion. Magara (1978), who is a pioneer, proposed using sonic-transit time logs to determine downhole porosity specifically as a means of defining mudstone compaction trends for estimating erosion. Issler (1992) adopted this approach for defining porosity in mudstones, the compaction curves derived from porosity became the basis for estimating the amount of erosion. He showed a reference compaction curve (porosity-depth) in a part of the basin that has no erosion comparing with the sonic-porosity logs in wells within other parts of the basin to identify the amount of erosion.

Magara (1978) proposed sonic-transit time and depth relationship for estimating thickness of erosion (Figure 2.12). The normal trend of this curve is used to extrapolate to the surface, a surface (datum depth, $z_0$) gives approximately 200 μs/ft of surface transit time ($\Delta t_0$)

suggesting no erosion in this area. On the other hands, the distance between the erosional surface and the level at which the extrapolated value equal $\Delta t_0$ is the approximate thickness of the sedimentary rocks removed by erosion. Magara (1978) believes from the knowledge of mudstone compaction in several different basins that in most basins the value $\Delta t_0$ will not exceed 210 μs/ft.

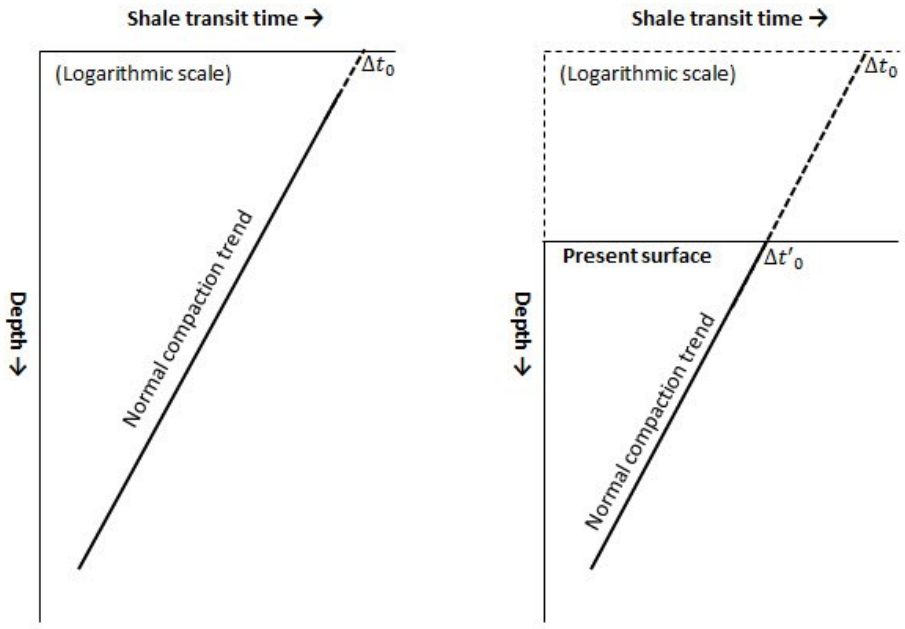


**Figure 2.12 Schematic showing the normal compaction trend of shale transit time-depth plots for estimation of eroded thickness (Magara, 1978)**

## 2.2 Fluid injection into sandstones as rock dilation

### 2.2.1 Introduction of fluid injection

Fluid injection is the placement of fluids into the subsurface through a well bore. The practice of fluid injection has become essential to many petroleum industries. The main proposes of the fluid injections are used to increase production and prolong the life of oil producing fields. To recover oil beyond primary production, engineers usually implement water flooding as a process in which field operators pump water into the reservoir through injection wells with the aim of displacing oil toward equipped production wells.

Nowadays, a growing concern that increasing levels of greenhouse gases, especially carbon dioxide ($CO_2$) emission, in the atmosphere is contributing to climate change. Therefore, a promising approach is CCS has been conducted to mitigate atmospheric greenhouse gas concentrations. Recent experience from $CO_2$ injection demonstrates that CCS in deep sedimentary formations is technologically feasible. However, the injection induced any change in storage formation pressure and temperature influencing some stress-strain changes

in and around the injection zone. Even a small pressure change and straining of the rock might result in small microseismic events including fractures and local stress concentrations that could be released locally. If pressure becomes sufficiently high, more substantial, irreversible mechanical changes could occur, *e.g.,* creating new fractures, straining the well assembly, reactivating larger faults within reservoir and ground surface deformation.

### 2.2.2 Simulation of $CO_2$ sequestration

Geomechanical simulation of the evolution of geological structure has used in some form for two or three decades, especially simulation of the deformation of viscous rocks. The inter-linking of geosciences and engineering in cross-disciplinary studies has become increasingly popular in recent years. Geomechanical modeling is now recognized as an essential part of many appraisal and development projects.

In a geological $CO_2$ sequestration project, a vital concern of monitoring and verifying the subsurface movement and phase behavior of the injected $CO_2$ is important to ensure the storage integrity. Consequently, geomechanical simulations of fluid injection and extraction (production) in porous media are used to be an important tool for assessing feasibility, safety and productivity of such operations. As $CO_2$ injected, the additional fluid influences on localized pressure buildup, causing pore expansion and fluid density increases, eventually land-surface uplift problem.

Various researches have been conducted to date evaluating under which hydrogeological condition the injected volume of $CO_2$ can be safely stored for long term (hundreds or even thousands of years). Minkoff *et al.* (2003) studied on fluid flow and mechanical deformation caused by hydrocarbon production at the Belridge Field in California, USA, using coupling of reservoir (IPARS) and mechanical (JAS3D) simulators. Rutqvist and his colleagues have done many researches during 2002-2012 about geomechanical simulations of $CO_2$ sequestration by using the coupled process simulator TOUGH-FLAC. Similarly, Ouellet *et al.* (2011) used coupled simulators of reservoir (ECLIPSE) and mechanics (VISAGE) to assess containment in $CO_2$ storage at Ketzin case study, Germany.

The stress-strain relationship is fundamental for modeling mechanical deformation and the associated coupled process in porous and fractured rock. Hook's law (Elastic theory) has been generally used to describe this stress-strain relationship for elastic mechanical processes (Liu *et al.*, 2009). The geomechanical models are built based on laboratory measurements and require input from a variety of discipline, *e.g.*, petrophysics, geology and geophysics. For examples, Lewis *et al.* (2007) suggests that the development of dilation and compaction can be predicted with some confidence by a well-chosen and well constrained geomechanical model but for a simulation to be of any real value there must be some check of its validity. Crook *et al.* (2006) and Couples *et al.* (2007) both based their geomechanical simulation on laboratory deformations. Couples *et al.* (2007) have also calibrated their materials to laboratory data using a simulated axi-symmetric experimental deformation of a cylindrical

test sample. They stated that there is a good match between the stress and strain states obtained in the laboratory and in the simulation across the full evolution of the system.

### 2.2.3 Surface uplift problem induced by $CO_2$ sequestration

Surface uplift is important because the injection of $CO_2$, in general, produces an increase pore pressure will change the stress field cause deformations in the rock mass. Therefore, the pressurization is considered to be a main process generating vertical expansion of the reservoir. The vertical expansion of the reservoir may result in a ground surface uplift.

The study of the surface uplift problem caused by $CO_2$ sequestration is still scanty and there are a few researches which have been published. However, there has been a significant drive to integrate satellite interferometric synthetic aperture radar (InSAR) with geomechanical modeling to link surface deformation with movement and storage of injected $CO_2$. Significant research into linking geomechanics with InSAR observations has shown that integrated InSAR and geomechanical simulation has strong potential in accurately imaging $CO_2$ migration, estimating injected $CO_2$ volume and containment of $CO_2$ (Rutqvist *et al.*, 2009, 2010; Vasco *et al.*, 2010; Angus *et al.*, 2012).

The research from Rutqvist *et al.* (2009, 2010) showed a study on surface uplift caused by $CO_2$ sequestration at In Salah, Algeria, using the observed surface deformation from InSAR to constrain geomechanical simulation. Moreover, they showed the surface deformation from InSAR can be useful for tracking the fluid pressure and for detection of a permeable leakage path through the overlying caprock layers. Their works reported that, at In Salah industrial $CO_2$ storage project, surface uplifts with magnitude of 4 mm/year as shown in Figure 2.13 and 2.14.

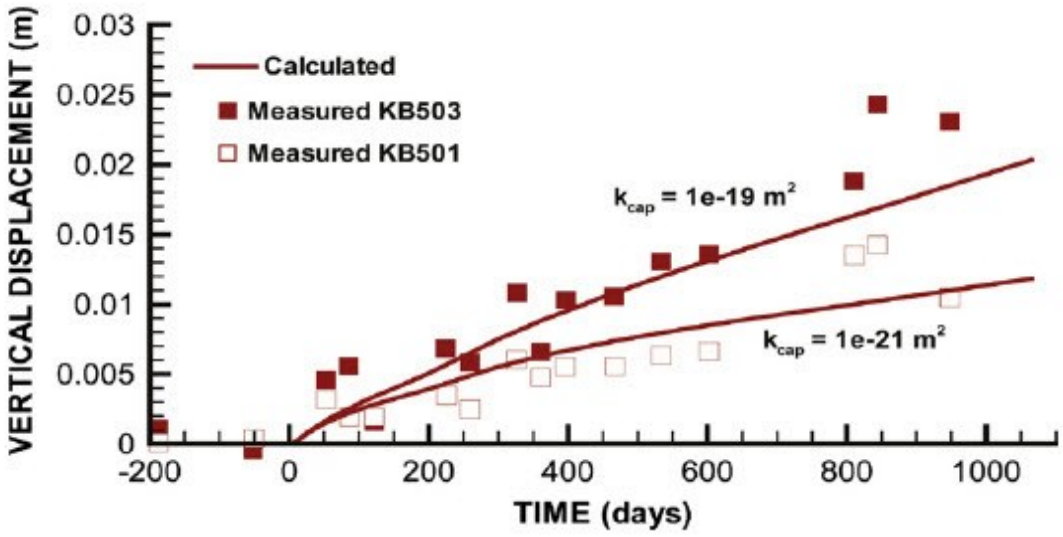


**Figure 2.13 Comparison of simulated and measured vertical surface uplift at In Salah, Algeria (Rutqvist, 2010)**

(a)

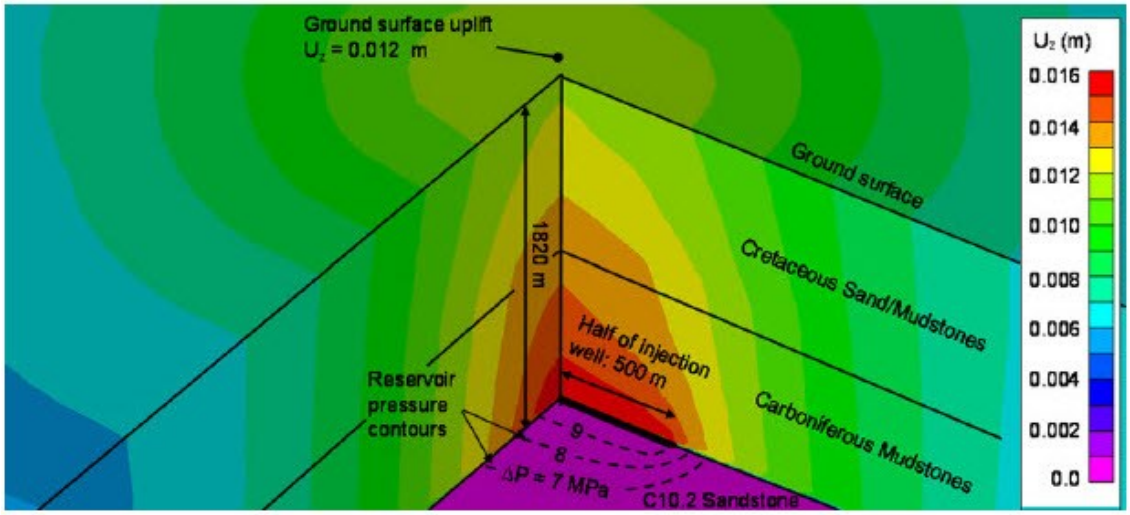


(b)

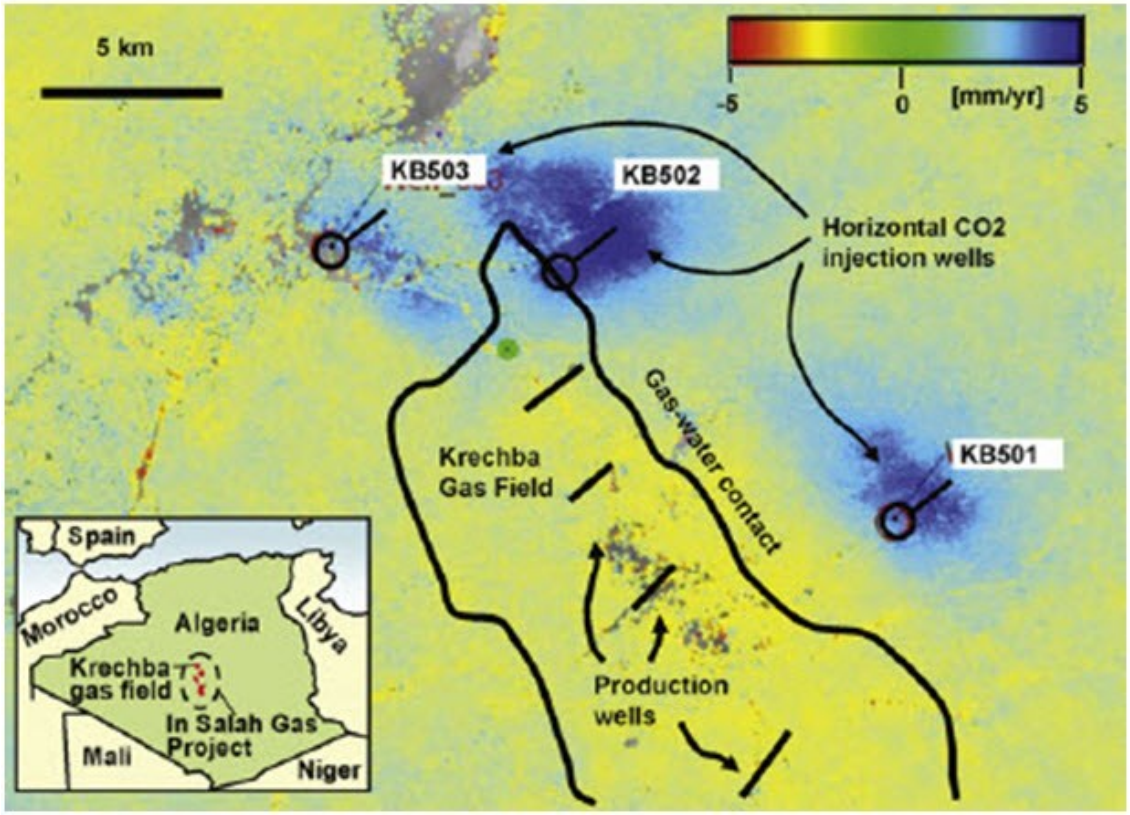


**Figure 2.14 Surface uplift at In Salah, Algeria (a) The result from geomechanics simulation (b) The result from InSAR (Rutqvist, 2010)**

## 2.3 The relationship between porosity and bulk modulus of rock

Rock deformation is based on the concepts of hydrostatic and linear poro-elasticity theories, rock permeability, porosity, bulk modulus, pore pressure, and confining pressure play a significant role in the rock deformation. There are evidences, revealing that the closing and shortening of tapered crack tips (Mavko and Nur, 1978) or the decreasing compliance of grain contacts (Murphy *et al.*, 1993) are possibly cause of changes in porosity and dry bulk modulus of rock. Consequently, the changes of porosity (effective porosity) because movements of particles, are close to or away from each other, can relate to dry bulk modulus of rock, and finally, influencing on rock strains and deformations (Figure 2.15).

Several researches have been conducted to study on dry rock modulus as a function of porosity, and inferring velocity and density changes due to reservoir fluid change as a function of porosity. Mavko and Mukerji (1995) stated that the pore space compressibility of a rock is the direct physical link between the dry and fluid-saturated moduli, and is therefore the basis of Gassman's equation (Eq. 2.12) for fluid substitution.

Gassmann's equation was used to convert the time-dependent pore pressure and saturations resulting from the flow simulation into changes of elastic rock parameters (Gassmann, 1951). Gassman's equation computes effective bulk moduli of rock saturated ($K_{sat}$) with a given composition of pore fluid from the elastic moduli of the dry rock. The equation is

$$\frac{K_{sat}}{K_m - K_{sat}} = \frac{K_d}{K_m - K_d} + \frac{K_f}{\phi(K_m - K_f)} \qquad (2.12)$$

where $K_f$ is the total fluid bulk modulus, $K_d$ is the dry bulk modulus of rock and $K_m$ is the matrix or mineral bulk modulus.

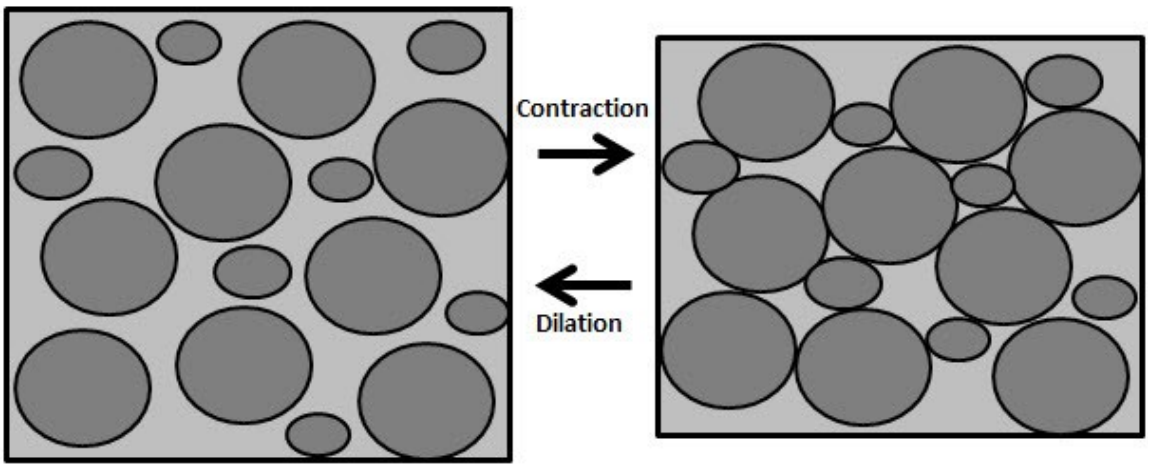


**Figure 2.15 Schematic rock contraction (compaction) and dilation influencing effective porosity changes**

Russell and Smith (2007) examined two approaches (*i.e.* pore space stiffness approach and critical porosity approach) of pore space compressibility, which are used to determine a relationship of dry bulk modulus and effective porosity, with quantitative data of sandstones

obtained by Han *et al.* (1986). Their results show that the pore space stiffness produced a better fit to the data than the critical porosity approach. Thereby, the pore space stiffness, $K_\phi$, which is the inverse of the dry rock space compressibility at a constant pore pressure, is related to the dry rock bulk modulus, $K_d$, the mineral bulk modulus, $K_m$, and porosity, $\phi$, by the relationship (Mavko *et al.*, 1998):

$$K_d = K_m \left( \frac{1}{1+\frac{\phi}{k}} \right) \tag{2.13}$$

$$k = K_\phi / K_m \tag{2.14}$$

where $k$ is the pore space stiffness over matrix bulk modulus ratio. The value of $k$ can be determined by a graph as shown in Figure 2.16.

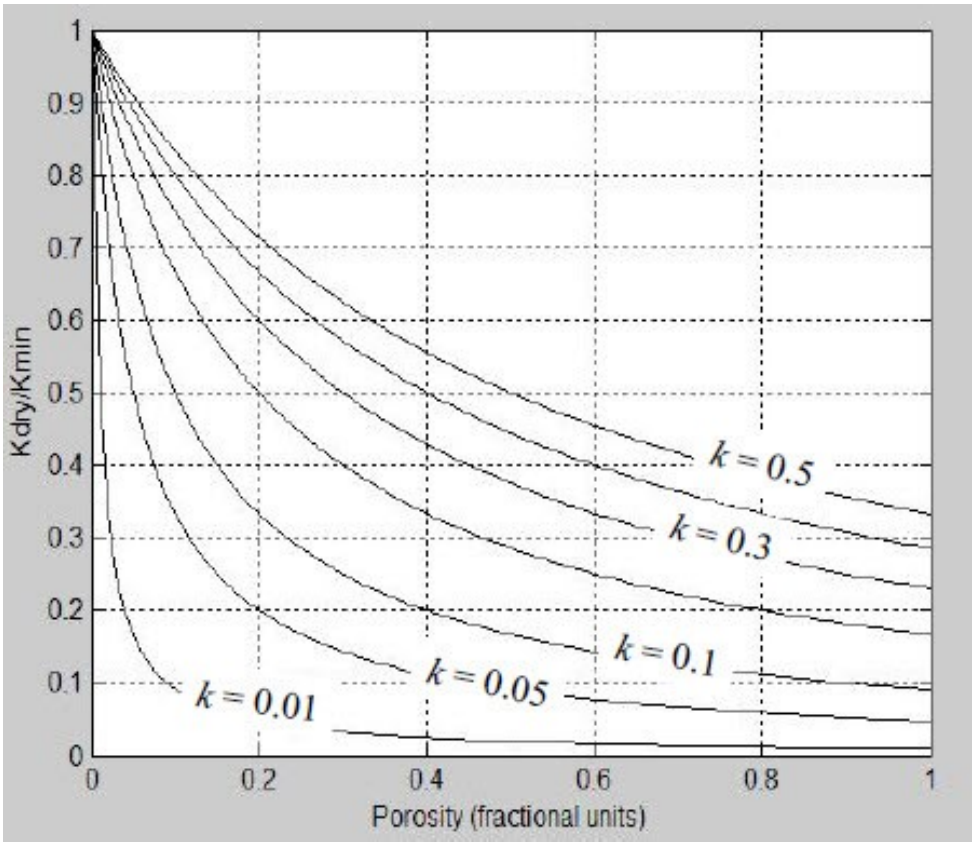


**Figure 2.16 Bulk modulus of dry rock over mineral bulk modulus ratio curves for varying values of k (Russell and Smith, 2007)**

Regarding the basic idea of the pore stiffness method; for a given pressure, $K_\phi$ should stay constant over range of porosities. Russell and Smith (2007) proposed a re-computation of $K_{d\ (new)}$ at different porosity (effective porosity), $\phi_e$, expressed by:

$$K_{d\ (new)} = \left[ \frac{1}{K_m} + \frac{\phi_e}{K_\phi} \right]^{-1} \tag{2.15}$$

In addition, Liu *et al.* (2009) demonstrated the relationship between porosity and dry bulk modulus of rock of Berea and Weber sandstones. They accomplished calculations of porosity and dry bulk modulus changes of both sandstones that match with measured data. Their results showed that changes of porosity strongly related to dry bulk modulus during confining pressure increase, especially at low confining pressure (< 25 MPa). The relationship of porosity and dry bulk modulus of Berea and Weber sandstones will gradually decrease when confining pressure increases as shown in Figure 2.17.

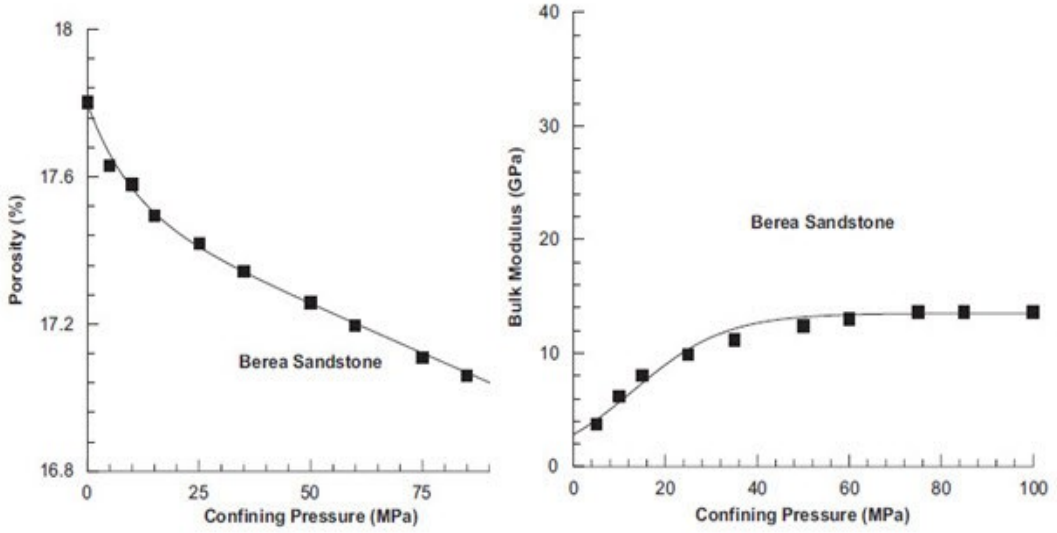


(*a*)

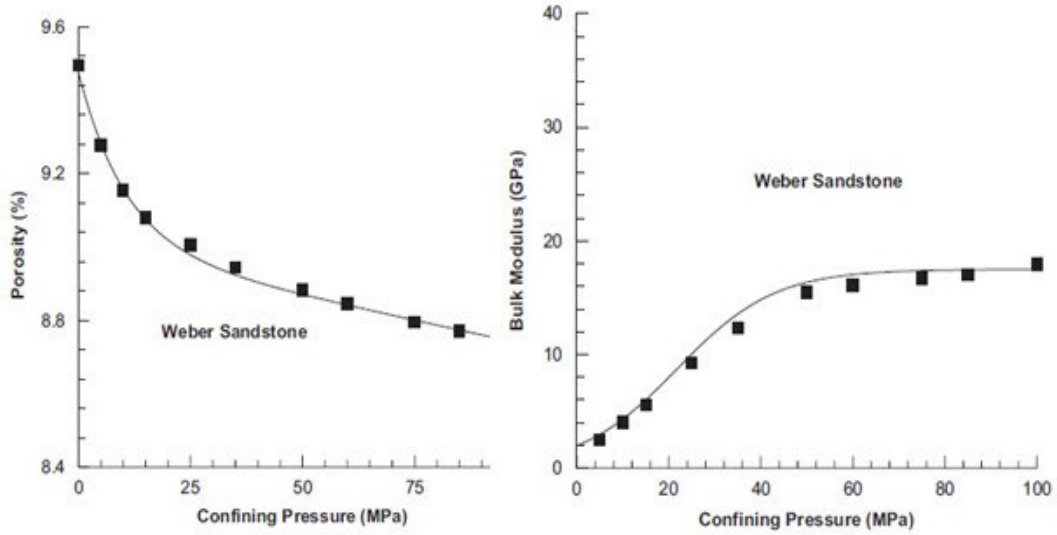


(*b*)

**Figure 2.17 Comparisons between calculated data (line) and measured data (square annotation) of relationship of porosity and dry bulk modulus from Liu *et al.* (2009) (*a*) Berea sandstone (*b*) Weber sandstone**

## 2.4 Effect on Biot's coefficient during compaction and dilation of rocks

Biot's coefficient is related to dry bulk modulus of rock. Biot (1941) defined the effective stress as the difference between the total stress and a fraction called Biot's coefficient, $\alpha$, of the pore pressure, which can put in Eq. 2.3 as follows:

$$\sigma_e = \sigma_v - \alpha P_p \tag{2.16}$$

Likewise, during compaction and dilation mechanism is related to the change of Biot's coefficient and the change of Biot's coefficient during those processes is questioned and it is still arguments. However, Alam *et al.* (2010) demonstrated that mechanical compaction reduce porosity, but only lead to a minor decrease in $\alpha$.

Terzaghi (1925 and 1943)'s concept is suitable for loose grainy sediment and stated that $\alpha$ is unity; therefore the differential stress (total stress – pore pressure) is equal to the effective stress. Consequently, in cemented rock, resistant to the overburden load is partly obtained from the rock skeleton and $\alpha$ is less than unity (Alam *et al.*, 2010).

Based on Alam *et al.* (2010)'s research, $\alpha$ is unity for loose sediments, while $\alpha$ below unity indicates the development of contact cement between particles or grains and stiffening of the sediment. Hence, their work stated that during mechanical compaction porosity decreases, but $\alpha$ remains close to one, as compaction requires movement of particles or grains relative to each other. Recrystallization in itself should not influence $\alpha$, unless it leads to contact cementation, where the sediment stiffens, so that $\alpha$ declines although porosity a little decreases or remains constant. Furthermore, $\alpha$ shows decreasing with depth, it is sensitive only deeper part of basins or it can be said that it is sensitive only on chemical compactions (because cementation is a mechanism of chemical compaction processes).

Although several authors have found that pore pressure associated with the Biot's coefficient play a significant role in deformation. Mese and Tutuncu (2000) obtained experimental data on bulk compressibility that vary by an order of magnitude depending on the way the load was applied *e.g.* by increasing the confining pressure or by decreasing the pore pressure.

# CHAPTER 3

# EFFECT OF TIME ON MUDSTONE COMPACTIONS

## 3.1 Introduction

Assembled compaction curves of mudstones (Skemption, 1944; Engelhardt and Gaida, 1963; Miyazaki, 1966; Meade, 1966; Baldwin and Butler, 1985; Dzevanshir *et al.*, 1986; Mondol *et al.*, 2007) have revealed that only mechanical compaction (compaction processes as a function of effective stress or burial depth) cannot explain variations of compaction curves.

Effect of geological time on the compaction is far more difficult for us to analyze than overburden. It is because an experiment is impossible for geologic time. Terzaghi (1925, 1943) did the consolidation experiment and demonstrated that an excess pore pressure relating to porosity as a function of time. Van Olphen (1963) stated the time relating to diagenesis of clay mineral that many clay lattices in older sediments appear to have been dehydrated completely under normal compaction, while partial dehydration occurs on young sediments. Especially, Burst (1969) was firstly to study on time effects of compaction of mudstones using the compiled data of a wide range of geological age (Manger, 1963). He showed a trend of a gradual decrease of porosity of mudstones with increasing geological ages. He did not show, however, a mathematical relationship between time and porosity of mudstones over geologic times (Figure 2.3). The mathematic expression of porosity as function of time and depth has been proposed by Dzevanshir *et al.* (1986). They set up the mathematic equation for mudstone compactions with consideration of time and lithology (ratio of shales to total thickness), but their tested results were scanty and were not clear.

This chapter presented re-analysis and re-construction published compaction data of mudstones. The different ages of data were used to be quantitative data for proving time effect. Also, the information of geologic histories and porosity acquisitions were given as a good discussion on mudstone compaction. Based on theory of consolidation proposed by Terzaghi (1925, 1943), Fowler and Yang (1998) proposed an equation of porosity as a function of burial depth and time for slow compaction processes over geological ages. Consequently, a mathematic expression of compaction of mudstones can be set up with consideration of time and depth, and the mudstone compaction curves can be drawn. Due to time is another factor that should be paid more attention in a certain long time range. A mathematic expression of compaction of mudstones can be set up with consideration of time and depth. Consequently, a compaction concept method can be modified to improve accurate prediction of pore pressure with considering time effect in mudstone or shale formation.

### 3.1.1 Re-construction porosity-time plots of Burst (1969)

Based on effect of time was re-studied and analyzed as shown in previous sections, the data plots on porosity-time of Burst (1969), as shown in Figure 2.3, can be reproduced. Although Burst (1969)'s plots showed that the porosity of mudrocks tend to decline as a function of increasing time. However, his plot was not clear because he only plotted ranges of porosities with times, and depths (or age range of sample) were not specified, *i.e.* effect of time did not only influence on the decline of the porosity because mechanical compaction (burial depth) was still dominant.

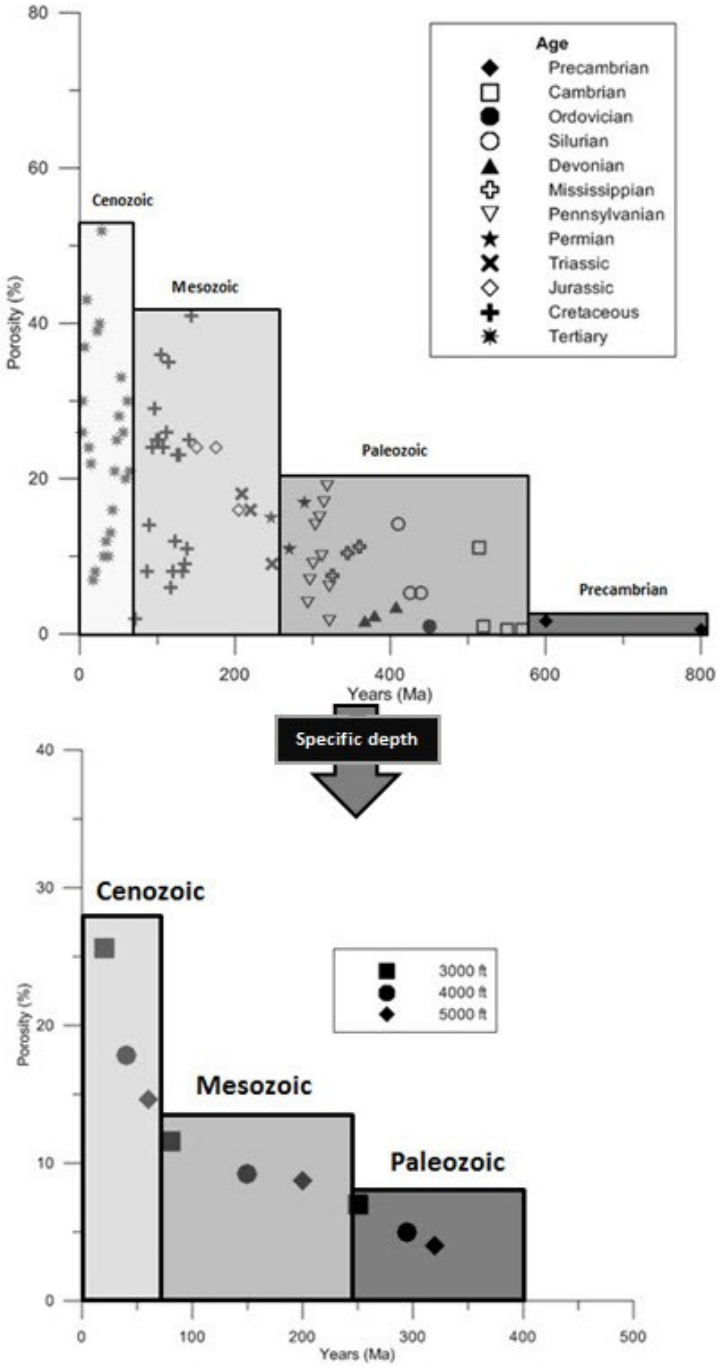


**Figure 3.1 Re-construction of porosity-geologic time plots from Figure 2.3 (Burst, 1969)**

Consequently, this section selected specific depths at 3000, 4000 and 5000 ft. (Meaning effective stress does not affect compaction processes at each depth) to reveal an effect of time, as shown in Figure 3.1, and eventually found that porosity declines as a function of geologic time as same as Burst (1969).

## 3.2 Objective

The purposes of this study were (1) to re-analyze and re-construct on mechanical compaction of mudstones (2) to show effect of time on mudstone compactions (3) to set up mathematic equation of mudstone compaction based on effect of time and (4) to adjust a compaction concept method for pore pressure prediction base on time effect of mudstone compactions.

## 3.3 Mathematic equation of porosity-depth-time relationship

Compaction of soils and clays has been described by Terzaghi's equation (Terzaghi, 1925, 1943). Terzaghi's equation includes time as one of variable parameters. This directly indicates effect of time on sediment compaction. To reveal the effect of time on mudrock compaction, this study assumed that conditions of compaction, *i.e.* permeability of sediments are much smaller, and changes of water saturation and relaxation of excess pressures due to changes of stress state take place much slower than in aquifer sediments. Water cannot migrate rapidly from one part to another (or adjacent more permeable layers that promote expulsion of excess water). This phenomenon produces a time lag between a change of forces that cause compaction and corresponding change of water saturation in sediments. The excess pressure ($u$), the pressure difference between the static and pore pressure, in the water contained in compacting beds of clay is a function of the time ($t$) and depth ($z$) as shown in Terzaghi (1925, 1943)'s equation (Eq. 3.1), where $c_{vc}$ is called that the coefficient of compaction.

$$\frac{\partial u}{\partial t} = c_{vc}\frac{\partial^2 u}{\partial z^2} \tag{3.1}$$

Following Terzaghi set up assumptions for Eq. 3.1, *i.e.* (1) the process of consolidation proceeds very slowly, (2) the voids are completely filled with water, (3) the rocks are homogeneous and (4) only water moves in the framework, Eq. 3.1 can be rewritten by using the porosity instead of the excess pressure as a function of time and depth of slow compaction following Fowler and Yang (1998)'s equation:

$$\frac{\partial \phi}{\partial t} = \lambda'\frac{\partial^2 \phi}{\partial z^2}, \quad \lambda' = \lambda\frac{(1-\phi_0)^2}{\phi_0} \tag{3.2}$$

$$\lambda = \frac{k_0}{M}, \quad k_0 = \frac{K_0\gamma_w}{\mu} \tag{3.3}$$

where $\lambda$ is the compaction number, $\phi_0$ is the initial porosity, $M$ is the sedimentation rate, $\mu$ is the fluid viscosity, $\gamma_w$ is the unit weight of water, $K_0$ is the initial permeability, and $k_0$ is the

initial permeability coefficient. This study analyzed Eq. 3.2, based on assumptions that the depth and time are independent variables and other effects on mudstone compaction are omitted, using a variable separation method of second order partial differential equation as obtained:

$$\phi(z,t) = \phi_0 e^{-(az+a^2\lambda' t)} \tag{3.4}$$

Eq. 3.4 is a mathematical expression of compaction of mudstones considering both time and depth, and it also shows that if time factor is omitted, Eq. 3.4 will be reduced to Athy's model as shown in an Eq. 2.1 (This study ignored mutual dependence of $z$ and $t$ in a geological process). An actual set of data from a well represents geological processes and histories of the stratigraphic succession pass through. Hence, as long as this study stick to the actual data, the ignorance of mutual dependence of $z$ and $t$ can be implicitly expressed in analysis of the actual data based on Eq. 3.4 is cancelled in an evaluation of constants $\phi_0$ and $a$, etc.

### 3.3.1 Mudstone compaction curves considering with time effect

The theoretical parameters of mudstone compaction are listed in Table 3.1; they are initial porosity ($\phi_0$) which was reported that the surface porosity of mudstones range around 60 – 65 %, initial permeability ($K_0$), fluid viscosity ($\mu$), and unit weight of water ($\gamma_w$) were used by the standard numbers of mudstones and water, the sedimentation rate ($M$) was assumed for slow compaction model of mudstone compaction, and constant value of exponential function ($a$) which was obtained by an average of constant values of exponential function from several published compaction curves. By using those parameters based on geological consideration for various basins used in Eq. 3.4. Mudstone compaction curves varying with times from 0 to 250 Ma (Cenozoic to early Paleozoic age) can be drawn as shown in Figure 3.2.

**Table 3.1: Assuemed parameters for mudstone compaction curves varying with time**

| Parameters | Value | Unit |
|---|---|---|
| Constant value of exponential function ($a$) | 0.48 | $Km^{-1}$ |
| Initial porosity ($\phi_0$) | 65 | % |
| Unit weight of water ($\gamma_w$) | $1x10^4$ | $N/m^3$ |
| Initial permeability ($K_0$) | 0.38 | μD |
| Fluid viscosity ($\mu$) | $0.8x10^{-3}$ | Pa·s |
| Sedimentation rate ($M$) | 1 | mm/y |

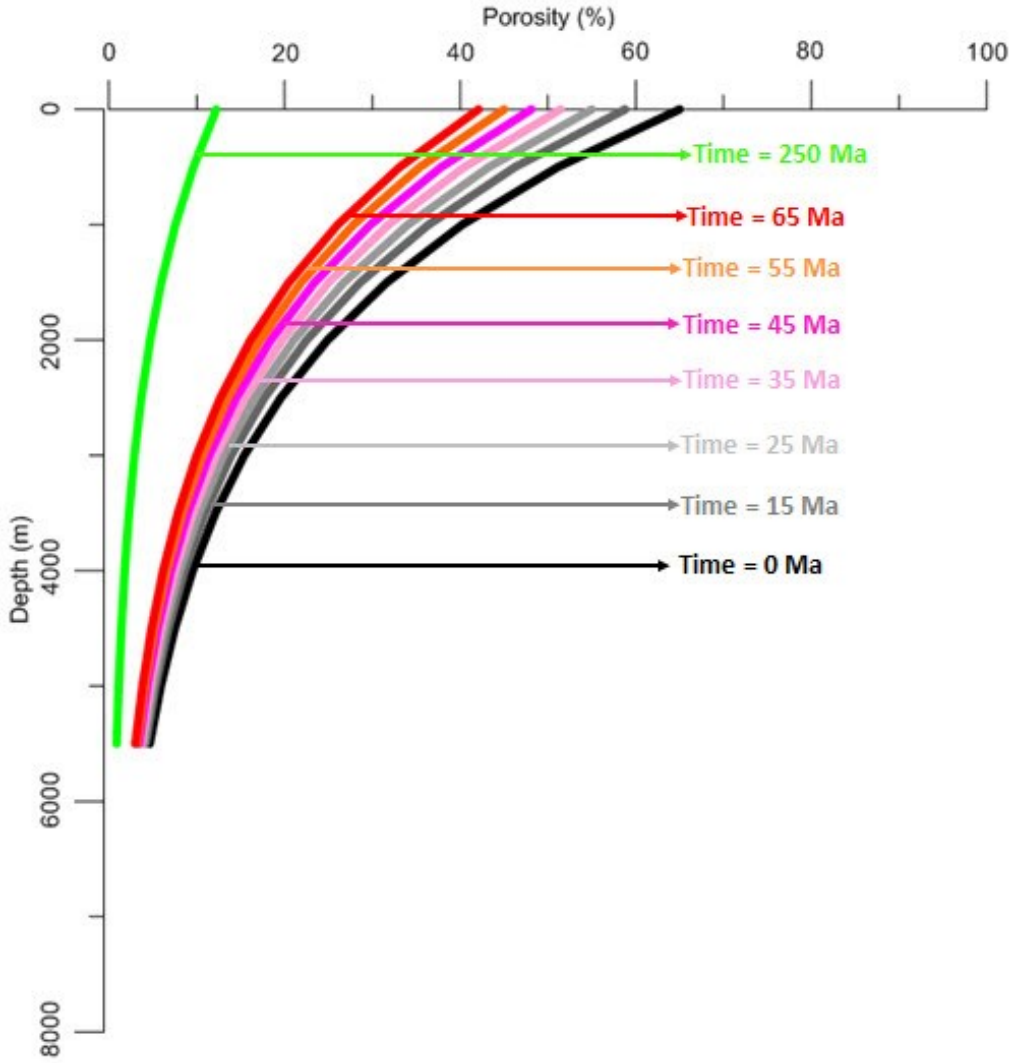


**Figure 3.2 Mudstone compaction curves considering with time effect**

### 3.3.2 Mudstone compaction curves considering with time effect on compilation curves of Mondol *et al.* (2007)

According to compilation curves of mudstone compaction created by Mondol *et al.* (2007) showed variations and did not have explanations of variations. Therefore, mudstone compaction curves varying with times were drawn on a compilation of mudstone compaction curves created by Mondol *et al.* (2007) as shown in Figure 3.3.

The circle in Figure 3.3 represented the same data that were used in this study. Therefore, variations of Mondol *et al.* (2007)'s curves can also be explained by mudstone compaction curves varying with times. Athy (1930)'s curve in Figure 3.3, which is known as Paleozoic mudstone, is consistent with mudstone compaction curves with starting time of Paleozoic period (250 Ma). However, at the shallow part shows discrepancy between both of these curves. This discrepancy will discuss and find out in the next chapter. Similarly, Hedberg

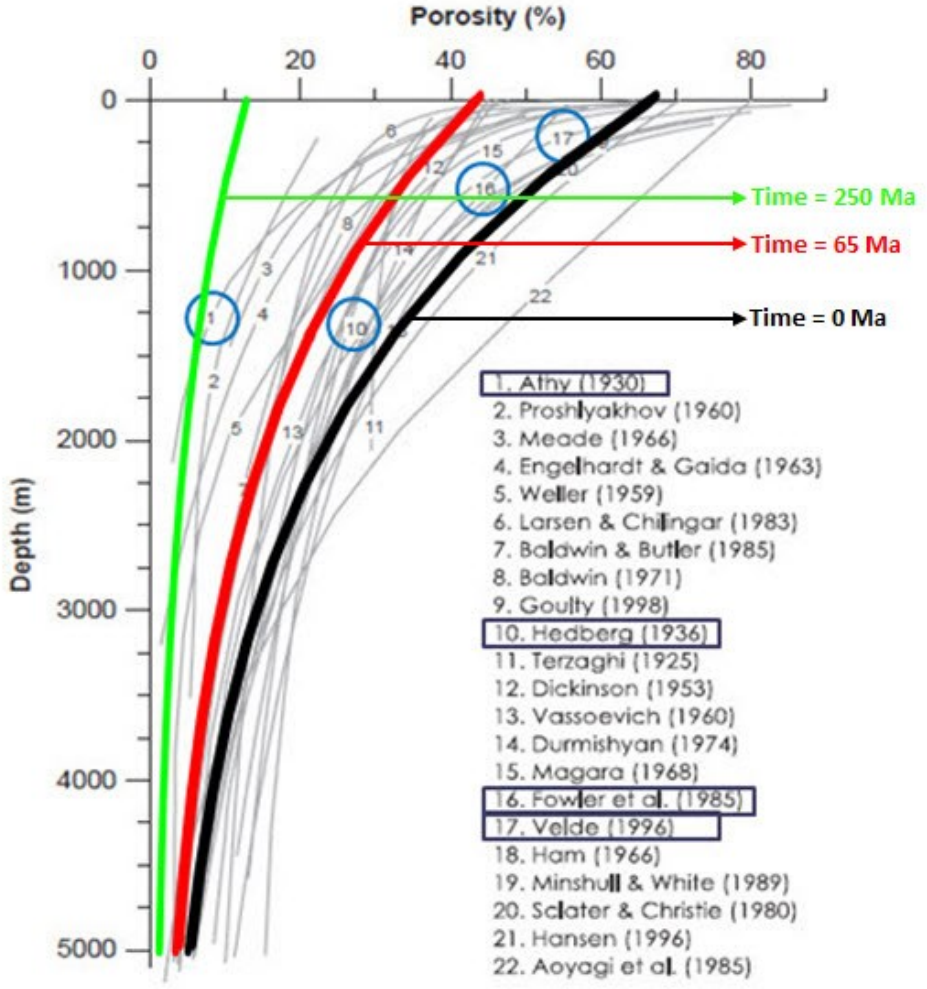


**Figure 3.3 Mudstone compaction curves considering with time effect on compilation curves of Mondol *et al.* (2007)**

(1936), Velde (1996) and Fowler *et al.* (1985)' curves, which are Cenozoic mudstones, are within mudrock compaction curves varying with Cenozoic period (time from 0 to 65 Ma).

## 3.4 Data collection

Mudstone compaction data used in this study came from several sedimentary basins. The porosity and density are theoretically related and known as the indicators of the compaction of sediments. All data have no information on major erosions and unconformities. The data used in this study are listed in Table 3.2 along with basin location, bottom depth, porosity measurement, amount of data, and reference.

Figure 3.4 represents varieties of basins of data that were used in this study. The geographic map shows that the data were taken by both onshore and offshore basins, including Japan (No. 1 and 3.7), Gulf of Oman (No. 2), U.S.A. (No. 4), Venezuela (No. 5), Barbados (No. 3.2), Italy (No. 3.8), Antarctic Ocean (No. 3.3), Indian Ocean (No. 3.5), Pacific Ocean (No. 3.1), Philippines (No. 3.4) and Atlantic Ocean (No. 3.6), and the obtained data can be represented

mudstone compaction data of around world. All amounts of data used are more than 700 data. The numbers on the geographic map are correlated the No. in the Table 3.2, which identify locations of basins.

**Table 3.2: Data description**

| No. | Basin location | Bottom depth (km) | Porosity Measurement | Amount of data | Reference |
|---|---|---|---|---|---|
| 1 | Akita | 3.00 | Direct measurement | 143 | Aoyagi *et al*. (1979; p.41) |
| 2 | Makran | 5.00 | Wireline measurement | 25 | Fowler *et al*. (1985; p.429-430) |
| 3.1 | N Pacific | 0.05 | Direct measurement | 138 | Velde (1996; p.196) |
| 3.2 | Barbados | 0.46 | | | |
| 3.3 | Antarctic | 0.30 | | | |
| 3.4 | Sulu Sea | 1.00 | | | |
| 3.5 | Indian Ocean | 1.30 | | | |
| 3.6 | E Atlantic | 0.30 | | | |
| 3.7 | Niigata | 4.50 | | | |
| 3.8 | Po Valley | 2.50 | | | |
| 4 | Oklahoma | 2.00 | Direct measurement | 368 | Athy (1930; p.12) |
| 5 | Maracaibo | 2.00 | Direct measurement | 37 | Hedberg (1936; p.254) |


**Figure 3.4 Geographic map of data locations**

### 3.4.1 Information of porosity acquisition

The porosity data No. 1 were from the core samples obtained at 16 wells in Akita oil field, Japan. The natural densities of the samples were measured within a few hours, just after taken from wells, and then were converted to porosity data by that assuming specific gravity of the present sea water as 1.025, thus the average specific gravity of the grain is 2.65, as followed:

$$\phi = \frac{\rho_g - \rho}{\rho_g - \rho_l} \tag{3.5}$$

where ρ is the natural density, $\rho_g$ is the grain density, $\rho_l$ is the density of pore water, and $\phi$ is the porosity.

For No. 2, porosity data were estimated by seismic velocity data using an empirical relationship derived by Hamilton (1978). First the seismic velocity was converted to bulk density ($\rho_s$), and then the bulk density was converted to porosity ($\phi$) by using following equation:

$$\rho_s = \phi\rho_w + (1 - \phi)\rho_g \tag{3.6}$$

a grain density ($\rho_g$) of 2.762 g/cm$^3$ and a pore water density ($\rho_w$) of 1.050 g/cm$^3$ are assumed from measurements on Deep Sea Drilling Project (DSDP) site 222.

For group of data No. 3 (*i.e.* 3.1, 3.2, 3.3, 3.4, 3.5, 3.6, 3.7 and 3.8) the porosity data were obtained from several basins. Almost all data were taken from Ocean Drilling (ODP) and DSDP. The porosity data were acquired from consolidation test in laboratory. The laboratory test is for porosity measurements as a void ratio and the compacting force as pressure exerted by the solids. The porosity ($\phi$) is related to void ratio ($e$) by Eq. 3.7.

$$e = \frac{\phi}{(1-\phi)} \tag{3.7}$$

In cases of data No. 4 and 5, porosities were estimated from density data as followed:

$$\phi = \left[1 - \left(\frac{Bulk\ density}{Absolute\ density}\right)\right] \cdot 100 \tag{3.8}$$

where bulk density is the density of thoroughly dried rock, *i.e.* pore space free of liquids, and absolute density (or called grain density) is the density of constituent particles of a rock, *i.e.* rock substance free from pore space. However, they are different way to obtain the density data. The bulk density of data No. 4 was acquired by weighing a sample in mercury with a Jolly balance and a sufficient mass being suspended to submerge the sample. While, the data No. 5 used Melcher method and pycnometer method in order to measure bulk density and absolute density, respectively. In addition, this study assumed the absolute density of data No. 4 remains constant and equal 2.762 g/cm$^3$ (Fowler *et al.*, 1985) for calculating in Eq. 3.8.

### 3.4.2 Basin information

The geologic information of data No. 1 referred to Miyazaki (1966). The samples were taken from Akita oil field and range from the mudstone of the Sasaoka formation to the black shale of the Funakawa formation. In fact, the density distribution on each well seems to be pretty normal. Each well is situated near the crest of gentle anticline, where can be recognized no structural disturbances in sediments.

While, the data No. 2 were taken from abyssal plain sediments in the Makran accretionary prism of northwest Indian Ocean. The oceanic Arabian plate is subducting shallowly northwards beneath the continental Eurasian plate. The abyssal plain sediments were stated that they are undeformed sediments and very little erosion takes place. According to they do not exhibit major internal deformation, thus they do not undergo tectonic consolidation.

Basin histories of group of data No. 3 stated that the samples were not affected by diagenesis and were critical to any interpretation of general sedimentary compaction phenomenon in ocean basins as it was the beginning stages of particle re-arrangement which must necessarily condition later stages of volume reduction which are only due to pressure.

The basin information of the Oklahoma basin in data No. 4 stated that all the samples studied were taken from areas of structural deformation and some of compaction may have resulted from vertical and lateral pressures in the earth's crust. The samples were acquired from wells in the Mervine, South Ponca, Thomas, Garber, and Blackwell fields. The sediments range from Permian age to base of Pennsylvanian age with no intervening unconformity.

Finally, the data No. 5 was obtained from the Geological Laboratory of Venezuela Gulf Oil Company. These data came from the study of core samples of Tertiary mudstones from wells drilled in the large geosynclinal basins of Venezuela. The samples were taken from a deep test in undisturbed and essentially horizontal Tertiary strata far removed from areas of major tectonic disturbance and the strata consisted in large part of mudstones which were free from appreciable sand impurity. In addition, absence of major unconformities in the section makes it possible to assume that the existing overburdens are maximum overburdens.

### 3.4.3 Data Analysis

Assembled data were plotted on porosity-depth relationship as shown in Figure 3.5, and then the specific depths (500 and 1500 m) were mentioned to show that mechanical compaction (burial depth or effective stress is kept constant) is certainly one of the main controlling factors of compaction of mudstones, but porosity still declines even mechanical compaction (burial depth or effective stress is kept constant) does not influence on compactions.

Furthermore, the factors that influence on mudstone compaction are shown in Table 3.3. Those factors are basin type, lithology, thickness of strata, age of stratum and compaction

factors. The compaction factors, *i.e.* porosity of mudstone at datum depth ($\phi_0$) and constant value of exponential function ($a$), were determined by fitting curves of Eq. 2.1.

Table 3.3 revealed that the variations of compaction curves of mudstones can be due to several factors and the compaction is affected by several factors which control compaction under localized environments. Time (or geologic age) is likely to be a major factor that influences variations of compaction processes of mudstones. It is because the coefficients of compactions show an increasing tendency with increasing time in the summary table.

**Table 3.3: Data analysis**

| No. | Basin location | Basin type | Lithology | Thickness of strata (km) | Age of stratum | Compaction factor | |
|---|---|---|---|---|---|---|---|
| | | | | | | $\phi_0$ (%) | $a$ (km$^{-1}$) |
| 1 | Akita and Hokkaido | Back-arc | Black shale | 0.2 - 3 | Mio-Cretaceous | 72 | 0.656 |
| 2 | Makran | Abyssal | Silt and Clay sediment | 0 - 5 | Paleo-Neogene | 54 | 0.476 |
| 3.1 | N Pacific | Deep-water | Clay-rich sediment | 0.05 - 4 | Pleistocene | 56 | 0.486 |
| 3.2 | Barbados | | | | Eo-Holocene | | |
| 3.3 | Antarctic | | | | Plio-Pleistocene | | |
| 3.4 | Sulu Sea | | | | Mio-Pleistocene | | |
| 3.5 | Indian Ocean | | | | Paleo-Neogene | | |
| 3.6 | E Atlantic | | | | Plio-Holocene | | |
| 3.7 | Niigata | Back-arc and Convergent | | | Mio-Holocene | | |
| 3.8 | Po Valley | | | | Plio-Holocene | | |
| 4 | Oklahoma | Convergent | Red shale | 0.5 - 2 | Perm-Penn | 36 | 1.006 |
| 5 | Maracaibo | Back-arc | Greenish gray mud | 0.08 - 2 | Paleo-Neogene | 41 | 0.698 |

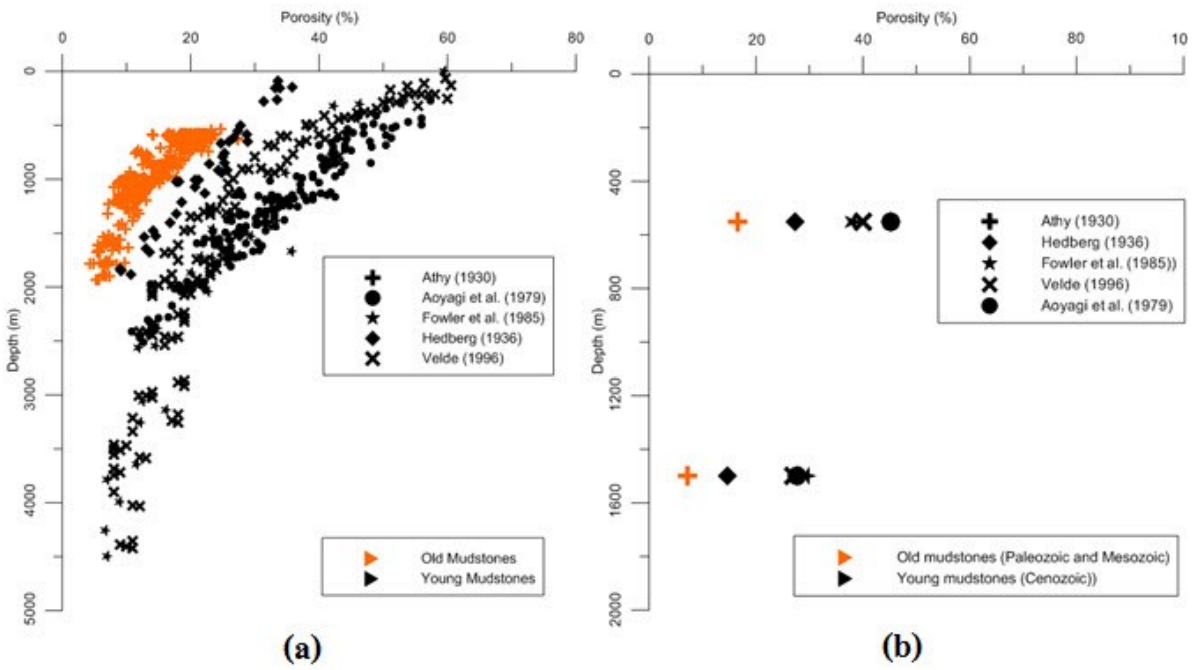


**Figure 3.5 Data plots of different times on porosity-depth relationship (a) Scattered data on mudstone compactions (b) Depth specifications revealing effect of time**

## 3.5 Mudstone compaction curves varying with time on data plots

The mudstone compaction curves varying with times plots with actual data are shown in Figure 3.6. The graph shows an acceptable match between compaction curves and actual data based on time variations (Figure 3.6). The scattering of actual data from Cenozoic age to staring time of Paleozoic age can also be explained as effect of time on mudstone compactions, but this study used assumed parameters to constrain only time factor influences on mudstone compactions. The order of 100 million years is necessary for us to recognize clearly the effect of time on mudstone compaction.

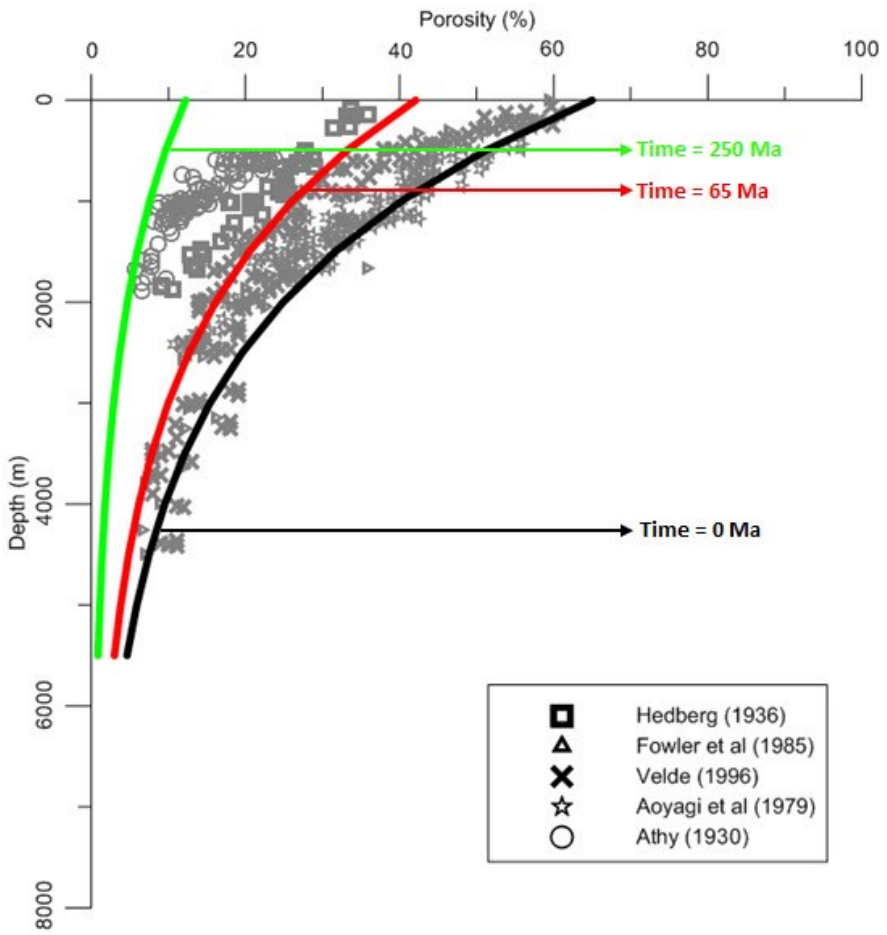


**Figure 3.6 Mudstone compaction curves considering with time effect on assembled data**

## 3.6 3D-plots of porosity-depth-time relationship

In this section, the data of porosity, depth and time were plotted on 3D graph, as shown in Fig. 3.7, in order to determine matching between mudstone compaction curves varying with times and actual data on 3D-plots. The porosity data were transformed by natural logarithm, while the time data were plotted in ranges of geologic times. The plane fitting of the data is in accord with mathematic model of time effect (Eq. 3.8) in natural logarithm function as shown in Eq. 3.9.

$$ln\,\phi = ln\,\phi_0 - az - a^2\lambda' t \tag{3.9}$$

Fig. 3.7 shows that the data could be fitted by plane fitting of Eq. 3.9. This can explain the mathematic model that has been setup in this chapter can use and represent compaction data considering with time, and it can confirm that the mathematic model which has been setup in exponential function corresponding with function among porosity, depth, and time.

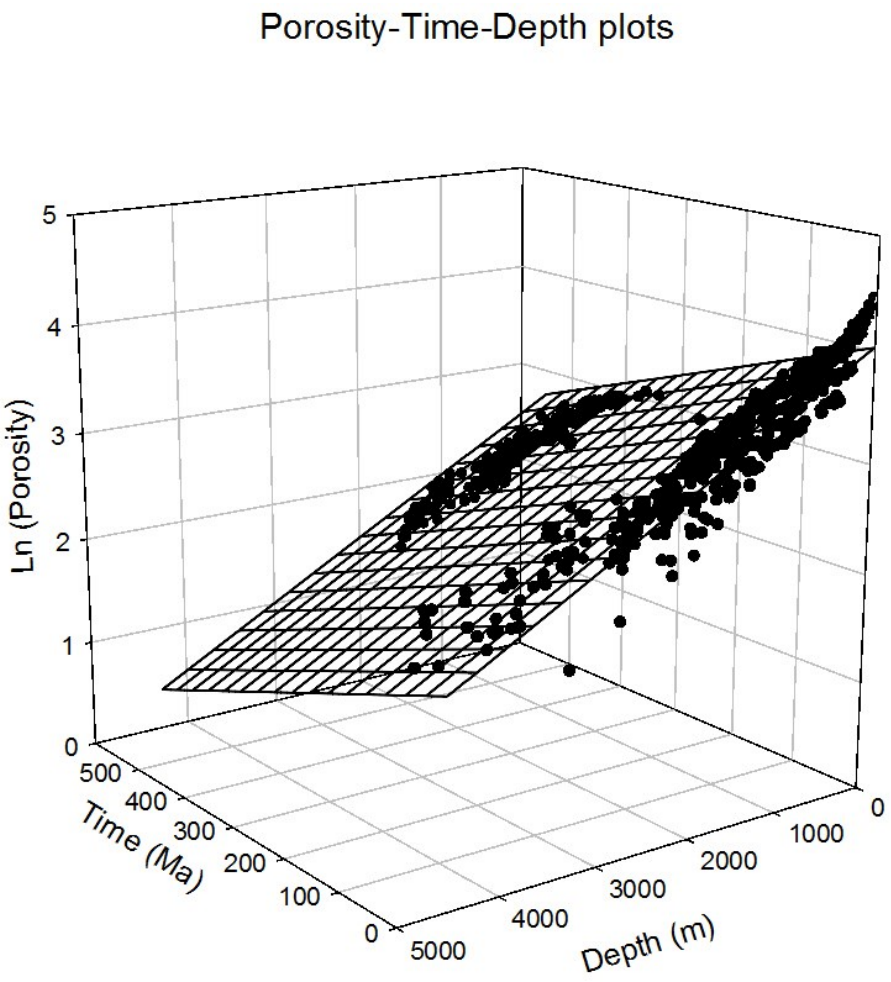


**Figure 3.7 Data plots and plan fitting on 3D graph of relationship among porosity-depth-time**

## 3.7 Parameter verifications

The parameters were determined by least square method of 3D plots, so the calculated parameters of compaction, *i.e.* initial porosity ($\phi_0$), initial permeability ($K_0$), constant value of exponential function ($a$) and $\lambda'$, were calculated to compare with theoretical parameters as shown in Table 3.4.

**Table 3.4: Comparison between assumed and calculated parameters**

| Parameters | Theoretical value | Calculated value | Unit |
|---|---|---|---|
| Constant value of exponential function ($a$) | 0.48 | 0.49 | $Km^{-1}$ |
| Initial porosity ($\phi_0$) | 65 | 56.5 | % |
| Initial permeability ($K_0$) | 0.38 | 0.13 | μD |
| $\lambda'$ | 0.029 | 0.010 | - |

The comparisons show that the calculated parameters from 3D plots are consistent with assumed parameters; it means that the property and condition, which were assumed in order to calculate and draw mudstone compaction curves varying with time, were satisfactorily reasonable and can be represented to demonstrate effect of time on mudstone compactions.

## 3.8 Application to pore pressure prediction

Pore pressure has a direct impact on drilling safety and further exploration, in overpressured zones, and it is important as total stress to determine effective stress. The effective stress controls the mechanical behavior of geomaterial as strength and stiffness. Both stability of well bore and seismic velocity are realization of this mechanical behavior. Pore pressure also controls hydraulic gradient, which controls fluid flow in a basin. This issue is very important in the petroleum industry and the pore pressure in mudstone is one of the last items on the list of primary mechanical parameters.

It is possible that time effect controlling pore pressure is another factor controls the compaction processes of mudstones. A depth profile of densities of formation waters is virtually linear for a stratigraphic unit in a common sedimentary basin. This study shows that effect of time is convoluted into effect of burial depth. Time effect should be considered effects of burial depth ($z$), that mainly represents the process of mechanical compaction, influencing conventional equations of pore pressure prediction.

### 3.8.1 Adjustment of compaction concept method considering with time effect

Due to the mathematic expression with porosity as a function of depth and time, *i.e.* Eq. 3.4, the equation give a basis to depict hydrostatic trend of pore pressures in subsurface. Pore pressure prediction in mudstone can be modified in order to improve a result.

Using the relationships of porosity and effective stress as same as Eq. 2.2, so Eq. 2.8 and 2.9 can be re-written by consideration of time effect in explicit forms as shown below:

$$\sigma_e = \frac{1}{a}\left(ln\frac{\phi_0}{\phi} - a^2\lambda' t\right) \tag{3.10}$$

$$\sigma_n = \frac{1}{a}\left(ln\frac{\phi_0}{\phi_n} - a^2\lambda' t\right) \tag{3.11}$$

Combining Eq. 3.10 and 3.11, one has:

$$\sigma_e = \sigma_n\left(\frac{ln\frac{\phi_0}{\phi} - a^2\lambda' t}{ln\frac{\phi_0}{\phi_n} - a^2\lambda' t}\right) \tag{3.12}$$

Finally, considering $\sigma_e$ in both Eq. 3.12 and Eq. 2.10, and substituting the derived $\sigma_e$ into Eq. 2.3, the equation of pore pressure prediction using compaction concept with consideration of effects of burial depth and time is derived as expressed:

$$P_p = \sigma_v - (\sigma_v - P_{p,n}) \frac{ln\frac{\phi_0}{\phi} - a^2\lambda' t}{az} \tag{3.13}$$

Eq. 3.13 should be paid attention to that this equation is a modification of Eq. 2.11, as the conventional equation for predicting pore pressures in mudstone formations, with respect to time effect. The order of $a^2\lambda'$ should be negligible for a relatively short time in order of 1 to 10 million years. The order more than 100 million year makes time effect be visible in an actual stratigraphic succession.

## 3.9 Discussions and conclusions

Compaction of mudstones is defined as a function of porosity, and has been described in a burial diagenetic process to reduce porosity of mudstones. Mechanical process is the main among factors controlling the compaction, and is controlled mainly by overburden (*i.e.*, burial depths), effective stress and pore pressure. This study revealed that mechanical compaction (or burial depths) is certainly one of the main controlling factors of compaction of mudstones, but it cannot be a single factor to explain the relationship between porosity of mudstones and burial depths in a form of a compaction curve. The time effect can be observed clearly in scale of 100 million years. This work analyzed and classified effects of several factors, *i.e.* basin type, lithology, geologic age or time, thickness, etc. Such compaction factors, influencing scatters of data points from a normal trend, cause variations of mudstone compaction curves.

Time is an important factor to influence the compaction as well as overburden. Time after deposition of mud promotes its compaction. Effect of geological time on the compaction is far more difficult for us to analyze than overburden. It is because an experiment is impossible for geological time. Results of analysis of Table 3.3 and Figure 3.5 show that time (or age) is likely to be an effective factor influencing variations of compaction processes of mudstones. In addition, this study re-evaluated on time effect of mudrock compactions based on theory of consolidation (Terzaghi equation) proposed by Terzaghi (1925, 1943). Assuming the processes of compactions are very slow (compaction number, $\lambda$<1), mudrocks have low permeability, and the rock model is a homogeneous following Terzaghi's assumptions, and thus a differential equation of excess pore pressure considering with time and depth proposed by Terzaghi (1925, 1943) can be replaced by slow compaction model of Folwer and Yang (1998)'s differential equation.

A mathematical expression of compaction of mudstones can be set up with consideration of time and depth, and the mudstone compaction curves can be drawn. The scatters of porosity-depth plots in term of time effect were revealed and the variations on compilation curves of Mondol *et al.* (2007) can be classified by time effect. Finally, this study furnished results of

Dzevanshir *et al.* (1986) and supported that time factor should be paid more attention on mechanism of mudstone compaction. Furthermore, this study can also help us to understand the mechanism of mudstone compaction, especially at the shallow part that is dominated by the mechanical compaction.

The most world-widely used methods to predict pore pressure are based on compaction concept of mudstones. Porosity is a good indicator of mudstone compaction in determining an overpressured zone of sedimentary basin because it is predictive and economical in practice. Due to the mathematic equation of mudstone compaction with consideration of time effect was set up (Eq. 3.4), and thus it leads to adjust pore pressure prediction using compaction concept method based on time effect as shown in Eq. 3.13. If the pore pressure is more accurately predicted prior to drilling, drilling operators can reduce borehole trouble time and avoid drilling accidents. Eq.3.13 is a modification of Eq.2.11 and includes a term of time effect.

# CHAPTER 4

# EFFECT OF EROSION ON MUDSTONE COMPACTIONS

## 4.1 Introduction

Mudstone compaction involves complex processes causing reduced porosity. Porosity reduction is a key point during sediment compactions, but a compaction model and a fundamental behavior of compaction, especially mudstones, are still obscure. Mudstones are a more complex function of numerous natural factors than other sediments. Effect of geologic time has been studied for many years, and seems to be an effective factor on mudstone compactions. It means that mudstones in different geologic ages will produce the different compaction curves. Following in the compilation curves of mudstone compaction (Figure 1.2) by Mondol *et al.* (2007), Paleozoic compaction curve represented by Athy (1930) showed higher porosity reductions than other curves, though they were the same an exponential function.

Effect of time was firstly investigated by Sorby (1908). He found that very fine-grained deposits behaved as a thin adherent film of water played a most important part, after settling for a day, acted like an imperfect liquid containing, so that the particles must have been comparatively far from one another. His conclusion was that the change in void ratio (porosity) which occurs on settling and the much greater change brought about by contraction on drying, and thus the reduction in pore spaces in due not to the compression of the cavities but to deformation of the solid particles which tends to fill them up and this must have been brought about by the slow giving-way of minute grains during long geological periods. Burst (1969) continued the study on time effect that has been discussed in section 2.1.3. The re-consideration and re-construction of Burst (1969) have been presented in previous chapter, already.

Uplift accompanying erosion is tectonic activity in which the overburden is reduced during such processes, and the results influence on the original in situ pore pressure being contained by a much lower overburden, which results in a reduction of the effective stress as unloading mechanism (Chopra and Huffman, 2006). Therefore, areas where are affected by erosions, their porosity will be abnormally high because of overburden reduction in the succession. Based on geologic information of Oklahoma basins, the Athy (1930)'s was obliviously ignorance of erosion effect. Especially, the shallow part show rather high porosity corresponding with other Paleozoic mudstones of Manger (1963).Likewise, this chapter focused on the Athy (1930)'s data that they were rare Paleozoic data of mudstone compactions. The re-construction of the compaction curve of Athy (1930) based on effect of erosion at the shallow part was drawn. Finally, the re-constructed curves of Paleozoic mudstone compaction of Athy (1930) based on erosion effect comparing with mudstone

compaction curve considering with time at Paleozoic age are discussed, and a compaction model including compaction factors for Paleozoic mudstone could be proposed.

## 4.2 Objective

The purposes of this study were (1) to reveal effect of erosion on mudstone compaction (2) to correct compaction data of Paleozoic mudstone based on unloading mechanism.

## 4.3 Geologic information of Nemaha Uplift

According to the information of (Hedberg, 1936; Buldwin and Butler, 1985) reported that Athy (1930)'s data were somewhat handicapped, *i.e.* Hedberg (1936) stated that Athy (1930)'s data must be affected on porosity by the necessity of estimating the amount of eroded overburden, so the compaction curve should have been drawn with a steeper initial slope. It means that the empirical part of the curve between 600 – 1200 m (2000 – 4000 feet) might have been drawn with less curvature. While Buldwin and Butler (1985) stated that 425 m (1400 feet) of beds from Athy (1930)'s data had been eroded before the drill cores were taken. In addition, a result from effect of time on mudstone compactions showed the discrepancy between a mudstone compaction curve considering with Paleozoic time (250 Ma) and Athy (1930)'s data, especially at shallow part (500 – 1400 m) as shown in Figure 4.1. Likewise, the geologic information of Athy (1930)'s data were thoroughly re-considered, and they found that all data were taken from areas where had been occurred by uplift and erosion as known Nemaha Uplift.

The geologic information of Nemaha uplift were reported by Clark and Cooper (1927) and Dolton and Finn (1989). They revealed that younger rocks (Permain and Pennsylvanisn strata) of Nemaha Uplift in exposed in the shallow subsurface and showed gentle anticlines, domes, and arches as expressions of a much stronger deformation at depth in older rocks. The Nemaha uplift has seen a long history and involves sedimentary rocks of all Paleozoic periods. Thickness may exceed 10000 feet, but because of paleostructural growth, parts of older Paleozoic succession are locally absent by truncation, and some of younger Paleozoic sequence by non-deposition. Deposition of the Pennsylvanian rocks followed the major uplift of the Nemaha, and total thickness of Pennsylvanian rocks ranges from 750 feet (230 m) to over 6000 (1830 m) feet. There is no doubt as to the pre-Pennsylvanian age of the movements. For Permian rocks, they consist primarily of terrigenous red beds, mostly mudstones (shales). After deposition of the Permian and prior to mid-Cretaceous, the Nemaha uplift was subject to a second cycle of growth, causing additional folding of strata over older structures and renewed faulting along some of the bounding faults. Permian rocks on the Nemaha range in thickness from 0 to 1500 feet (460 m).

Geologic information of each field from Athy (1930)'s data are listed as follows. Firstly, the Ponca field is the first field to be discovered in Oklahoma. About 1905, the Ponca field was drilled to discover gas in Kay County. The structure of the Ponca field is found in a

pronounced anticlinal fold. The surface structure is somewhat obscure, but the folding becomes more pronounced with depth. Then, the Mervine field was drilled in 1913 as the first important oil field. The structure of the Mervine is a continuation of the Ponca fold. The Blackwell field is a continued field to be drilled in 1914. The surface structure is very hard to map because of the indefinite nature of the outcrops of mudstone occurring in the area, and the complex nature of the fold as shown by subsurface work. The third field is Garber field in Garfield County to discover in 1917. This field is only a field in Garfield County, while other fields are in Kay County. The structure information of the thin section of Cherokee shales present is due to the fact that this old hill was an island. The last field is the Thomas field, it was discovered in 1924. The structure information was obtained by core drilling. Rocks of Permian age were found from the surface to a depth of 1200 (365 m) to 1300 (396 m) feet in this area. They included a series of alternating gray and red mudstones about 450 (137 m) feet thick at the top. The Pennsylvanian system included a maximum thickness of 2800 (853 m) feet of blue and grey mudstones. The geologic history of this field is much the same as the Garber area. Figure 4.2 represents geologic map of Nemaha Uplift showing study areas of Athy (1930).

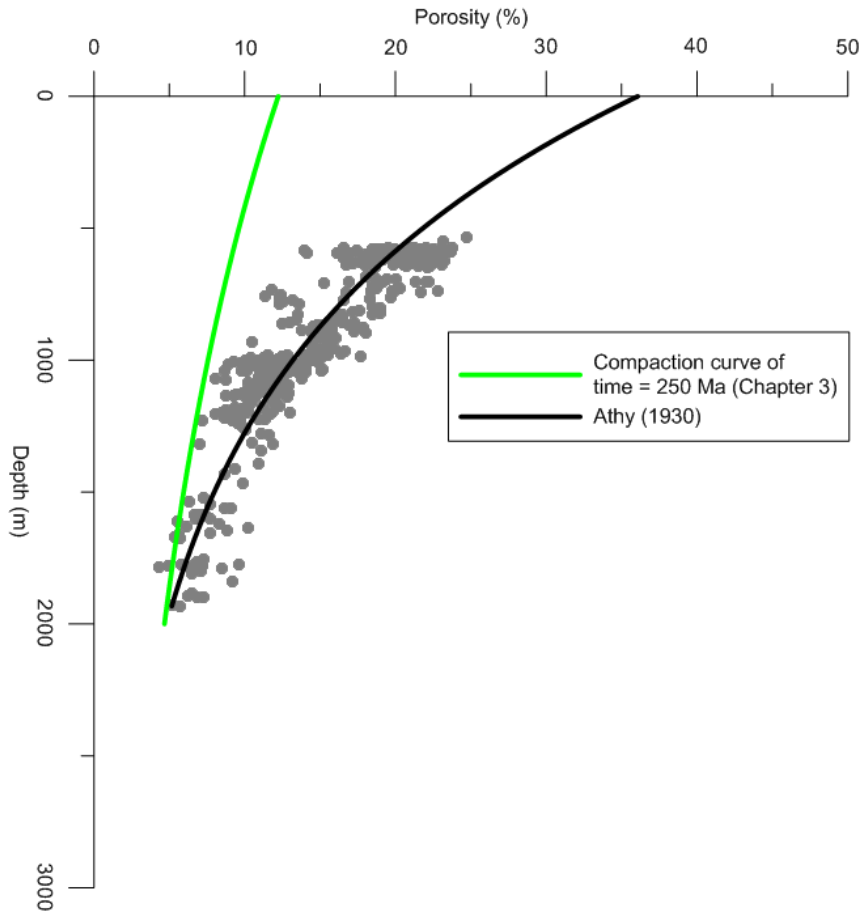


**Figure 4.1 Discrepancy in shallow part between Athy (1930)'s data and compaction curve of time = 250 Ma (Chapter 3)**

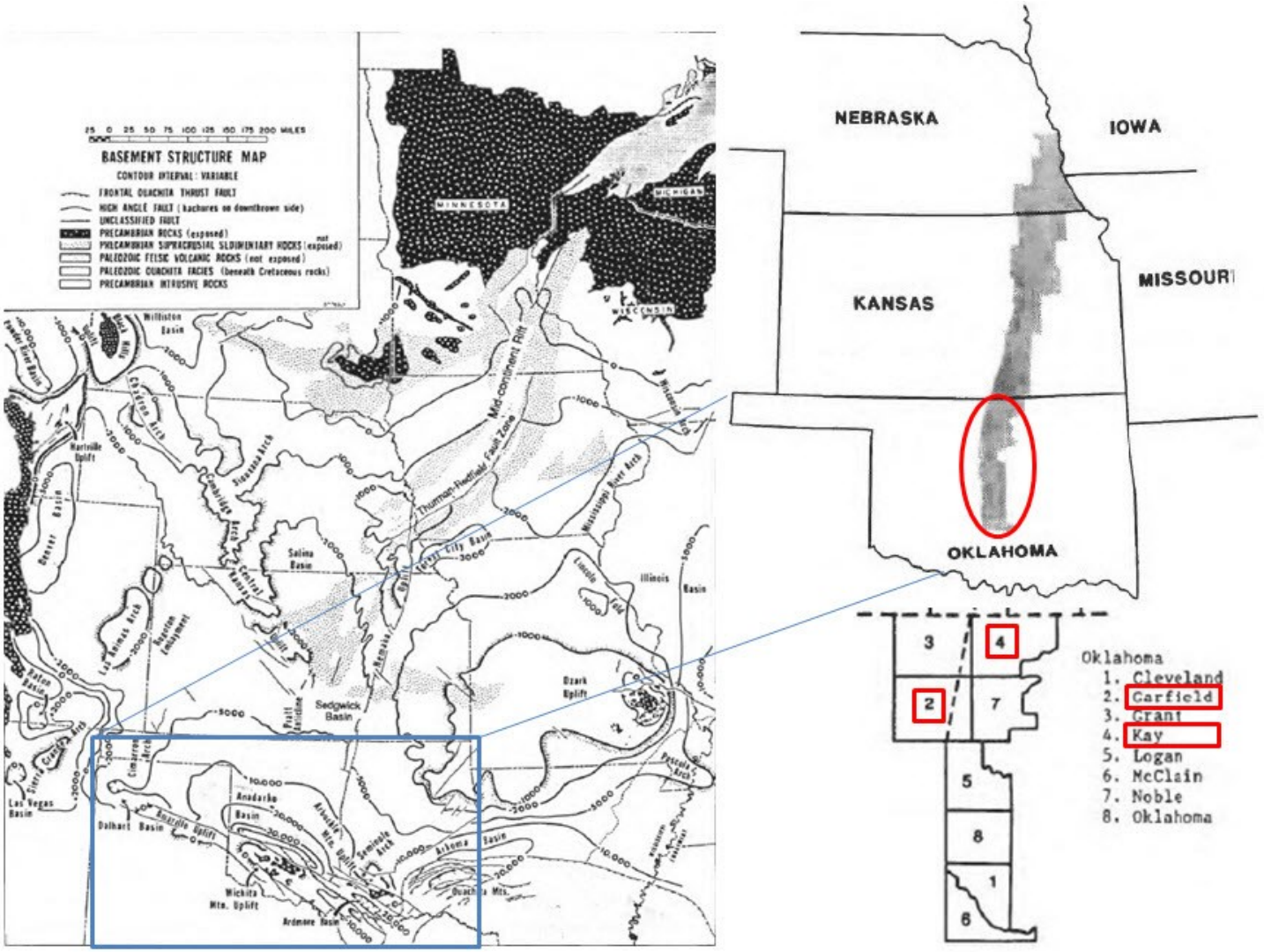


**Figure 4.2 Map of Nemaha Uplift showing study areas of Athy (1930)'s data modified from Dolton and Finn (1989)**

## 4.4 Application a concept of eroded thickness estimation to Paleozoic mudstone data of Athy (1930)

From the knowledge of geologic information, it was believe that the data from Oklahoma basins (Mervine, South Ponca, Thomas, Garber and Blackwell fields) could not be represented by only one curve. Although sonic-transit time is an effective tool for estimating thickness of erosion (Magara, 1978; Issler, 1992), a strong correlation of porosity-depth and sonic-transit time-depth relations can be shown in Figure 4.3.

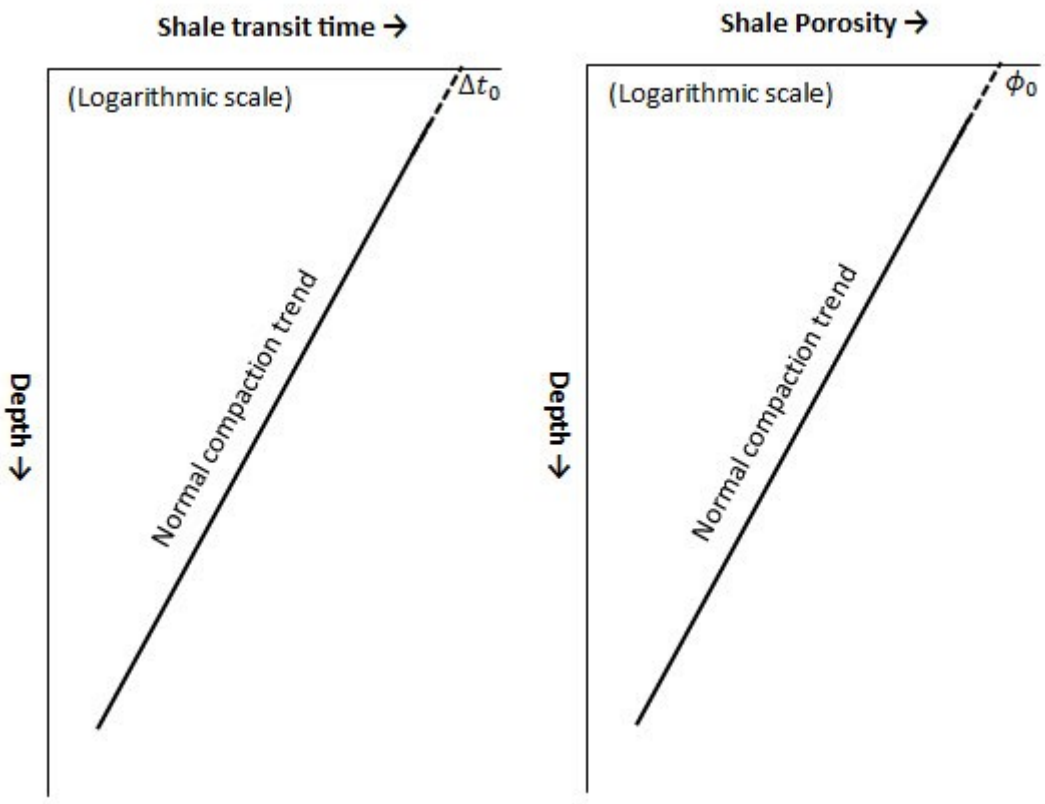


**Figure 4.3 Schematic showing transit time-depth and porosity-depth relationships of normal compaction trend (Magara, 1978)**

Due to mudstone porosity-depth relationship can be shown as a straight line on semi-log paper revealed that Athy (1930)'s were extrapolated and the surface porosity was about 35% (Figure 4.4). Porosities data of Athy (1930) were possibly come from sediment depositions after erosion processes. Consequently, a concept of estimation of eroded thickness by Magara (1978) was applied to Paleozoic mudstone data of Athy (1930), the normal compaction trend of Athy (1930)'s data was extrapolated in order to estimate thickness of erosions where was removed and disappeared. The porosity value corresponding to surface transit time (200 μs/ft), which is a good approximation transit time of clay-water mixture at the surface, is about 62 % (Magara, 1978).

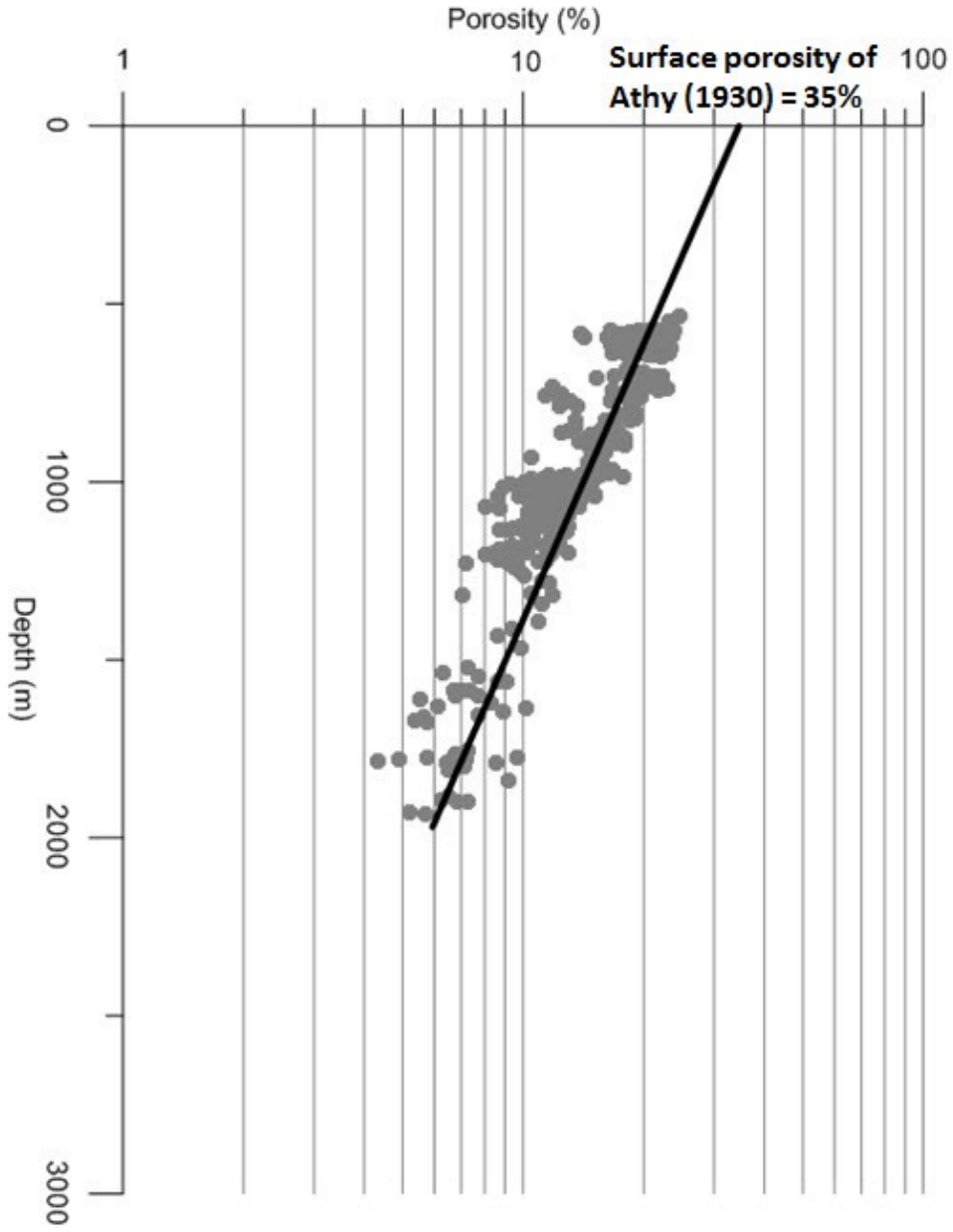


**Figure 4.4 Porosity-depth plots of Athy (1930)'s data on semi-log scale representing with two straight lines and revealing surface of erosion**

Therefore, the distance between the erosional surface and the level at which the extrapolated value of surface porosity (62 %) showed that the thickness of sedimentary rocks removed and disappeared by erosion ($\Delta z_e$) was 635 m. Figure 4.5 shows the extrapolation of the normal compaction line on semi-log scale of porosity-depth plot for estimating erosion thickness. This figure shows that there are 635 m of sedimentary thickness had been removed and disappeared.

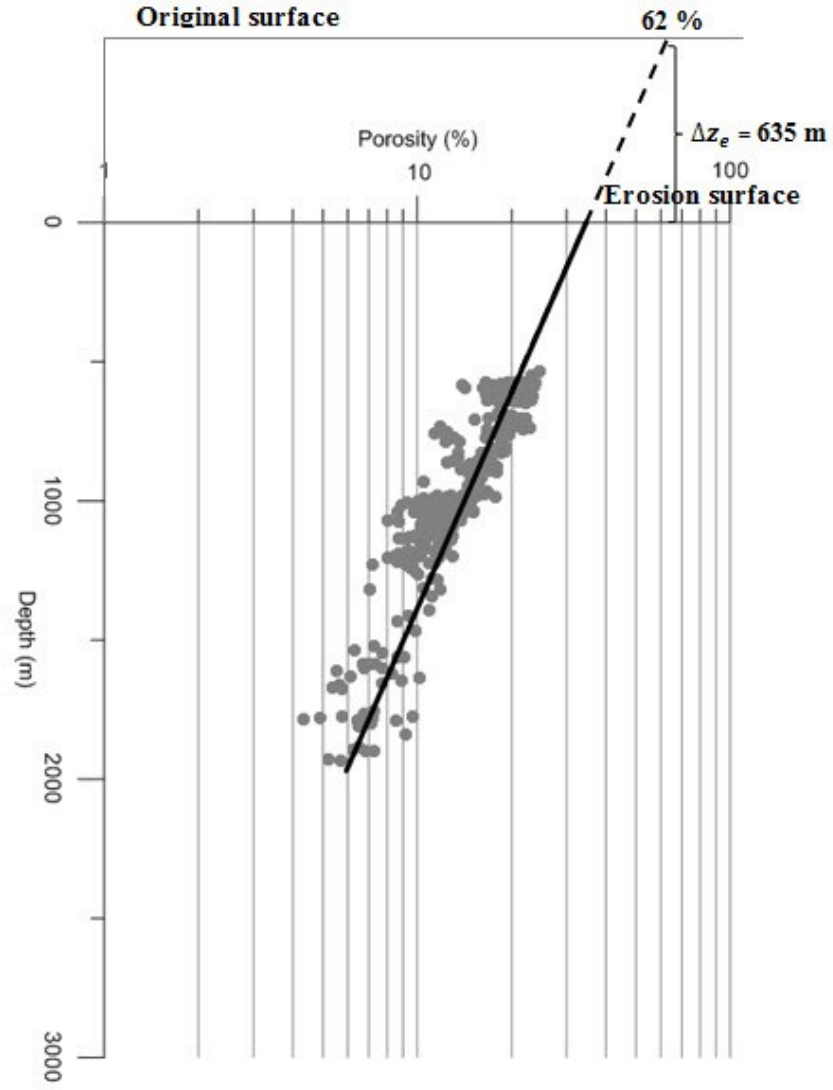


**Figure 4.5 Estimation of sedimentary thickness where was removed and disappeared by erosion on Athy (1930)'s data**

## 4.5 Effect of erosion on mudstone compaction and data correction

As Athy (1930)'s data were affected by erosion, the thickness of the sedimentary rocks removed and disappeared by erosion (635 m) can represent unloading mechanism. This means that there are some overburdens were lost as 635 m of sediment thickness during deposition in this section. More curvature of Athy (1930)'s data was resulted by effective stress decreases, and thus the data show abnormally high porosities. Likewise, the compaction model was corrected based on depth correction, *i.e.* the apparent depth of the data should be added by thickness of erosion, as follows.

$$z_{correction} = z + \Delta z_e \tag{4.1}$$

Where $z_{correction}$ is the corrected depth, $z$ is the apparent depth of Athy (1930)'s data and $\Delta z_e$ is the thickness of erosion which was removed and disappeared. Consequently, the depth used for exponential function of mudstone compaction model was replaced by $z_{correction}$. Therefore, porosity decreases exponentially as depth increases in this interval depth can expressed as:

$$\phi_{correction} = \phi_0 e^{-a(z+\Delta z_e)} \quad (4.2)$$

Based on Eq. 4.2 the porosity data of Athy (1930) were corrected as shown in Figure 4.6. Compaction factors ($\phi_0$ and $a$) of exponential model used to be the same with the normal compaction trend of Athy (1930), *i.e.* $\phi_0$ is 35 % and $a$ is 0.0015 $m^{-1}$. Hence, the modified compaction curve could be drawn by Eq. 4.2 as shown in Figure 4.7.

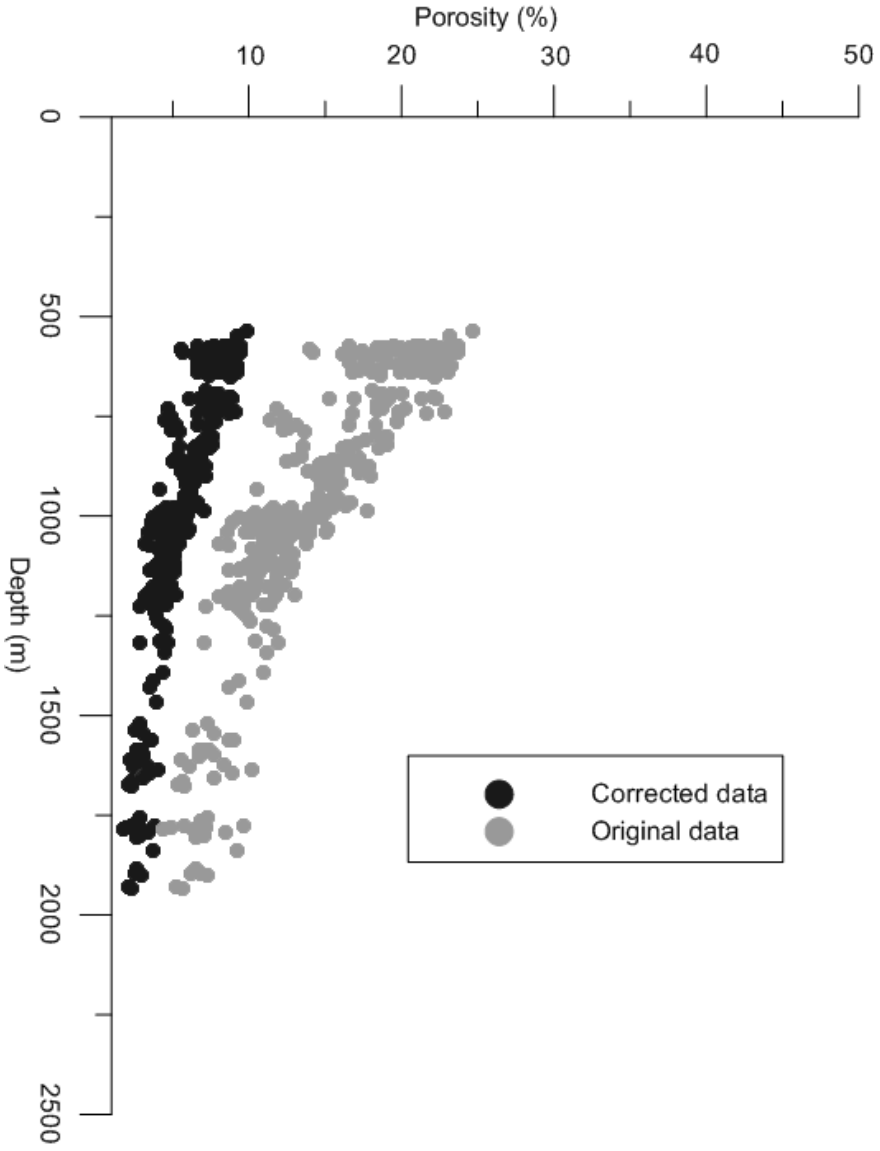


**Figure 4.6 Porosity correction of Athy (1930)'s data based on effect of erosion**

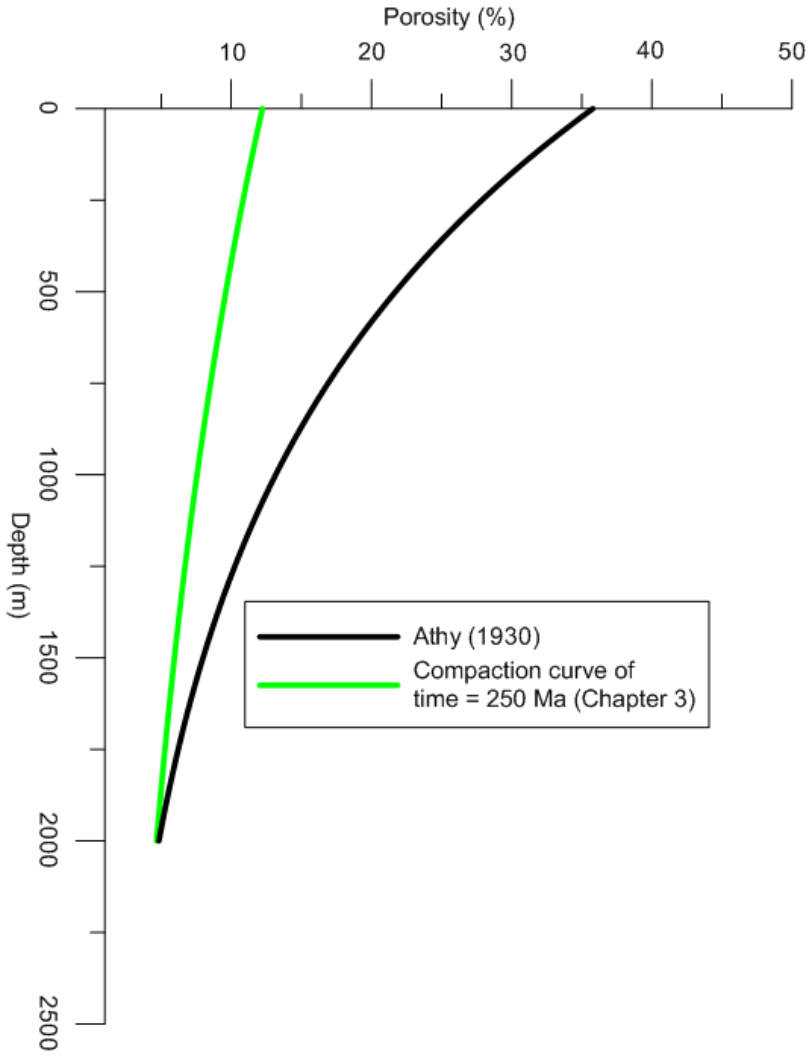


**Figure 4.7 Comparison between a compaction curve (original curve) of Paleozoic mudstone by Athy (1930), mudstone compaction curve after correction of unloading mechanism**

After correction the data show that they can be fitted and in accord with mudstone compaction curve considering with Paleozoic time ($t$ = 250 Ma of Figure 3.2). Figure 4.7 shows the comparison between the original compaction curves proposed by Athy (1930) and the mudstone compaction curve considering with Paleozoic time ($t$ = 250 Ma of Figure 3.2). It seems to be clear that the corrected data of Athy (1930) in this study was in consistent with the mudstone compaction curve considering with time of Paleozoic age ($t$ = 250 Ma, Figure 3.2), so that model of Paleozoic mudstone compaction can be proposed and it can confirmed that compaction curve of Paleozoic mudstones will be steeper trend than compaction curves of young mudstone, *e.g.* Mesozoic and Cenozoic mudstones. Finally, the initial porosity of Paleozoic mudstone should not exceed 20 % (corresponding with porosity data of Paleozoic mudrocks from Manger, 1963 as shown Figure 3.1) and the constant number of exponential function is about 0.2 $km^{-1}$.

## 4.6 Discussions and conclusions

Due to Athy (1930) presented compaction model of Paleozoic mudstone from well samples in Oklahoma, USA, without considerations of erosion and uplift effects in such areas. The shallow part of Athy (1930) was believed that there are some effects influencing on abnormal trend of shallow part of Athy (1930). Even though exponential curve was likely to be a better fit with Athy (1930)'s data, but when they were plotted on semi-log paper, it was obvious that Athy (1930)'s data were influenced by uplift and erosion processes. A discrepancy of his samples showed on semi-log paper of porosity-depth relationship. More curvature (or rapid porosity reduction) of shallow part (Hedberg, 1936) was possibly influenced by thickness of sedimentary rocks removed and disappeared by erosion. In addition, this study can confirm that statement of Buldwin and Butler (1985).

Effect of erosion on sediment compactions has been emphasized by Magara (1978), Issler (1992) and Nelson and Bird (2005). Uplift and erosion processes affect mudstone compaction as unloading mechanism. When unloading mechanism occurs in the subsurface, the increase in pore pressure causes the compaction process to stop, which causes the porosity and density cease changing with depth of burial. Consequently, a new deposition after erosions shows the different compaction trend comparing with old sediments. Likewise, a concept of eroded thickness estimation, which was proposed by Magara (1978), was applied to estimate the thickness of erosion at shallow part of Athy (1930)'s data. The compaction model of Athy (1930) could be modified based on depth correction. The result shows that thickness of erosion ($\Delta z_e$) could be inferred an absent overburden as unloading mechanism. Apparent depths of Athy (1930)'s data were added by $\Delta z_e$ as deposition of overburden load that was removed and disappeared by erosion. Then, Paleozoic mudstone compaction curve of Athy (1930) could be re-constructed, this curve was compared with the mudstone compaction curve considering with time of Paleozoic age ($t$ = 250 Ma, Figure 3.2). Based on the better match on both curves, hence, a compaction curve of Paleozoic mudstones can be proposed. Furthermore, the initial porosity of modified compaction model based on effect of erosion in this study were more corresponding with porosity range of Paleozoic mudrock data proposed by Manger (1963) than original compaction model, which were somewhat high.

# CHAPTER 5

# STANDARD CURVE OF MUDSTONE COMPACTIONS

## 5.1 Introduction

As known that mudstone compaction has related to the oil and gas migration, especially shale gas which is trapped in shale (or mudstone) formation and one of the most rapidly expanding trends in oil and gas exploration and production today. Also by using compaction curves, prediction and detection of overpressure zones are one of the most important contributions to the petroleum exploration.

Intentions have been given an answer to the doubts of discrepancies in mudstone compaction curves, especially the shallow part (< 2000 m), dominated by mechanical compaction. Time (Geologic time) and temperature were studied as major factors influence the mudstone compactions. In order to coming out these effects, the data were classified depending on geologic ages and geothermal gradients. The data which were plotted on porosity-burial depth vary with geologic ages and geothermal gradients. Furthermore, with respect to clay mineral dehydration and fluid expansion in mudstones caused by time and temperature effects, respectively, can be corrected by equations which was proposed by Keith and Rimstidt (1985).

Re-vision and re-construction on data plots of mudstone compactions after time and temperature corrections can be re-plotted. The reconstructed plots match well with one another than shown by original plots. It is possible that this study will be able to establish mathematic expression of compaction and propose a standard curve of mudstone compactions. The standard curve of compaction for mudstones will be very useful to apply for prediction and detection of overpressures and basin modeling works.

## 5.2 Objective

The purposes of this study were (1) to correct effects of time and temperature on mudstone compactions (2) to try an establishment of a standard curve of mudstone compaction.

## 5.3 Data collection

The data used in this study are shown in Table 5.1. Almost data are as same as the data that used in chapter 3, however, for quantitative accuracy, the data were added to use in this study, *i.e.* data No. 6 and 7. In addition, geologic age and geothermal gradient, which are main factors, used to classify effects of time and temperature are shown in Table 5.2.

**Table 5.1: Added data description (Data No. 1-5 are the same as shown in Table 3.2, No. 6 and 7 are added data)**

| No. | Basin location | Bottom depth (km) | Porosity Measurement | Amount of data | Reference |
|---|---|---|---|---|---|
| 1 | Akita and Hokkaido | 3.00 | Direct measurement | 143 | Aoyagi *et al*. (1979; p.41) |
| 2 | Makran | 5.00 | Wireline measurement | 25 | Fowler *et al*. (1985; p.429-430) |
| 3.1 | N Pacific | 0.05 | Direct measurement | 138 | Velde (1996; p.196) |
| 3.2 | Barbados | 0.46 | | | |
| 3.3 | Antarctic | 0.30 | | | |
| 3.4 | Sulu Sea | 1.00 | | | |
| 3.5 | Indian Ocean | 1.30 | | | |
| 3.6 | E Atlantic | 0.30 | | | |
| 3.7 | Niigata | 4.50 | | | |
| 3.8 | Po Valley | 2.50 | | | |
| 4 | Oklahoma | 2.00 | Direct measurement | 368 | Athy (1930; p.12) |
| 5 | Maracaibo | 2.00 | Direct measurement | 37 | Hedberg (1936; p.254) |
| 6 | Central California | 0.3 | Direct measurement | 35 | Meade (1966; p. 1086) |
| | Maracaibo | 3.0 | | | |
| | Po Valley | 2.0 | | | |
| 7 | Colombia | 2.0 | Direct measurement | 33 | Johnson (1950; p. 337) |

**Table 5.2: Time and temperature information of data**

| No. | Basin location | Geologic age | Geothermal Gradient (°C/km) |
|---|---|---|---|
| 1 | Akita and Hokkaido | Miocene | 30-60 |
| 2 | Makran | Tertiary | ~ 35 |
| 3.1 | N Pacific | Pleistocene | ~55 |
| 3.2 | Barbados | Eocene-Holocene | ~15 |
| 3.3 | Antarctic | Pliocene-Pleistocene | ~ 52 |
| 3.4 | Sulu Sea | Miocene-Pleistocene | ~ 127 |
| 3.5 | Indian Ocean | Tertiary | 30-50 |
| 3.6 | E Atlantic | Pliocene-Holocene | 25-50 |
| 3.7 | Niigata | Miocene-Holocene | ~ 30 |
| 3.8 | Po Valley | Pliocene-Holocene | ~ 18.8 |
| 4 | Oklahoma | Pennsylvanian-Permian | ~ 25 |
| 5 | Maracaibo | Tertiary | ~ 16 |
| 6 | Central California | Pliocene-Pleistocene | 13.8-22 |
| | Maracaibo | Tertiary | ~ 16 |
| | Po Valley | Miocene-Pliocene | ~ 18.8 |
| 7 | Colombia | Cretaceous | 12-23 |

## 5.3.1 Porosity acquisition and basin history information

The information of porosity acquisition and basin history of data No. 1-5 have been discussed in section 3.4.1 and 3.4.2 of chapter 3, already. Therefore, this section will discuss only on the data which were added to use in this study, *i.e.* data No. 6 and 7. Remarkably, the Athy (1930)'s data that used in this chapter are the data after correction of unloading mechanism.

The data No. 6 were taken as averages from the trends graphically reported in the cited publications (Meade, 1963; Storer, 1959; Hedberg, 1936). All data converted from density data which acquired from laboratory test. In case of basin history information, there is little information on composited data No. 6. The sediments are all Cenozoic. Most of the sediments consist of clastic, inorganic, and terrigenous detritus. One of the composited data is the data in Venezuela basin which was already discussed above (Data No. 5), while other data are Po Valley basin of Storer (1959) and central California basin of Meade (1963).

While, porosity data of No. 7 were estimated from density data as followed Eq. 3.8, the bulk density of data No. 7 came from wireline measurements of wells in Colombia and the

absolute density was assumed to remain constant and equal 2.762 g/cm$^3$ (Fowler *et al.*, 1985) for calculating in Eq. 3.8 as same as the calculated porosity of data No. 4. The information of basin history of data No. 7 are very scanty, so it was just reported that the data No. 7 obtained from several wells of Mesozoic mudstones in Colombia.

## 5.4 Plots of porosity-depth relationship considering with time

Due to the issue of effect of time has been clearly revealed on mudstone compactions as discussed in chapter 3. However, in this section, the data were divided into two groups, *i.e.* first group is old mudstones (Paleozoic and Mesozoic ages) which are high porosity reductions represented by Data No. 4 and 7. While, second group is young mudstones (Cenozoic age), which are low porosity reductions, represented by data No. 1,2,3,5, and 6 as shown in Figure 5.1.

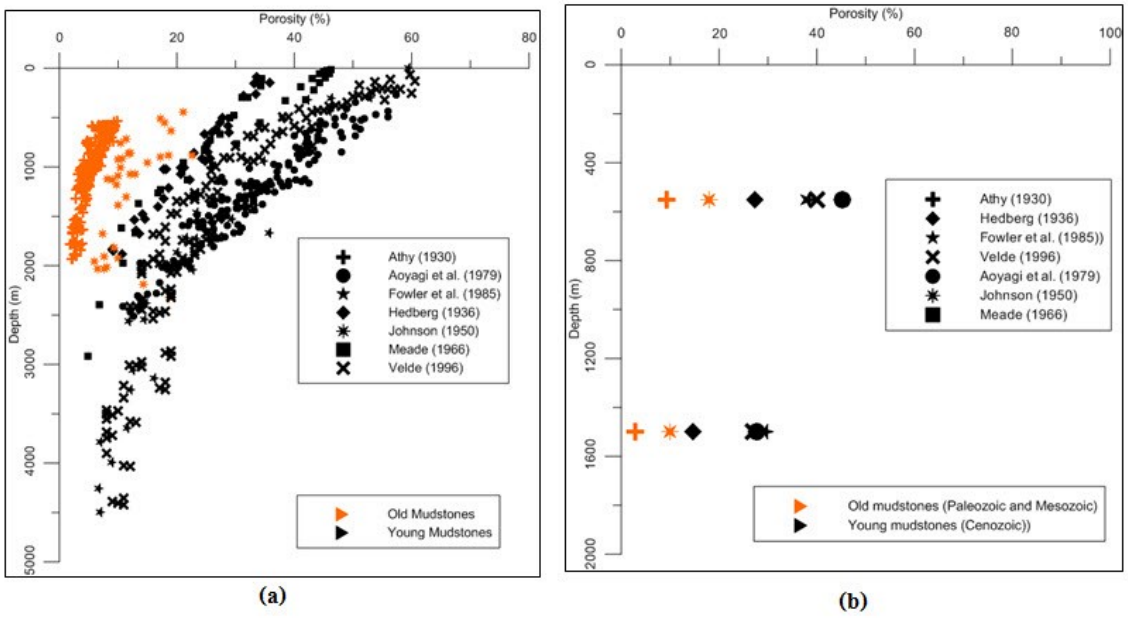


**Figure 5.1 Data plots of porosity-depth relationship classifying with time**

The Figure 5.1 shows that the data scattered wildly on porosity-depth relationship, especially at the shallow depth, and the data seem to be convergent when the depth is deeper. Furthermore, the data were likely to be able to separate obviously into two groups by using time classification. In this chapter, the effect of time was deduced by dehydration of many clay lattices was completed in old sediments under normal compaction, while partial dehydration has occurred on young sediments (Van Olphen, 1963). Secondary compression (porosity decrease not caused by effective stress) and erosion, which are possible reasons for high porosity reduction in the old mudstones comparing with young mudstones, were not considered in this chapter.

## 5.5 Plots of porosity-depth relationship considering with temperature

Even though temperature is a main factor in the chemical processes in deep part of mudstone compactions, but the evidences of Barker (1972), Bradley (1975) and Magara (1974, 1978) showed that it also influences the shallow part dominated by the mechanical compaction, if sedimentation and burial continued in the geological past, the under-compacted section would be influenced by the aquathermal effect. In addition, Domenico and Palciauskas (1979) incorporated the effects of a geothermal gradient in theoretical models to determine the conditions under which thermal effect provide an important contribution to the total excess pressure development. They found that high porosity at given depths could also be achieved under conditions of fluid flow, provided that burial produces a thermally induced increase in water volume. Cekerevak and Laloui (2004) presented the results of an experimental study of thermal effects on the mechanical behavior of saturated clay.

Another point of view is the theory of consolidation proposed by Terzaghi (1925, 1943). He stated that loss of water (consolidation) of sediments corresponds to absorption of water (Fluid expansion) to increase of heat. In addition, fluid expansion is in accord with a second stage of de-watering processes which was studied by Burst (1969). He stated that when heat accumulations is sufficient to mobilize the interlayer water, one of the two remaining interlayers is discharged into bulk system. Hence, the fluid expansion of high geothermal environments lead to the de-watering processes will be slower than the areas which have normal geothermal environments.

In this study studied on temperature effect using geothermal gradient of each location as listed in Table 5.2, and then the geothermal gradient divided two groups of data as plotted in Figure 5.2. The first group is the geothermal gradient higher than 30 ◦c/km as known high temperature mudstones, and another group is the geothermal gradient lower than 30 ◦c/km which is low temperature mudstones. Geothermal gradient influences the fluid pressure in the formation. Low porosity reduction is due to the increase in geothermal gradient. Consequently, the low porosity reduction can be considered as fluid expansion of de-watering processes of rocks.

Figure 5.2 shows clearly that even effect of temperature is a main controlling factor of chemical compaction at the deep part of the basin, but it is also one of factors, which influences on mechanical compaction at the shallow part. The figure shows quite clear on temperature classification and, in this study, effect of temperature on mudstone compactions was deduced by fluid expansion of de-watering processes.

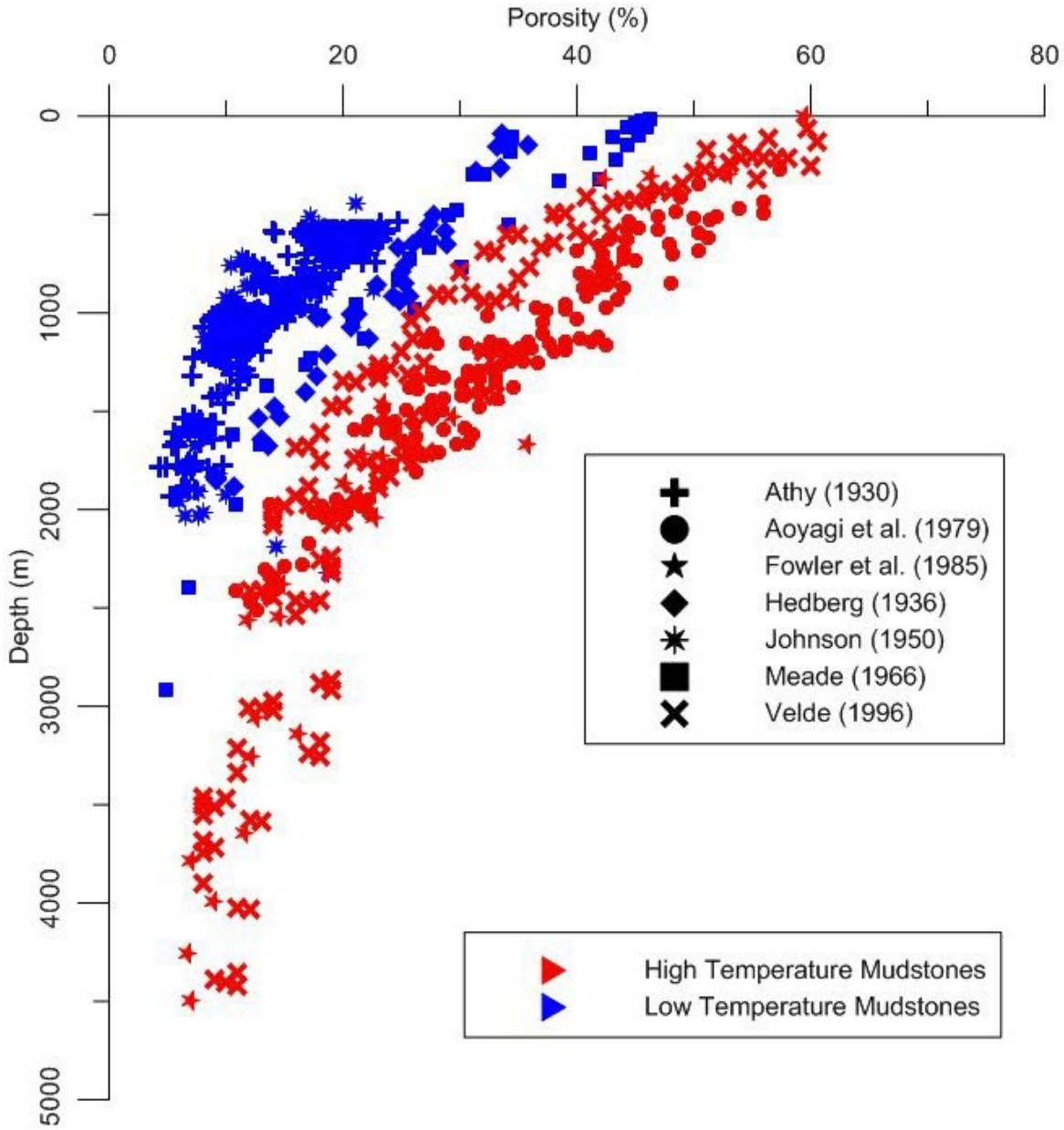


**Figure 5.2 Data plots of porosity-depth relationship classifying with temperature**

## 5.6 Porosity correction

Due to Terzaghi model (3.4) and Keith and Rimstidt (1985) model can use to correct the porosity during compaction with considerations of time and temperature effects. Thus, this study assumed that the scatters of porosity data during compaction are caused by time and temperature effects regarding different geological ages and thermal expansion. Terzaghi model were applied to correct porosity data considering different ages of mudstones, and Keith and Rimstidt model were applied to correct porosity data considering fluid expansion is caused by temperature increasing. Finally, the establishment of a standard compaction curve for mudstones can be drawn and proposed.

### 5.6.1 Time correction

According to Van Olphen (1963), many clay lattices in Paleozoic and Mesozoic ages appear to have been dehydrated completely under normal compaction, while partial dehydration has occurred on young sediments (Cenozoic age). Hence, it is possible that porosity scatters of mudstone compactions, especially in mechanical compaction, are caused by different ages (Time effect).

The porosity correction for time effect can be applied by using Eq. 3.4. In this study, time $(t)$ was assumed that the smectite to illite transformations occurs after 65 Ma (Cenozoic age) and the parameters that were used in Eq. 5.1 are the same as shown in theoretical parameters of Table. 3.1. From geologic information, Ages of Athy (1930)'s data and Johnson (1950)'s data are in early Paleozoic and Cretaceous (Mesozoic) ages, so $t$ used to correct porosity data are 250 and 144 Ma, respectively. Consequently, the correction of porosity data based on clay dehydration can be used applied equation of Eq. 3.4 as follows.

$$\phi_a = \phi / e^{-a^2 \lambda' t} \tag{5.1}$$

Eq. 5.1 was applied for converting the porosities of old mudstones to recent or young mudstones. The high porosity reductions of the old mudstones caused by complete dehydration of smectite to illite transformations, comparing with incomplete dehydration of young mudstones, were corrected by the smectite-illite dehydrations at times of the porosity data in old mudstones (Paleozoic and Mesozoic ages) of data No. 4 and 7.

The results show that the corrected porosities comparing with the original data were higher than the original data as shown in Figure 5.3. Remarkably, the original data of Athy (1930) in Fig. 5.3 are the data that have been corrected by unloading effect in previous chapter, and after that they were corrected based on clay dehydration by Eq. 5.1.

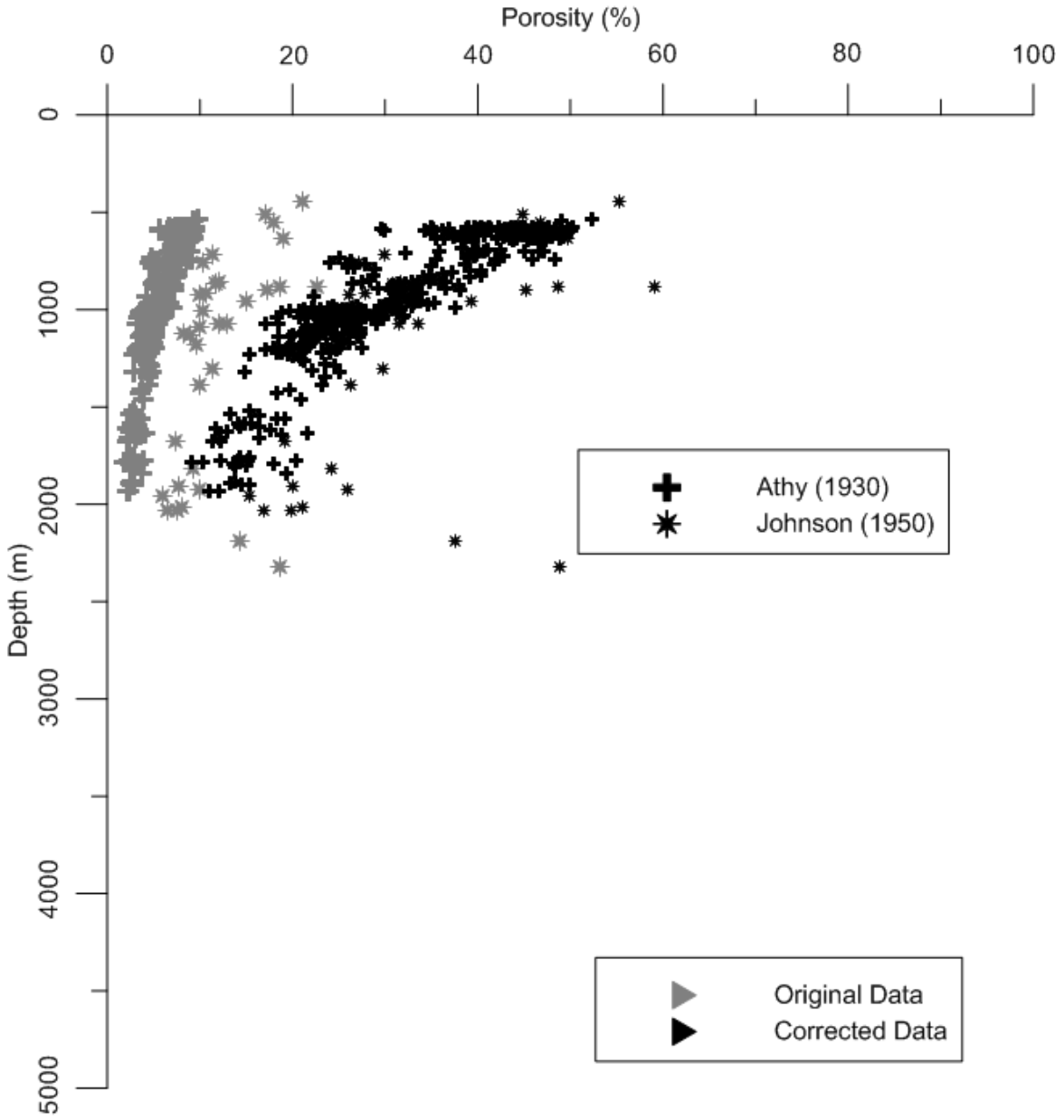


**Figure 5.3 Time correction on data plots of porosity-depth relationship**

## 5.6.2 Temperature correction

Magara (1978) found that amount of water expelled by compaction decreases with burial depth, but the subsurface temperature tends to expand volume of water (fluid expansion). In addition, the fluid expansion is in accord with increases of expelled water in a second stage of de-watering processes which was studied by Burst (1969). Hence, the fluid expansion of high geothermal environments lead to the de-watering processes will be slower than the areas having normal geothermal environments.

Equations for thermal correction proposed by Keith and Rimstidt (1985) were applied to correct porosity data. They showed that the specific fluid volume change with depth, which is expressed:

$$V_{sp} = 2.6x10^{-8}z + 9.5x10^{-4} \quad (5.2)$$

where $V_{sp}$ is the specific volume of fluid and $z$ is the burial depth.

In addition, the change of porosity with depth changing caused by thermal expansion($\left(\frac{d\phi}{dz}\right)_{therm}$) is expressed by specific fluid volume change with depth as expressed:

$$\left(\frac{d\phi}{dz}\right)_{therm} = \left(\frac{\phi}{V_{sp}}\right) \cdot \frac{dV_{sp}}{dz} \quad (5.3)$$

where $\frac{dV_{sp}}{dz}$ is the change of specific fluid volume with depth changing.

Finally, according to a depth interval ($\Delta Z$), thus the adjusted porosity is given by:

$$\phi_a = \phi - \left(\frac{d\phi}{dz}\right)_{therm} \cdot \Delta Z \quad (5.4)$$

The porosities were corrected based on temperature effect as porosity was converted from high temperature environments to normal temperature environments using Eq. 5.4. Because of the depth interval ($\Delta Z$) of our high temperature mudstone data is around 5000 m, thus it was believed that during 5000 m the specific fluid volume is changed by high temperature environments following Eq. 5.2 and 5.3. The porosity data which were corrected for temperature effect include data No. 1, 2 and 3. The corrected porosity comparing with the original data were plotted on porosity-burial depth plots as shown in Figure 5.4.

Figure 5.4 shows that the corrected porosities were lower than the original porosities. However, this correction might have some errors because the parameters referred by Keith and Rimstidt (1985), 40 °C/km as geothermal gradient, while this study used these parameters representing several geothermal gradients higher than 40 °C/km.

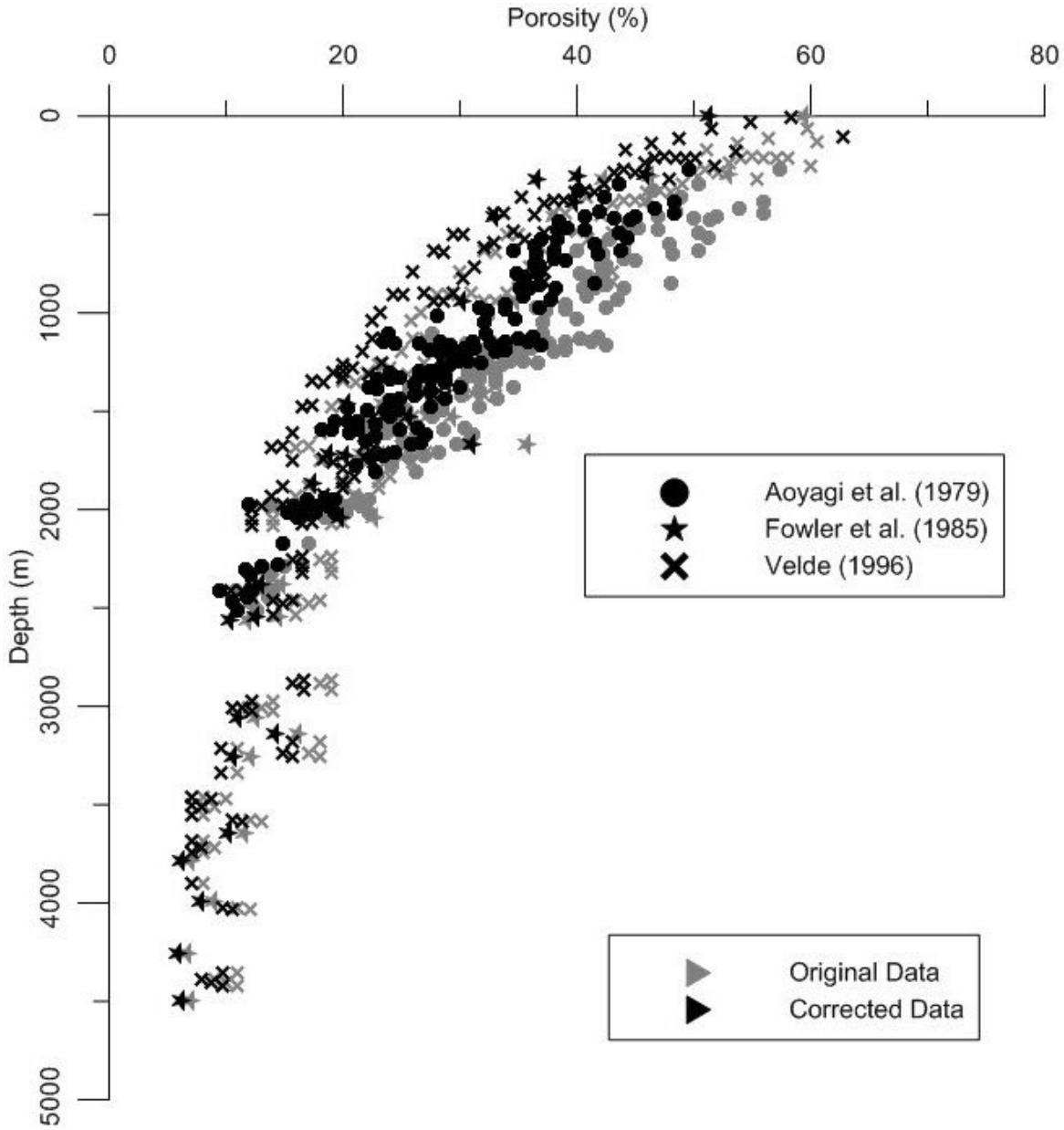


**Figure 5.4 Temperature correction on data plots of porosity-depth relationship**

## 5.7 Standard curve of mudstone compactions

Time and temperature factors influence variations of mudstone compaction curves, especially on mechanical compaction (shallower 2000 m). Re-plots of corrected data (No. 1-3, 4 and 7) and data which do not need for corrections (No. 4 and 6) were demonstrated in Figure 5.5.

The graphs seem to improve matching with one another than compared with original plots and the scatters of data reduced obviously after the corrections were operated. A trend curve represents the corrected curves toward a standard curve of mudstone compactions, especially during mechanical compaction (~500-2000 m).

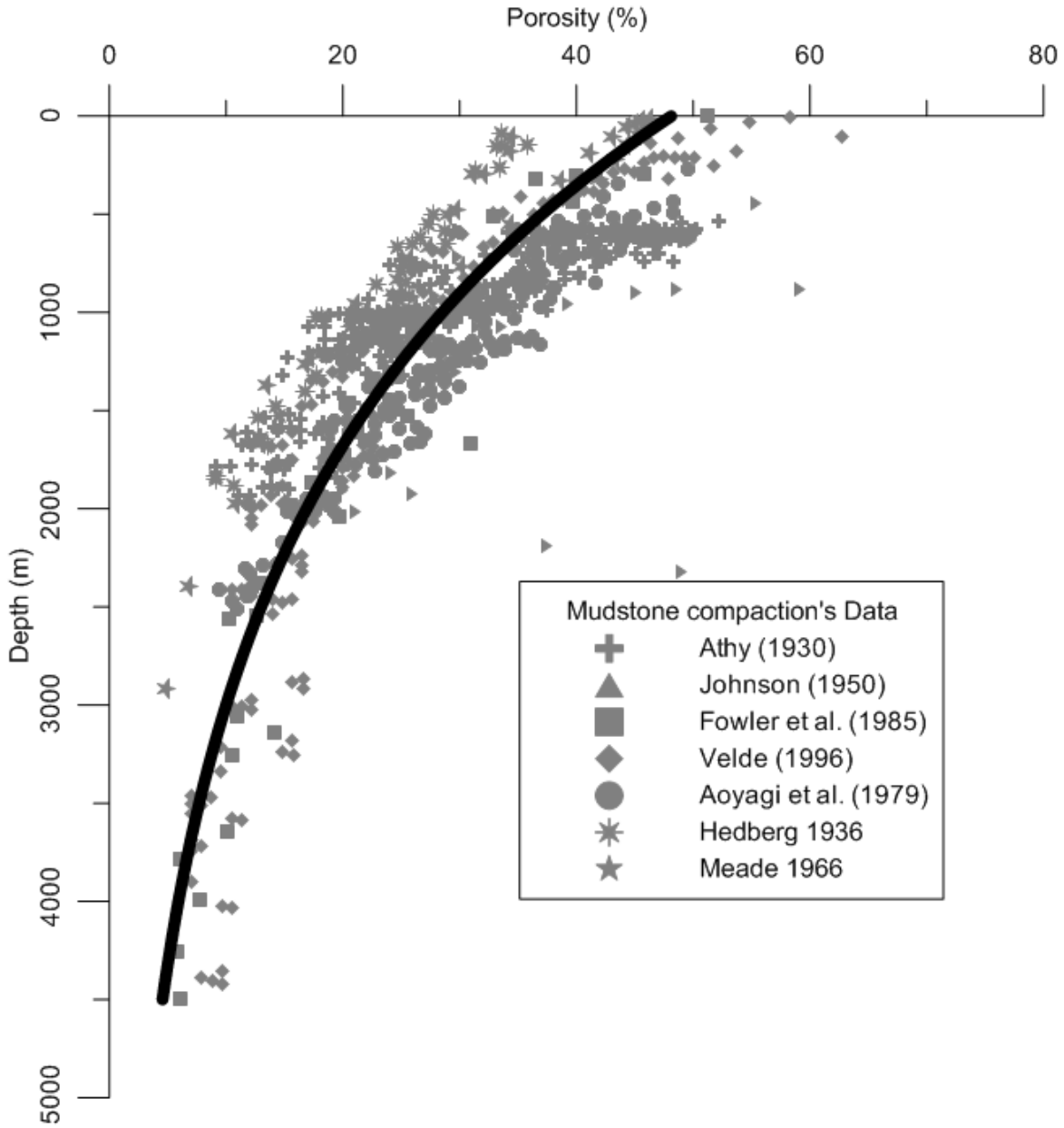


**Figure 5.5 Standard curve of mudstone compactions**

The standard curve is in accord with exponential model (Eq. 2.1) proposed by Athy (1930). Compaction factors, *i.e.* porosity of mudstone at datum depth ($\phi_0$) and constant value of exponential function ($a$) of standard curve of mudstone compaction can be determined and show in Table 5.3. Consequently, this curve (black curve) can be called a standard compaction curve for Cenozoic mudstones.

However, these corrections might have some errors because assumed parameters, referred by Keith and Rimstidt (1985), were used in this study were not acquired to represent each basin. Nevertheless, this study will be a guideline toward establishment of a standard compaction curve for mudstones.

**Table 5.3: Compaction factors of standard curve of mudstone compactions**

| Compaction factors | |
|---|---|
| $\phi_0$ (%) | $a$ (km$^{-1}$) |
| 45 | 0.5 |

## 5.8 Discussions and conclusions

The data plots on porosity-depth relation show that the wide scatters of mudstone compactions can be implied by effect of time and temperature. Based on time and temperature classifications, in this study, the data can be divided into three groups as shown in Figure 5.6. The first group is the data of young (Cenozoic age) and high temperature mudstones. The second group is the young and low temperature mudstones, while the third group is the old (Paleozoic and Mesozoic ages) and low temperature mudstones.

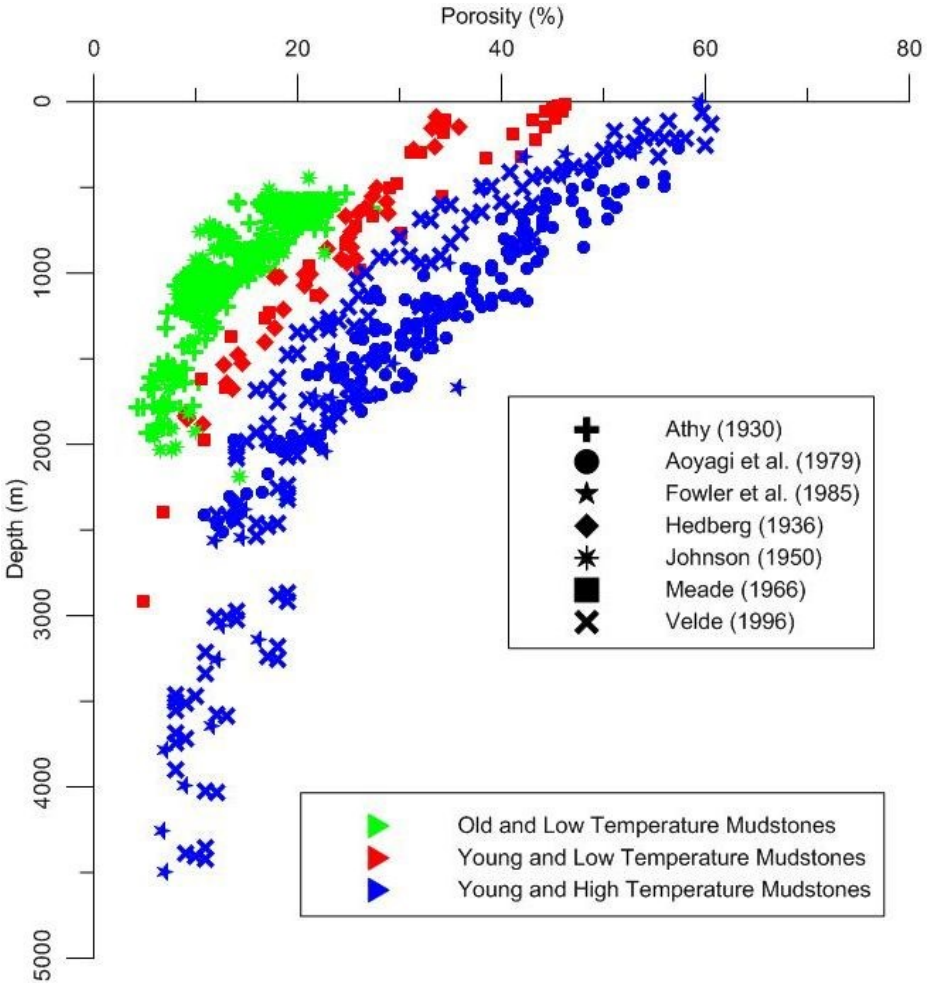


**Figure 5.6 Group divisions of mudstone compactions based on time and temperature classifications**

High porosity reductions of old mudstones caused by time effect are possible to relate to the different clay mineral dehydrations. Similarly, low porosity reductions of high temperature mudstones caused by temperature effect are possible to relate to fluid expansion. Consequently, porosity data were corrected and re-constructed on the porosity-depth relationship using concept of clay dehydration (Van Olphen, 1963) and the equations proposed by Keith and Rimstidt (1985), and show in Figure 5.3, 5.4 and 5.5.

The standard curve of compaction for mudstones will be very useful to apply for prediction and detection of overpressures and basin modeling works. The overpressure zones can be roughly evaluated before an exploration, if time and temperature of basins are known based on this guideline. Furthermore, in basin modeling works, reconstruction of basin geometries normally use default compaction curves and default thermal properties, the parameters which influence on compaction curves, *i.e.* time and temperature, are normally not considered in basin analysis. Consequently, the standard curve of compaction will be useful to improve accuracy in basin modeling works.

# CHAPTER 6

# SIMULATION OF SUPERCRITICAL $CO_2$ INJECTION INTO BEREA SANDSTONE

## 6.1 Introduction

Fluid production of a hydrocarbon reservoir normally causes a decrease in pore pressure, an increase in effective overburden load and surface subsidence. On the other hands, injection of fluid into formation, in general, produces an increase in pore pressure, which will change stress field causing deformations in the rock mass; the same processes, an underground injection of compressed fluid can be produced the ground surface to uplift because of a reduction of effective stress in the formation. Nowadays, geomechanics is extensively interested because many hydrocarbon fields are geometrically complex and irregular, and the rock properties are spatially variable, such an assessment can be conveniently done on a numerical model of the field understudy (Orlic, 2008). Petroleum geomechanics has evolved differently from civil and mining geomechanics. Petroleum geomechanics is newer and has based on physics, analysis and field observations rather than on laboratory testing and empirical models (Dusseault, 2011).

This study used geomechanical simulation to analyze and re-produce laboratory results of core sample in term of deformations. Strain changes of core sample in laboratory testing can be inferred to reservoir deformation relating to a surface uplift in field observation. Using FLAC3D simulator with a coupled fluid-mechanic interaction feature to simulate deformations of a core sample based on stages of laboratory experiments. The experiment was divided into three stages in order to measure the strain, *i.e.*, (1) Confining pressure change stage, (2) Water injection stage (Pore pressure changes) and (3) Supercritical (S.C.) $CO_2$ injection stage, with continuous tests, respectively. The relationship of effective porosity and effective bulk modulus changes proposed by Russell and Smith (2007), Mavko *et al.* (1998) and Gussmann's equation (Gussmann, 1951) was applied for simulations. Finally, the simulation results can help to understand the deformations of core sample in laboratory testing, especially a case of $CO_2$ injection in which it relates to Carbon dioxide Capture and Storage (CCS) project.

## 6.2 Objective

The purposes of this study were (1) to re-produce and analyze deformation of a homogeneous and isotropic rock (2) to monitor a motion of S.C.$CO_2$ in the rock sample influencing homogenous rock deformation.

## 6.3 Information of laboratory experiments for strain measurements

Laboratory experiment was setup to emulate surface uplift problem in CCS site. A main objective in this experiment is to try capturing the motion of S.C.$CO_2$ front in the rock sample by monitoring the strain of the sample. The strain changes of core sample were observed by using the optical fiber (Lawrence *et al*., 1999; Culshaw, 2000).

**Figure 6.1 Core sample of Berea sandstone**

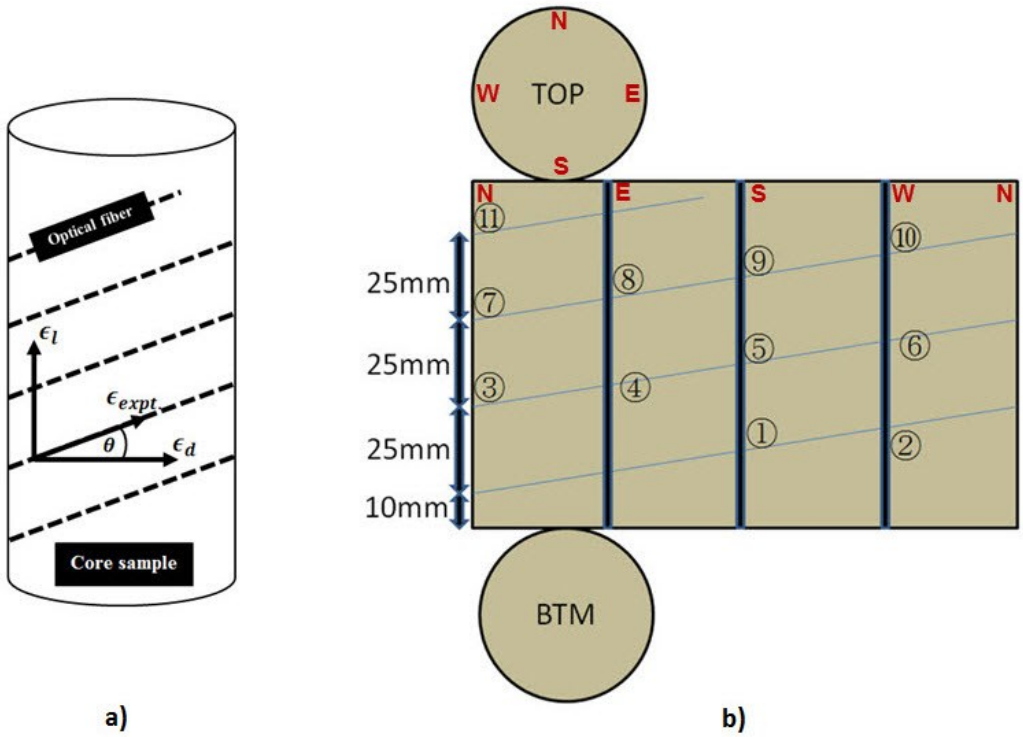


**Figure 6.2 Schematic of Berea core sample measuring by optical fiber a) overview of Berea sandstone core sample b) planar view representing the channel locations of optical fiber measurements of Berea sandstone**

A core sample of Berea sandstone (Figure 6.1) was selected as an ideal rock sample for the homogenous and isotropic reservoir. In addition, hydrostatic loading was used as external pressure condition in this testing. For avoiding rock deformation due to thermal effect, temperature was kept constant at 40°C throughout testing procedures. Since strains were measured continuously at each stage by optical fiber, the time series data of strain changes were obtained. 11 channels of optical fiber data are acquired; the locations and the directions of strain measurements are shown in Figure 6.2. A schematic of three stage experiments is shown in Figure 6.3 and the conditions of each stage are shown in Figure 6.4.

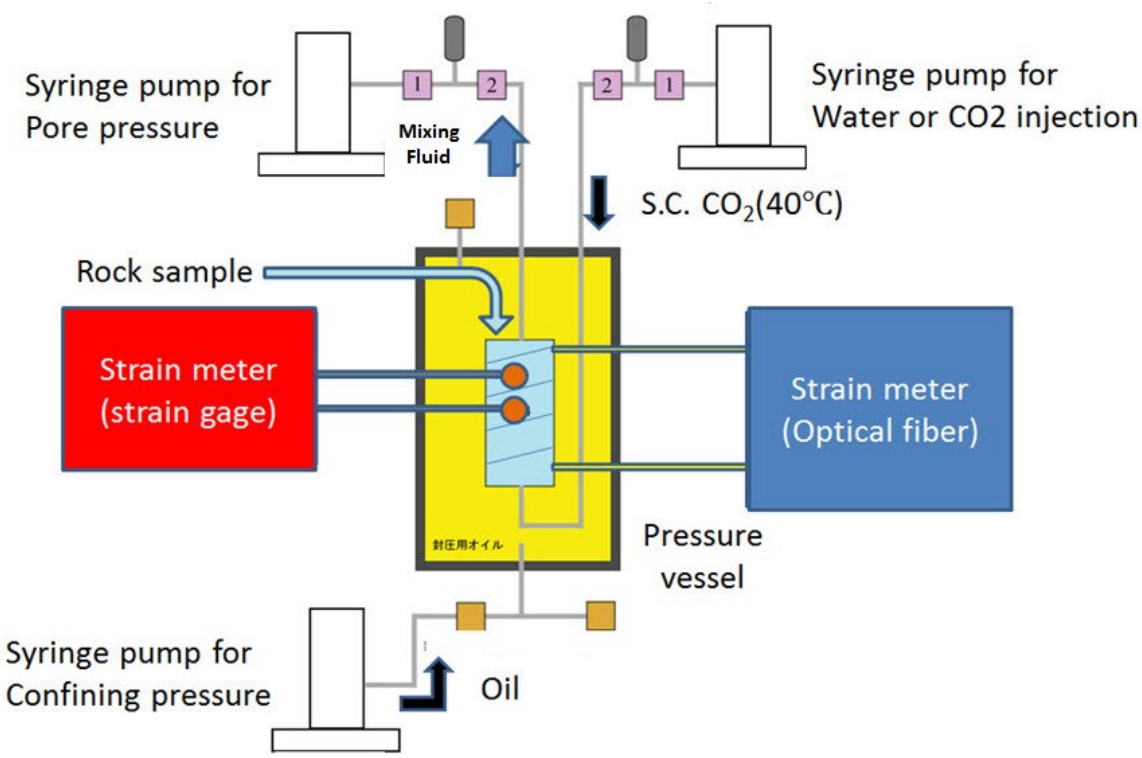


**Figure 6.3 Schematic of three stages in the laboratory measurements**

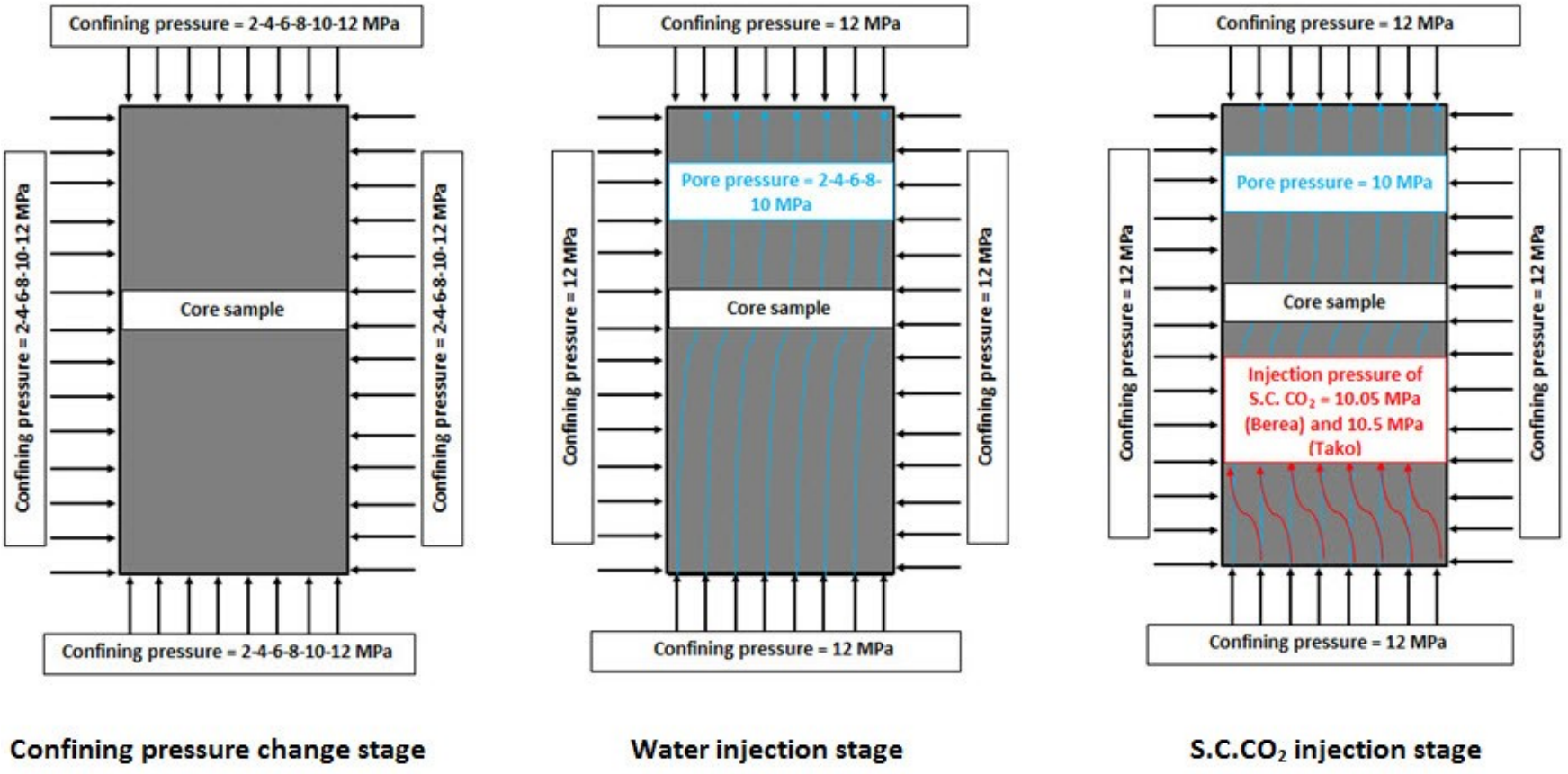


**Figure 6.4 Schematic of laboratory testing conditions**

## 6.4 Information of simulations for strain measurements

In this study, FLAC3D (Itasca, 2006a) was used as a simulator for Geomechanical simulations. It is a numerical modeling based on Finite Difference Method (FDM) codes for advanced analysis of soil, rock, and structural support in three dimensions and it can model complex behaviors which do not readily suit for Finite Element Method (FEM) codes, *e.g.*, large displacements, non-linear strain, unstable systems, and problems that consist of several stages. According to a coupled fluid-mechanic interaction feature it was satisfactorily able to simulate the time stepping change of strain according to fluid injection progress. Using FLAC3D reproduced time stepping behaviors of measured strain value from core sample experiment.

Due to insensitivity of stress-permeability relationship for sandstones (Rutqvist and Tsang, 2003), the changes in permeability are omitted in this study. In addition, the CT images of S.C.$CO_2$ saturation in a work of Shi *et al*. (2010) show that there is no noticeable evidence of gravity effect during the S.C.$CO_2$ injection, and therefore it can be negligible the gravitation loading in this simulation.

Model geometry was created corresponding to the core sample in the laboratory. The size of core sample is 5 cm of diameter and 10 cm of length. The core sample was discretized into 3-dimensional mesh, the mesh size in x, y, and z direction was 16x16x32 as shown in Figure 6.5. The calculating volumetric strains were consistent with the same location and direction of strain measurements of optical fiber (Figure 6.2) in the laboratory. The simulations required in unsupported system for the core sample, and thus the confining pressure with hydrostatic loading condition was performed as mechanical boundary condition and elastic model was used for simulations. Rock properties of Berea sandstone were used as input parameters, and they are shown in Table 6.1.

**Table 6.1: Physical properties of Berea sandstone**

| Parameter | Value |
|---|---|
| Dry bulk modulus ($K_d$, GPa) | 8.3 |
| Shear modulus ($G$, GPa) | 7.0 |
| Dry density ($\rho$, kg/m$^3$) | 2100 |
| Permeability ($K$, mD) | 100 |
| (Initial) Porosity ($\phi$, %) | 23 |
| Coefficient of pore space stiffness ($k$) | 0.05 |
| Pore space stiffness ($K_\phi$, GPa) | 1.8 |

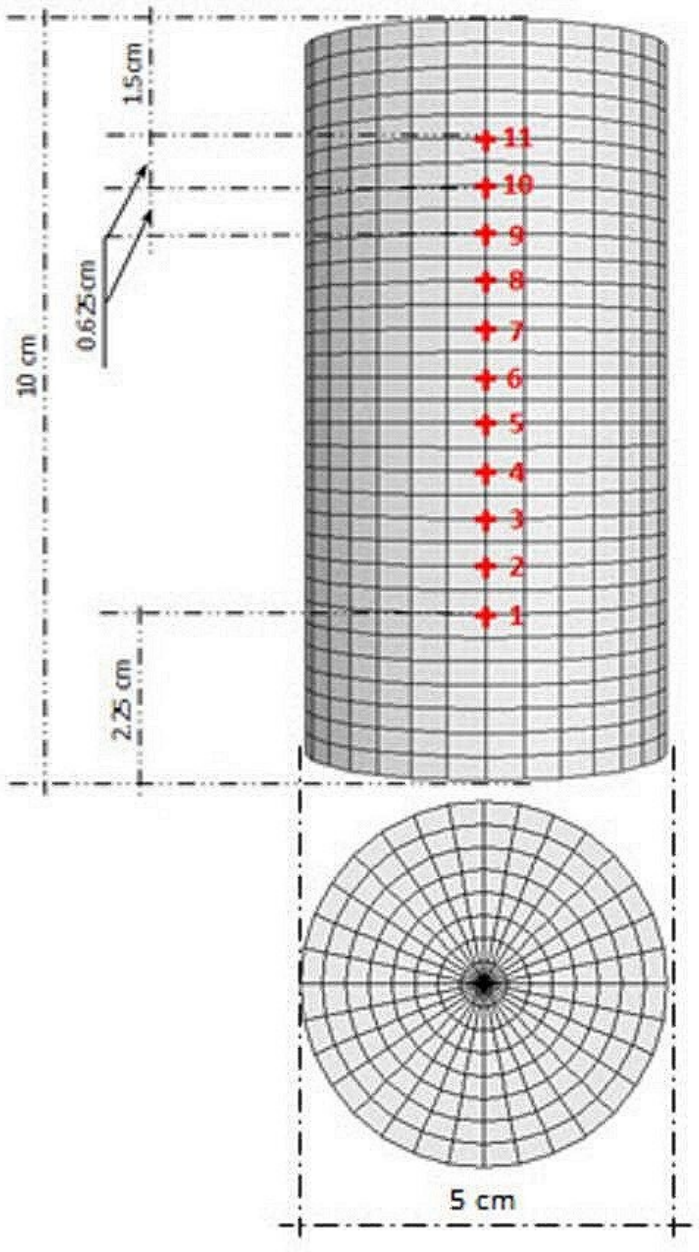


**Figure 6.5 Model geometry and the locations of simulation strains of Berea sandstone**

## 6.5 Simulation results vs. experimental results

In order to compare simulation and experimental results, they need to be converted a volumetric strain from simulation to experimental strain ($\epsilon_{expt.}$) in the direction which was measured by optical fiber. As an angle ($\theta$) between optical fiber direction and x-axis can be determined as shown in Figure 6.2a, and then a definition of volumetric strain of cylinder material can be expressed by Eq. 6.1. Hence, volumetric strains can be converted to experimental strain in the same direction of optical fiber by using Eq. 6.2. The following equations are used for conversion.

$$\epsilon_v = 2\,\epsilon_d + \epsilon_l \tag{6.1}$$

$$\epsilon_{expt.} = \frac{\epsilon_v}{(2\cos\theta + \sin\theta)} \tag{6.2}$$

where $\epsilon_d$ and $\epsilon_l$ are the diametrical strain and longitudinal strain, respectively.

## 6.6 Confining pressure change stage

In laboratory experiments, the confining pressure was exerted on a core sample with hydrostatic loading condition. Oil was injected from a syringe pump into a pressure vessel to control and change confining pressure (Figure 6.3 and 6.4). For protecting the sample from penetrating oil, the core sample was covered by silicone resin before it was taken inside the pressure vessel. At this stage, the core sample was in dry condition and the pore pressure kept at atmosphere pressure. According to the confining pressure was increased from 2 MPa to 4, 6, 8, 10, and 12 MPa, strain changes of rock sample were observed. Finally, strain was measured by optical fiber at each step of confining pressure changes (Figure 6.6). The observed values of strains were negative values because the core was shrinking according to the increasing of the confining pressures.

For simulation of this stage, rock is in a dry condition, and thus only mechanical processes were working in this stage and there is no the effect of fluid flow. Rock deformations or strain ($\epsilon$) are due to confining pressure ($P_c$) and dry bulk modulus of rock as followed:

$$\epsilon = -P_c/K_d \tag{6.3}$$

The calculating strain in FLAC3D is derived from nodal velocities, as usual. The strain rate ($\dot{\epsilon}_{ij}$) is then partitioned into deviatoric, $\dot{e}_{ij}$, and volumetric strain, $\dot{\epsilon}_v$, components:

$$\dot{\epsilon}_{ij} = \dot{e}_{ij} + \dot{\epsilon}_v \delta_{ij} \tag{6.4}$$

where $\delta_{ij}$ is the Kroenecker delta.

A nodal volumetric strain is calculated using the formula:

$$\dot{\epsilon}_{v,n} = \frac{\sum_{e=1}^{m_n} \dot{\epsilon}_{v,e} V_e}{\sum_{e=1}^{m_n} V_e} \tag{6.5}$$

where $\mathrm{m_n}$ are the elements surrounding node $(n)$, and $V_e$ is the volume of element $(e)$.

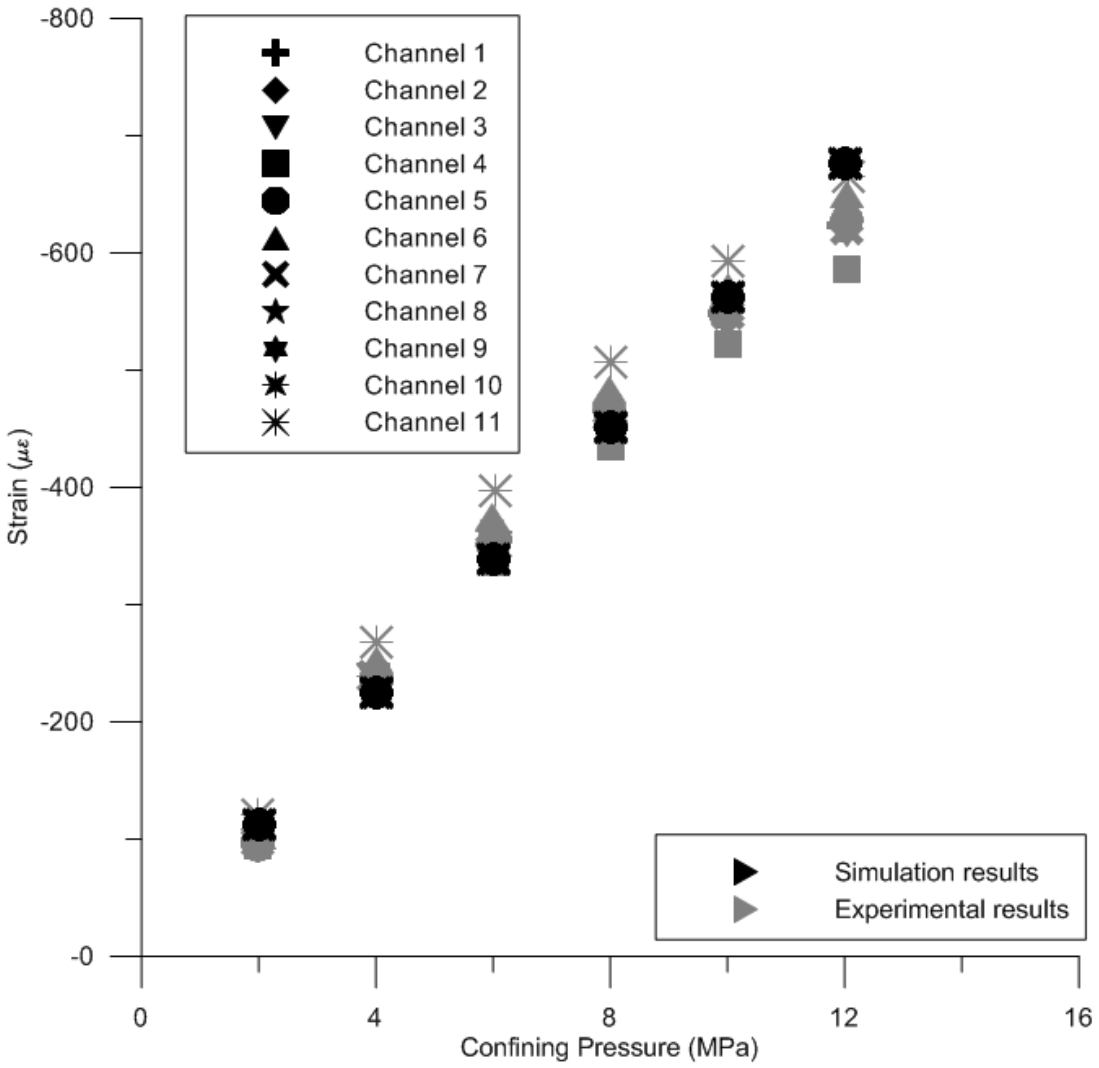


**Figure 6.6 Comparison between simulation and experimental results of confining pressure change stage of Berea sandstone**

## 6.6.1 Comparison of experimental and simulation results in confining pressure change stage

The strain decreases due to increase in confining pressure (Figure 6.6) in both case of simulation and experiment. This study simulated deformations of rock in this stage using dry bulk modulus of rock as input parameters (8.3 GPa), as shown in Table 6.1. The simulation results seem to be consistent with experimental results and almost straight line was obtained.

Figure 6.6 shows that during increase in confining pressure with hydrostatic loading condition, the effective porosity of rock might be decreased since the pore space compressibility, $K_\phi$, is smaller than the dry bulk modulus, $K_d$ (Table 6.1). Furthermore, this caused increase in dry bulk modulus because of pore connection closing following compaction concept (Figure 2.16). However, Figure 6.6 shows the strain change is straight line therefore this can be simulated by unchanged value of $K_d$ throughout confining pressure

changes. Since the curve of strain change is likely to be tilted after confining pressure at 12 MPa, this bending is possibly caused changes of pore space and grain contacts. The rock behaved deformations as a simple contraction in this stage.

With increasing confining pressure, variations of strain measurement at each location become visible. This can be explained by inhomogeneous of confining pressure exerted on the sample and the core sample itself. As the confining pressure was controlled by oil injection, the silicone resin was used to cover the rock to protect oil penetration; therefore, the sample condition was probably not equal at every location due to differences of silicone thickness. Moreover, the core (itself) is not completely homogenous, but the simulation model assumed it was a perfect homogenous model.

## 6.7 Water injection (pore pressure change) stage

After confining pressure was reached at 12 MPa, the confining pressure was kept constant following fluid injection stages. Then, water was injected into the core sample using water syringe pump until the pore pressure reaches the pre-specified values. The injection pressures of water were set 2 MPa to 4, 6, 8 and 10 MPa, therefore the effective pressure decreased from 10 to 2 MPa during the water injection stage.

At this stage, the valve at the outlet of water (see on Figure 6.3) was closed, and therefore the water did not flow out the core sample and it was not 100% water saturation state. The volume of injection water was measured at each injection pressure, and there were 34.02 ml and 35.20, 35.93, 36.65, 37.30 ml respectively, Strain changes of experimental results are shown in Figure 6.7 at each injection pressures were caused due to increased pore pressures.

There are no variations of strain measurement at each location in water injection stage (Figure 6.7) comparing with Figure 6.6. Because fluid was injected to sample directly and, after confining pressure was reached at 12 MPa, all of channels were set at zero microstrain before water injection in order to measure deformation of water injection. Hence, the results from each channel in this stage showed perfectly the same.

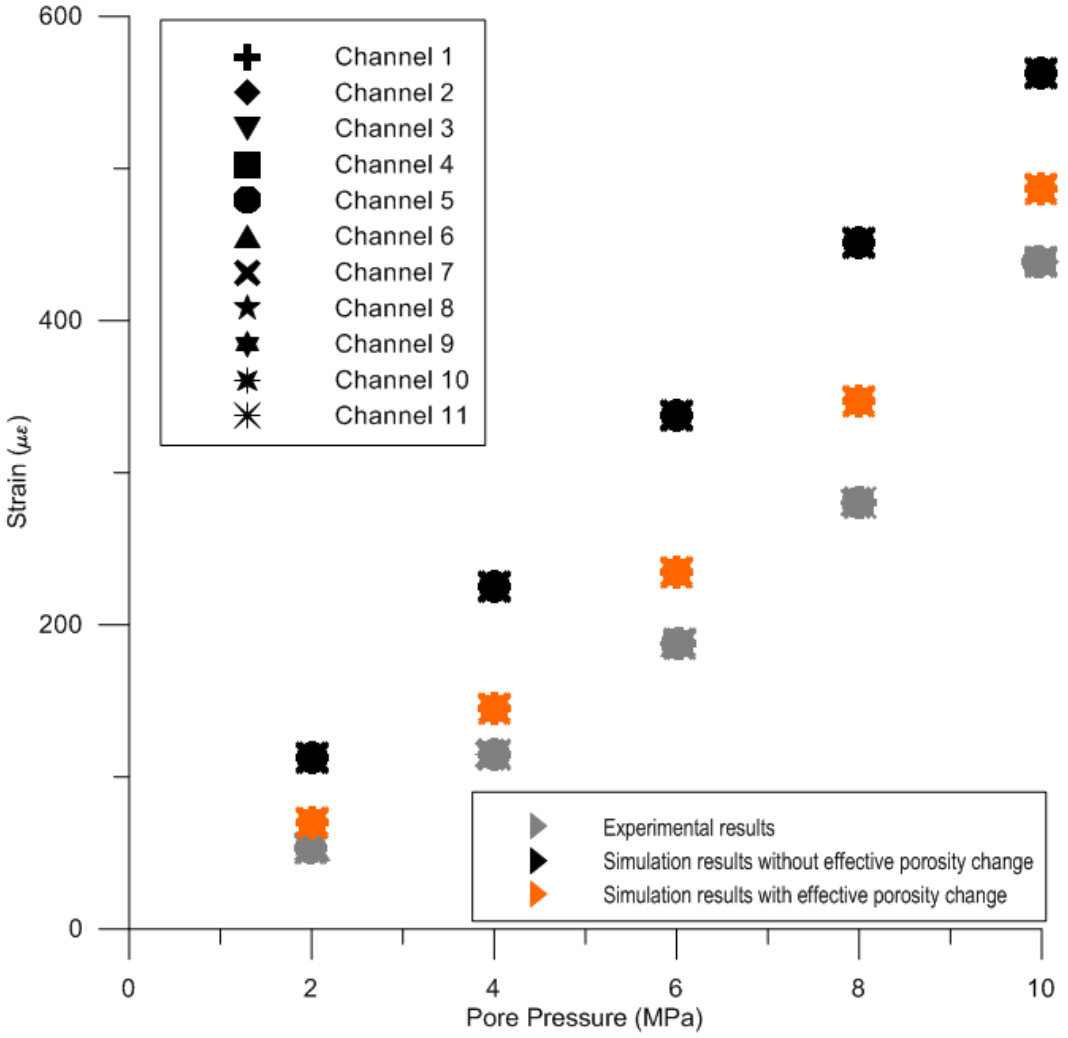


**Figure 6.7 Comparison between simulation and experimental results of water injection stage of Berea sandstone**

## 6.7.1 Stress (effective stress) – strain curve after water injection stages

Figure 6.8 shows experimental results of two stages such as confining pressure change and water injection stages on stress-strain curves. As rock was in a dry condition at confining pressure change stage, so effective stress increases were due to increases of confining pressure. While, in water injection stage, confining pressure was kept constant at 12 MPa, and thereby the effective stress decreased because of increase in pore pressure.

At first stage, strain decreased because of increase in effective stress (confining pressure increases) The curve shows almost a straight line that is consistent with theory of elasticity, while in the second stage, strain increased due to effective stress decreases (pore pressure increase). Since, permeability change was negligible, a non-linear stress-strain curve of water injection stage (Figure 6.7 and 6.8) might be explained by two parameters, *i.e.* porosity and bulk modulus of rock.

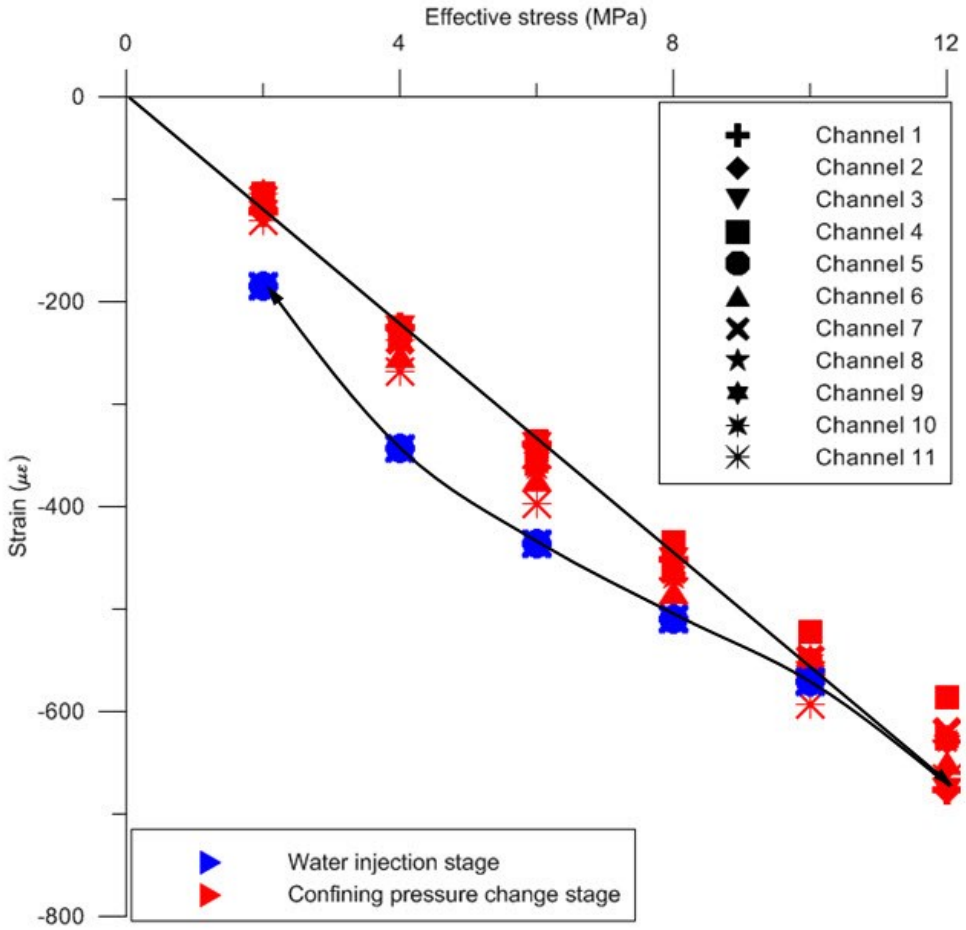


**Figure 6.8 Stress (effective) – strain curve of confining pressure change and water injection stages of Berea sandstone**

## 6.7.2 Simulation of strain change in water injection stage

In water injection stage, the coupled fluid flow and mechanical simulations were performed using FLAC3D. Strain changes with time are corresponding to fluid flow and mechanical changes. Changes in the variation of fluid content, $\xi$, are related to change in pore pressure, $P_p$, saturation, $S$, and mechanical volumetric strain, $\epsilon_v$. The response equation for the pore fluid is formulated as

$$\frac{1}{B}\frac{\partial P_p}{\partial t} + \frac{\phi}{S}\frac{\partial S}{\partial t} = \frac{1}{S}\frac{\partial \xi}{\partial t} - \alpha\frac{\partial \epsilon_v}{\partial t} \tag{6.6}$$

where $B$ is Biot modulus, $\phi$ is the porosity, $\alpha$ is Biot's coefficient. Alam *et al.* (2010) explained in their research that Biot's coefficient, $\alpha$, keep unity for loose sediments during effective stress changes. Hence, it may assume that during porosity decreases, but α remain close to one.

When the fluid is injected into rock, the injection pressure pushes the pore up to open. Hence, the effective porosity increases during steps of increase in pore pressure. The relationship of changes of effective porosity and dry bulk modulus of rock can be determined by Eq. 2.12 and 2.15, respectively. This section simulated and calculated strains at constant state of each injection pressure of water. The simulation results here show two cases of simulation, *i.e.* first case was simulated and calculated strains without effect of effective porosity changes, and second case was simulated strains with considering effective porosity changes. As mentioned above, effective porosity changes by pore closing or opening, then this change of effective porosity affects changes of dry bulk modulus $K_{d\ (new)}$(Figure 2.16 and Eq. 2.15). Also it needs to evaluate effective bulk modulus of rock which is saturated with water.

The data of injection volume of water from laboratory testing assuredly indicated that at confining pressure of 12 MPa the effective porosity increased continuously with increase in water injection pressure. The concept of effective porosity was adopted in order to evaluate bulk modulus of core sample saturated with water. Consequently, the input parameters of modifications of dry bulk modulus and effective bulk modulus of rock substituted with water were shown in Table 6.2. The $\phi_w$ in the Table 6.2 is the porosity which was occupied by injected water, while $\phi_e$ is the effective porosity which increased with increases of injection pressures. Therefore, the strain changes can be determined by simulations of strain changing at each stage of injection pressure based on concept of effective porosity change.

**Table 6.2: Information of injection volume of water, effective porosity, effective porosity of water and modification of effective bulk modulus of rock in case of Berea andstone 's experiments**

| $P_p$ (MPa) | $V_{H_2O}$ (ml) | $\phi_w(\%) = \frac{V_{H_2O}}{V^a_{rock}}$ | $\phi_e$ (%) | $K_{H_2O-sat}$ (GPa) |
|---|---|---|---|---|
| 2 | 34.02 | 17.3 | - | 12.3 |
| 4 | 35.20 | 17.9 | 0.6 | 32.2 |
| 6 | 35.93 | 18.3 | 0.4 | 33.3 |
| 8 | 36.65 | 18.8 | 0.5 | 32.7 |
| 10 | 37.30 | 19.0 | 0.2 | 34.6 |

[a] *Rock volume, $V_{rock}$, is 196.35 $cm^3$*

Figure 6.9 can be used to explain that when the porosity is change according to effective pressure change for example pore pressure change from 2 MPa to 4 MPa. At this stage assumed that $K_f$ is, the bulk modulus of water, equal to 1 GPa for a given pressure and temperature. This means that the effect of air, even the air exists in the pore space, was omitted, the bulk modulus of air is too small compared to the water. However, in case of S.C.$CO_2$ injection experiment, the fluid of the pore becomes S.C.$CO_2$. Therefore, the fluid bulk modulus ($K_f$) was changed to bulk modulus of $CO_2$ that is equal to 0.059 GPa. By using

the relationship of dry bulk modulus and effective porosity discussed above, it will simulate the strain behaviors of the rock sample at the following sections.

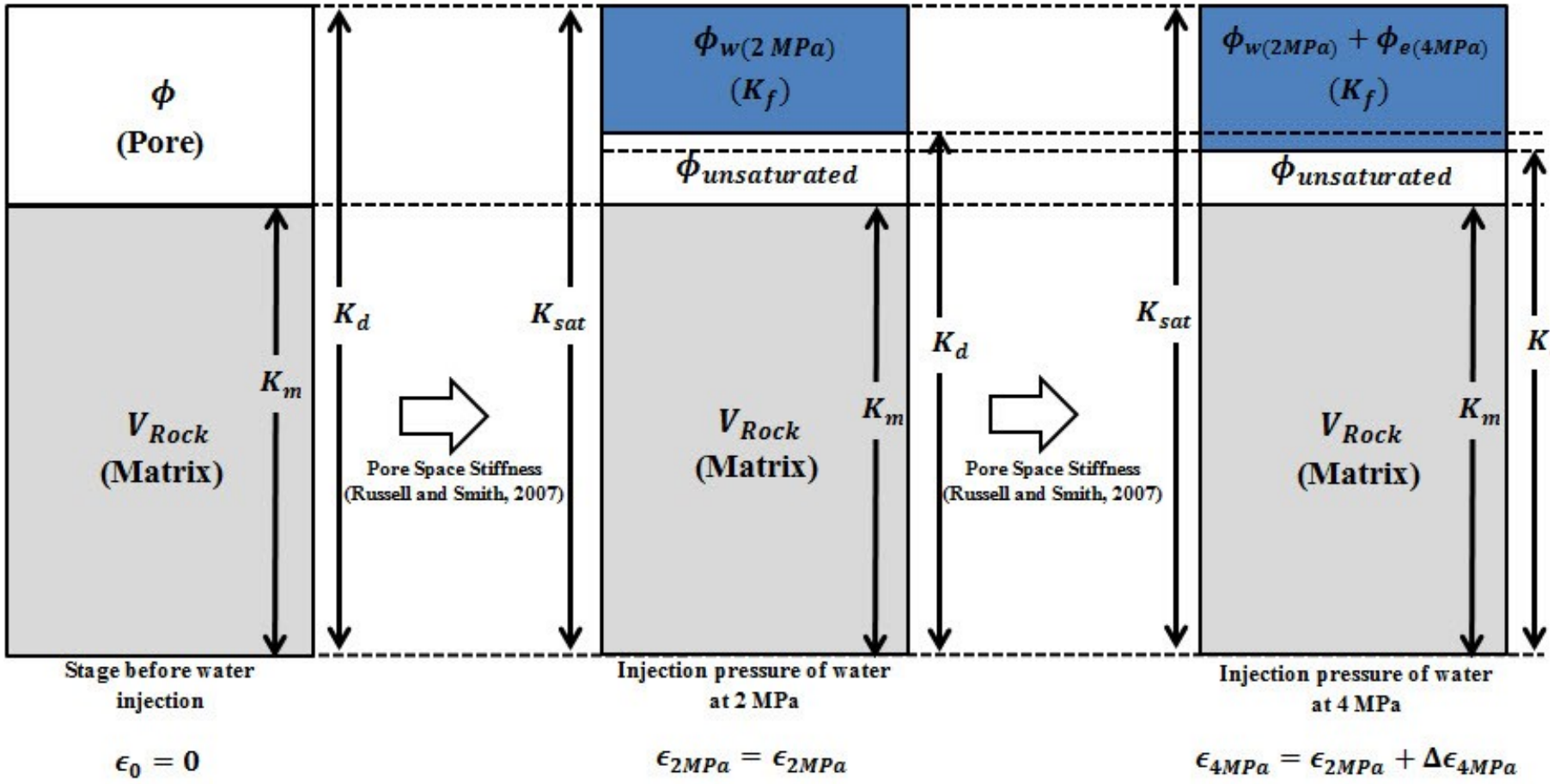


**Figure 6.9 Schematic of strain change simulations based on concept of effective porosity change**

### 6.7.3 Comparison of experimental and simulation results in water injection stage

Figure 6.7 shows that the simulation results without effective porosity change are totally different with experimental results. However, when applied effective porosity changes to the simulation, the simulation results were more consistent with experimental results. In addition, a trend of simulation results shows non-linear trend similar to experimental results. It might be explained by changes of effective porosity and effective bulk modulus of rock at each step, since injection pressure was not uniform. The results of both simulation and experiment are close together when a concept of effective porosity changes was applied to the simulation.

## 6.8 S.C. $CO_2$ injection stage

At conditions of 12 MPa confining pressure and 10 MPa pore pressure, $CO_2$ in supercritical state was injected from $CO_2$ syringe pump into the core sample from the bottom side of the core sample (see on Figure 6.3). The injection pressure of S.C.$CO_2$ was 10.05 MPa. Since the pressure difference between injection pressure and pore pressure was only 0.05 MPa, it takes long time to reach the stable state of strain changes. Also during injection of S.C.$CO_2$, the existing fluid was expelled from the top of the core sample through a water syringe pump. Strain was measured corresponding to elapsed time of S.C.$CO_2$ flows inside the core. The experimental results of time variation of strains according to the injection time are shown in Figure 6.10. In this experiment, injection rate of S.C.$CO_2$ was set as small amounts, so the low viscosity S.C.$CO_2$ could invade whole pores of the core sample. Finally, the change of strain became to zero after 12 hours of injection.

Comparing these three strain measurement experiments, the strain values of first and second stages are almost several hundred microstrains ($\mu\epsilon$) corresponding to the change of the effective pressures such as 2 to 10 MPa. At third stage experiment of S.C.$CO_2$ injection, the change of the effective pressure is only 0.05 MPa, however, the measured strain is also several hundred microstrains ($\mu\epsilon$). This is caused by the S.C.$CO_2$ properties, specially the low viscosity value of S.C.$CO_2$ (Rutqvist and Tsang, 2002; Chowdhury and Schmitt, 2012) compare to water.

A suspicion of strain changes at this stage is a high strain increment with elapsed time despite a small rate of pore pressure increase (0.05 MPa) was determined by simulation. These increased strains seem to be equal to an increase of strain at 7 MPa of pore pressure in water injection stage. A rate of pore pressure increase with 0.05 MPa is not certainly possible to generate a rate of strain increment in the laboratory testing for S.C.$CO_2$ injection stage. Consequently, this section considered that the high rate of strain increment of this stage is due S.C.$CO_2$ migration to narrow and small pores where water could not reach these pores during water injection stage because pore connections were closed together during increase of confining pressure.

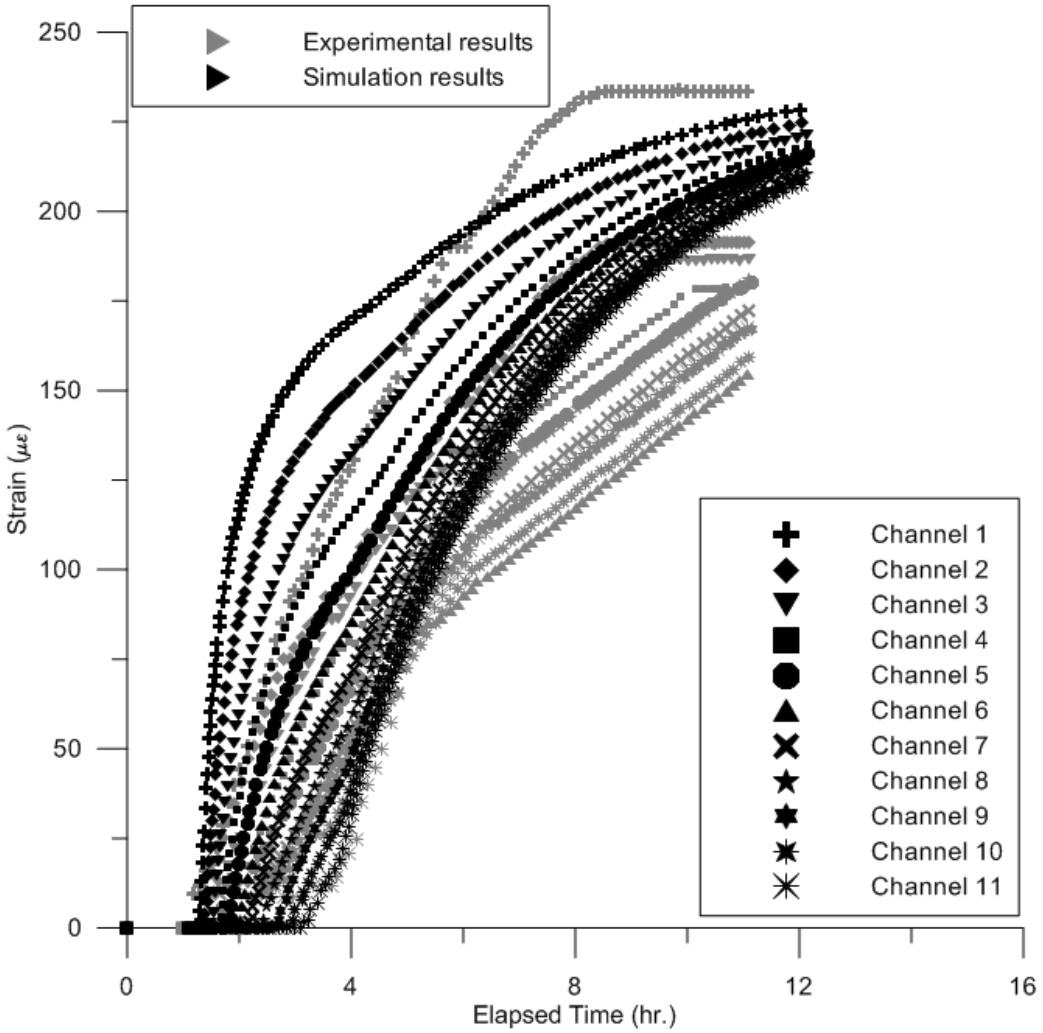


**Figure 6.10 Strain changes vs. elapsed time of S.C.$CO_2$ injection stage of Berea sandstone**

As known effective porosity at final stage of water injection, *i.e.* at 10 MPa of pore pressure the effective porosity is 19 % as shown in Table 6.2, and therefore pores, which will be occupied by S.C.$CO_2$ ($\phi_{CO_2}$), can be determined by a difference of initial porosity and effective porosity at 10 MPa of pore pressure (23 - 19 = 4 %). Afterward, a rock model was created to simulate a rock that has 4 % of porosity and effective bulk modulus of rock ($K_{(H_2O+CO_2)_{sat}}$), which saturated with S.C.$CO_2$, is 19.62 GPa as shown in Table 6.3.

**Table 6.3: Input parameters for simulation of S.C. $CO_2$ injection stage in Berea sandstone**

| $P_{CO_2-inj}$ (MPa) | $\phi_{CO_2}$ (%) | $K_{(CO_2)_{sat}}$ (GPa) |
|---|---|---|
| 10.05 | 4.0 | 19.62 |

Eq. 2.15 was used to determine a dry bulk modulus of rock due to porosity changes to 4 %, and then the effective bulk modulus of rock, which saturated with S.C.$CO_2$, was determined by Eq. 2.12. Finally, input parameters, as shown in Table 6.3, were used for simulation in this stage; they are S.C.$CO_2$ injection pressure ($P_{CO_2-inj.}$), porosity which will be occupied by S.C.$CO_2$ ($\phi_{CO_2}$), and effective bulk modulus of rock which saturated with S.C.$CO_2$ ($K_{(CO_2)_{sat}}$) Hence, in this stage, strain changes were generated from pore pressure change of 10.05 MPa.

## 6.8.1 Comparison of experimental and simulation results in S.C.$CO_2$ injection stage

Figure 6.11 represents changes of volumetric strains corresponding to pore pressure changes from simulation results. This figure is used to confirm that strain change of rock is in accord with changing pore pressure of rock. However, based on simulation results show that pore pressure change caused by S.C.$CO_2$ injection cannot be only one factor to consider rock deformation, the dry bulk modulus of rock change due to effective porosity change is also a factor which should be paid more attention.

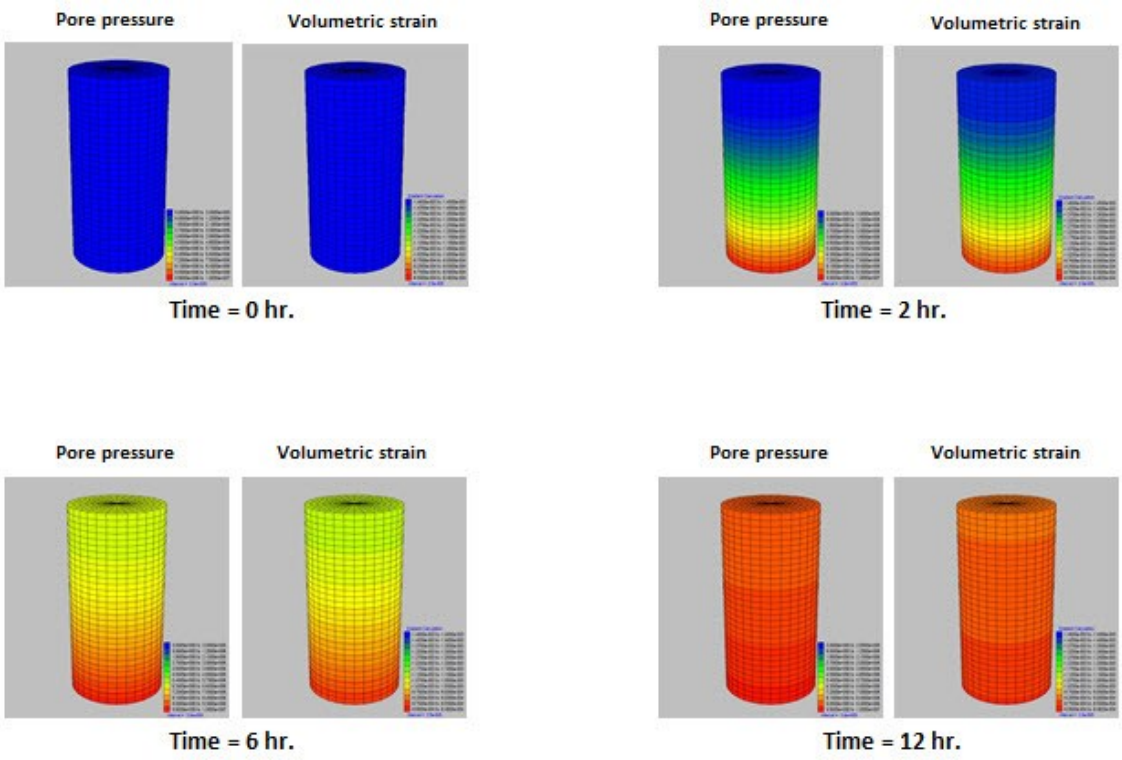


**Figure 6.11 Simulation results of volumetric strain changes with time corresponding with pore pressure changes in Berea sandstone**

In addition, motion of S.C.$CO_2$ front inside rock, which was represented by channel No. 1-11 of strain increases with elapsed times, can be explained by Figure 6.10. After applied a concept of effective porosity change to simulation in this stage, the simulation results showed

a good match with experimental results. There were differences on some channels between simulation and experimental results because the pore distributions in the real core sample were not perfectly uniform. The high rate of rock deformation is caused by the S.C.$CO_2$ properties, especially the low viscosity value compare to water, can move in the narrow pores with pore pressure change of 10.05 MPa.

## 6.9 Discussions and conclusions

Geomechanical simulation using FLAC3D simulator coupled with fluid-mechanic interaction feature was used in this study to explain rock deformations of laboratory experiments. At the same effective stress, the differences of strain changes because confining pressure and pore pressure increases, as shown in Figure 6.8, were significantly controlled by effective porosity and effective bulk modulus changes. Furthermore, a suspicion of high rate of strain increments in $CO_2$ injection stage can also be explained by changes of effective porosity and effective bulk modulus and the non-linear trend of experimental results of water injection stage is explained by non-uniform changes of effective porosity of water and effective bulk modulus of rock at each step of injection pressures. This study used information of injection volume of water from laboratory testing and Eq. 2.12, 2.15 and 6.7 to calculate effective porosity and effective bulk modulus of rock changes as input parameters as shown in Table 6.2 and 6.3 in cases of simulations. In addition, strain was increased corresponding to a flow of S.C.$CO_2$ front inside the core sample during S.C.$CO_2$ injection that can be monitored by a strain of each location (No. 1-11) of measurements and simulations.

Noticeably, this study revealed that increase of pore pressure or pressurization cannot be considered to be a main factor for the rock deformation caused by S.C.$CO_2$ injection into sandstone; the effective porosity change relating to change of dry bulk modulus of rock is also an important factor which should pay more attention.

The rock deformation due to injection or depletion of fluid inferring surface uplift and subsidence, has not been widely understood up-to-date. Geomechanics are used and discussed for how monitoring of geomechanical responses is used for detecting subsurface geomechanical changes and tracking fluid movements. Therefore, this study proposes and hopes that simulation results can help to understand the deformations of Berea sandstone, especially, for $CO_2$ injection in which it can be inferred on surface uplift problem of $CO_2$ storage in abandoned oil and gas fields, where are normally clastic (sandstone) reservoir rock.

# CHAPTER 7

# SIMULATION OF SUPERCRITICAL $CO_2$ INJECTION INTO TAKO SANDSTONE

## 7.1 Introduction

Keeping in mind that $CO_2$ in the supercritical state is highly sensitive to pressure change (Shukla *et al.*, 2011). The pressurization causes vertical expansion of the reservoir and changes in the stress field. These induced changes are proportional to the magnitude of the pressure increase and depend on the geometry and geomechanical properties of the reservoir and surrounding sediments. The vertical expansion of the reservoir may result in a ground surface deformation (Rutqvist, 2012). Laboratory core tests are the best source using for study on geomechanical model. According to rock formations in the real sites are not completely homogeneous and isotropic, and the simulations of heterogeneous rocks are still scanty.

Consequently, this study used geomechanical simulation to analyze and re-produce laboratory results of heterogeneous core sample in term of deformations as same as previous chapter. Strain changes of core sample in laboratory testing can be inferred to reservoir deformation relating to a surface uplift in field observation. Using FLAC3D simulator with a coupled fluid-mechanic interaction feature to simulate deformations of a core sample based on stages of laboratory experiments. The experiment remains to be divided into three stages in order to measure the strain, *i.e.*, (1) Confining pressure change stage, (2) Water injection stage (Pore pressure changes) and (3) Supercritical (S.C.) $CO_2$ injection stage, with continuous tests, respectively. There are just a few differences in cases of laboratory procedures. The relationship of effective porosity and effective bulk modulus changes proposed by Russell and Smith (2007), Mavko *et al.* (1998) and Gussmann's equation (Gussmann, 1951) was applied for simulations. Finally, the simulation results can help to understand the deformations of heterogeneous core sample in laboratory testing, especially a case of $CO_2$ injection in which it relates to Carbon dioxide Capture and Storage (CCS) project.

## 7.2 Objective

The purposes of this study were (1) to re-produce and analyze deformation of a heterogeneous and anisotropic rock from laboratory experiments (2) to monitor a motion of supercritical $CO_2$ in the rock sample influencing heterogeneous rock deformation.

## 7.3 Information of laboratory experiments for strain measurements

Laboratory experiment and main objective in this study were setup to emulate surface uplift problem in CCS site, and the strain changes of heterogeneous core sample were observed by using the optical fiber as same as Berea sandstone's experiments in previous chapter.

**Figure 7.1 Core sample of Tako sandstone**

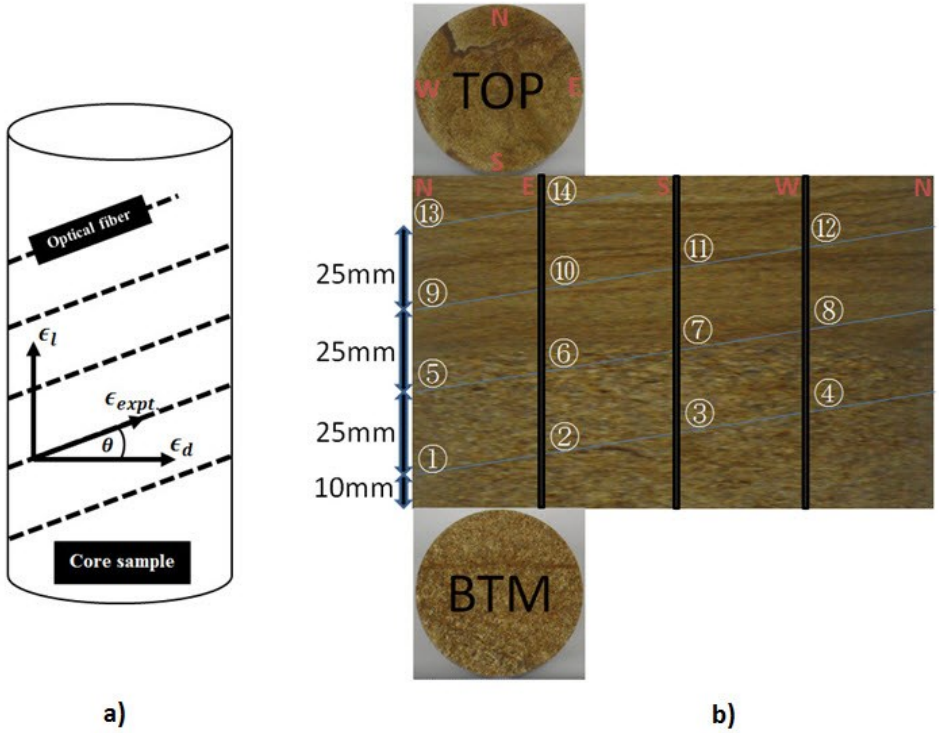


**Figure 7.2 Schematic of Tako core sample measuring by optical fiber a) overview of Tako sandstone core sample b) planar view representing the channel locations of optical fiber measurements**

A core sample of Tako sandstone (Figure 7.1) was selected as a heterogeneous and anisotropic reservoir and Tako core sample in this study shows clearly two parts, *i.e.* a bottom half of sample is coarse-grain part and a top half of sample is fine-grain part.14 channels of optical fiber data are acquired; the channel 1 to 7 were represented strain changes of coarse-grain part, while the channel 8 to 14 were represent strain changes of fine-grain part. The locations and the directions of strain measurements are shown in Figure 7.2. A schematic of three stage experiments can be seen in Figure 6.3 and the conditions of each stage can be seen on Figure 6.4 except the injection pressure of S.C.$CO_2$ was changed to 10.5 MPa.

## 7.4 Information of simulations for strain measurements

FLAC3D (Itasca, 2006a) was also used as a simulator for geomechanical simulations in this study. Model geometry was created corresponding to the two parts of core sample in the laboratory. The size of core sample is 5 cm of diameter and 10 cm of length as same as the Berea core sample. The core sample was discretized into 3-dimensional mesh, the mesh size of coarse-grain part in x, y, and z direction was 16x16x16, while the mesh size of fine-grain part was 32x32x32 as shown in Figure 7.3. The fine-grain part was thoroughly discretized because it has low permeability and porosity so that it will be considered more complex deformation than coarse-grain part. The calculating volumetric strains were consistent with the same locations and directions of strain measurements of optical fiber (Figure 7.2) in the laboratory. The simulations required in unsupported system for the core sample, and thus the confining pressure with hydrostatic loading condition was performed as mechanical boundary condition and elastic model was used for simulations. Rock properties of Tako sandstone were used as input parameters, and they are shown in Table 7.1.

**Table 7.1: Physical properties of Tako sandstone**

| Parameter | Value |
|---|---|
| Dry bulk modulus ($K_d$, GPa) | ~13.3 |
| Shear modulus ($G$, GPa) | ~7.0 |
| Dry density ($\rho$, kg/m$^3$) | 1900 |
| (Initial average) Porosity ($\phi$, %) | 27.8 |
| Permeability ($K$): | |
| - Fine-grain part (μD) | 100 |
| - Coarse-grain part (mD) | 10 |
| Coefficient of pore space stiffness ($k$) | 0.15 |
| Pore space stiffness ($K_\phi$, GPa) | 5.4 |

The volumetric strain from simulation in this study was also converted to experimental strain ($\epsilon_{expt.}$) in the direction which was measured by optical fiber by using Eq. 6.1 and 6.2 as explained in section 6.5 of Berea sandstone's simulations.

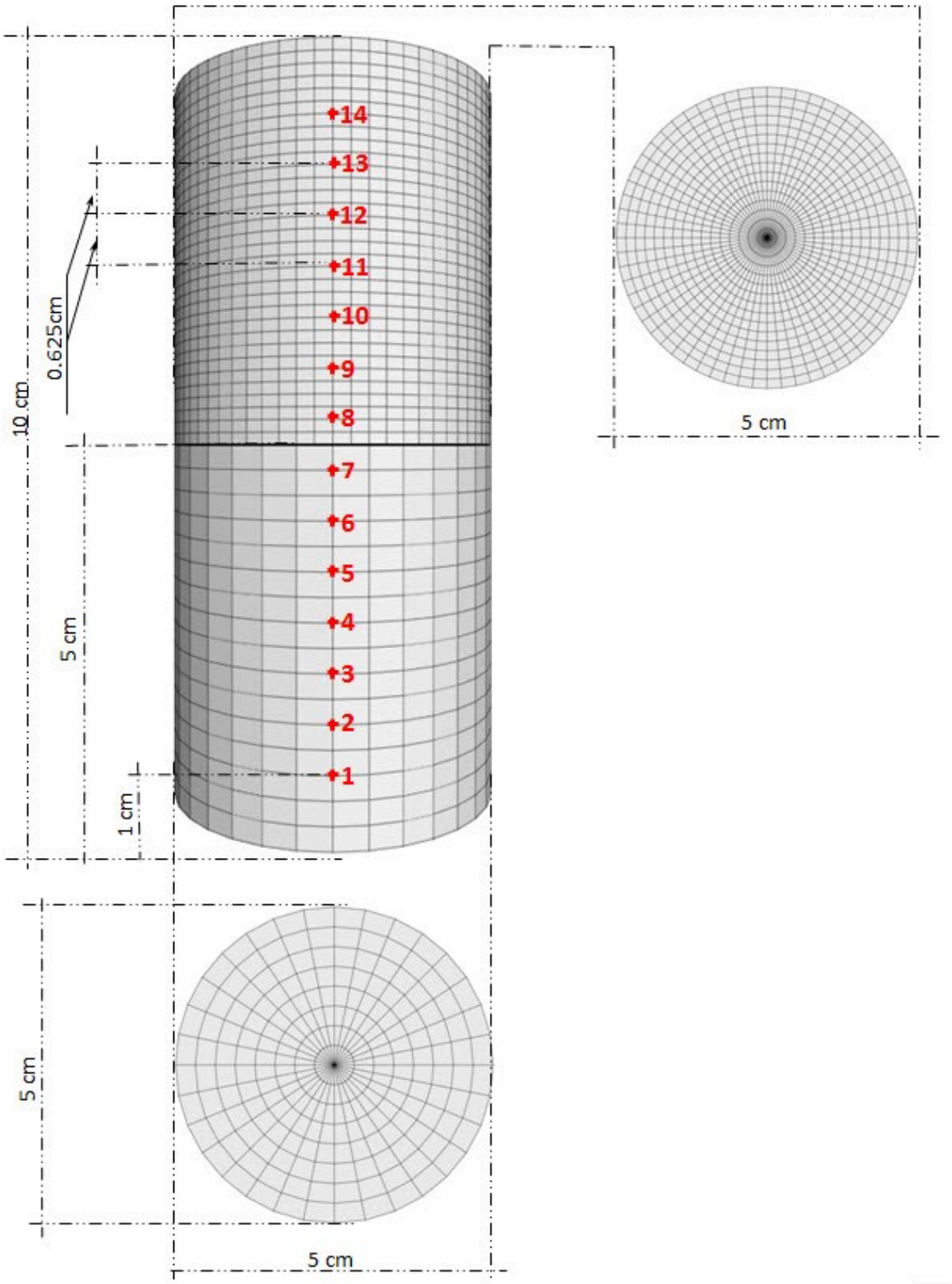


**Figure 7.3 Model geometry and the locations of simulation strains of Tako core sample**

## 7.5 Confining pressure change stage

All procedures in this stage were the same as Berea sandstone's experiments. The strain was measured by optical fiber at each step of confining pressure changes (Figure 7.4). The observed values of strains were negative values because the core was shrinking according to the increasing of the confining pressures.

In case of simulation, rock is in a dry condition, and thus only mechanical processes were working in this stage and there is no the effect of fluid flow. Rock deformations or strain ($\epsilon$) are followed Eq. 6.3 and the volumetric strain in FLAC3D is derived from Eq. 6.5.

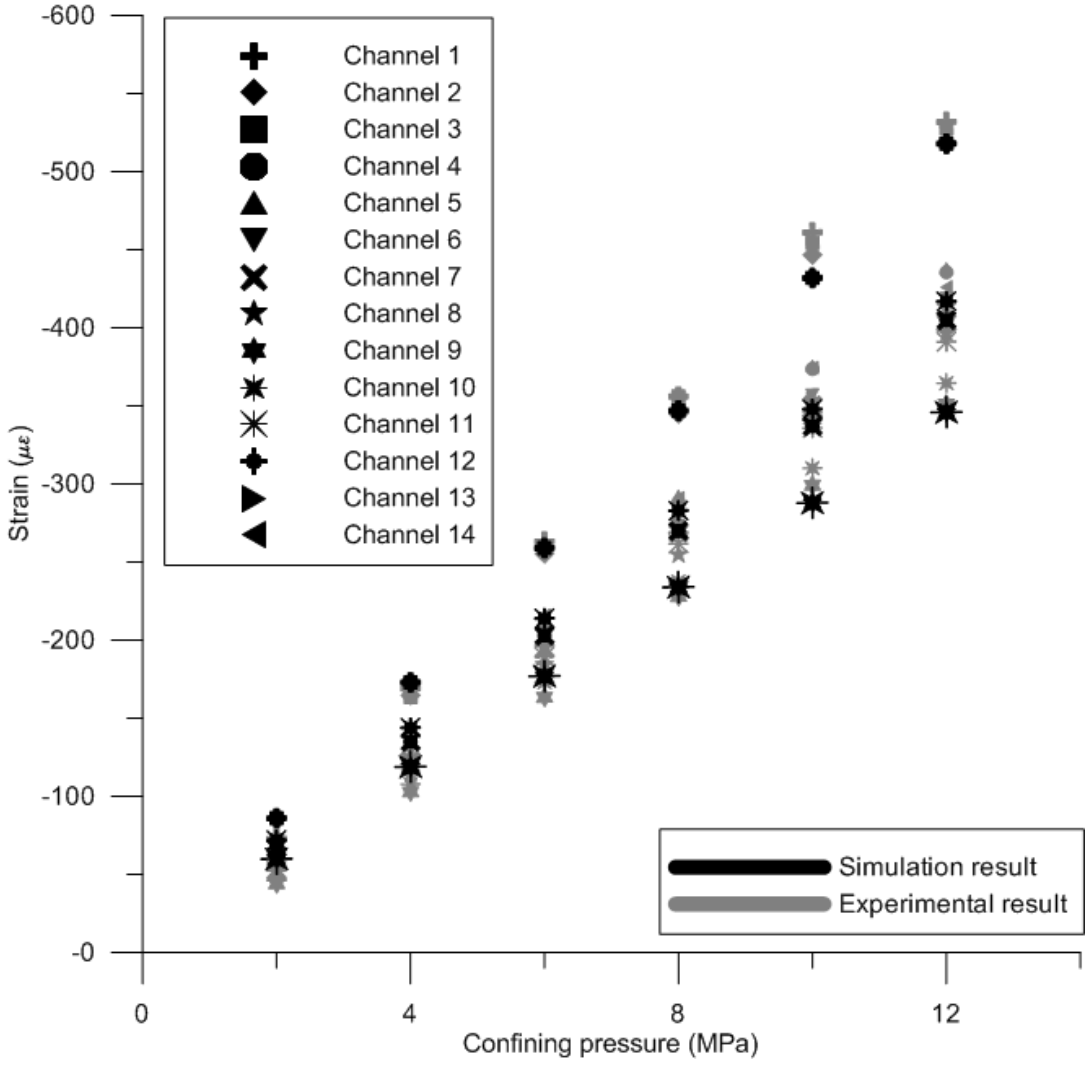


**Figure 7.4 Comparison between simulation and experimental results of confining pressure change stage of Tako sandstone**

### 7.5.1 Rock deformation in coarse-grain part at confining pressure change stage

Figure 7.4 shows very clear on the differences between two parts in deformations. However, at each part, they also show differences of deformation in which they will be discussed here and in the next section. In the coarse-grain part, Figure 7.5 shows two groups of deformation (shrinkage) in this stage. The first group, *i.e.* the channel no. 1-3, was more shrunk and was called coarse layer, while one another group (Channel no. 4-7) demonstrated the less deformation and was called coarse-transition layer. The differences show more increase with increasing of confining pressure.

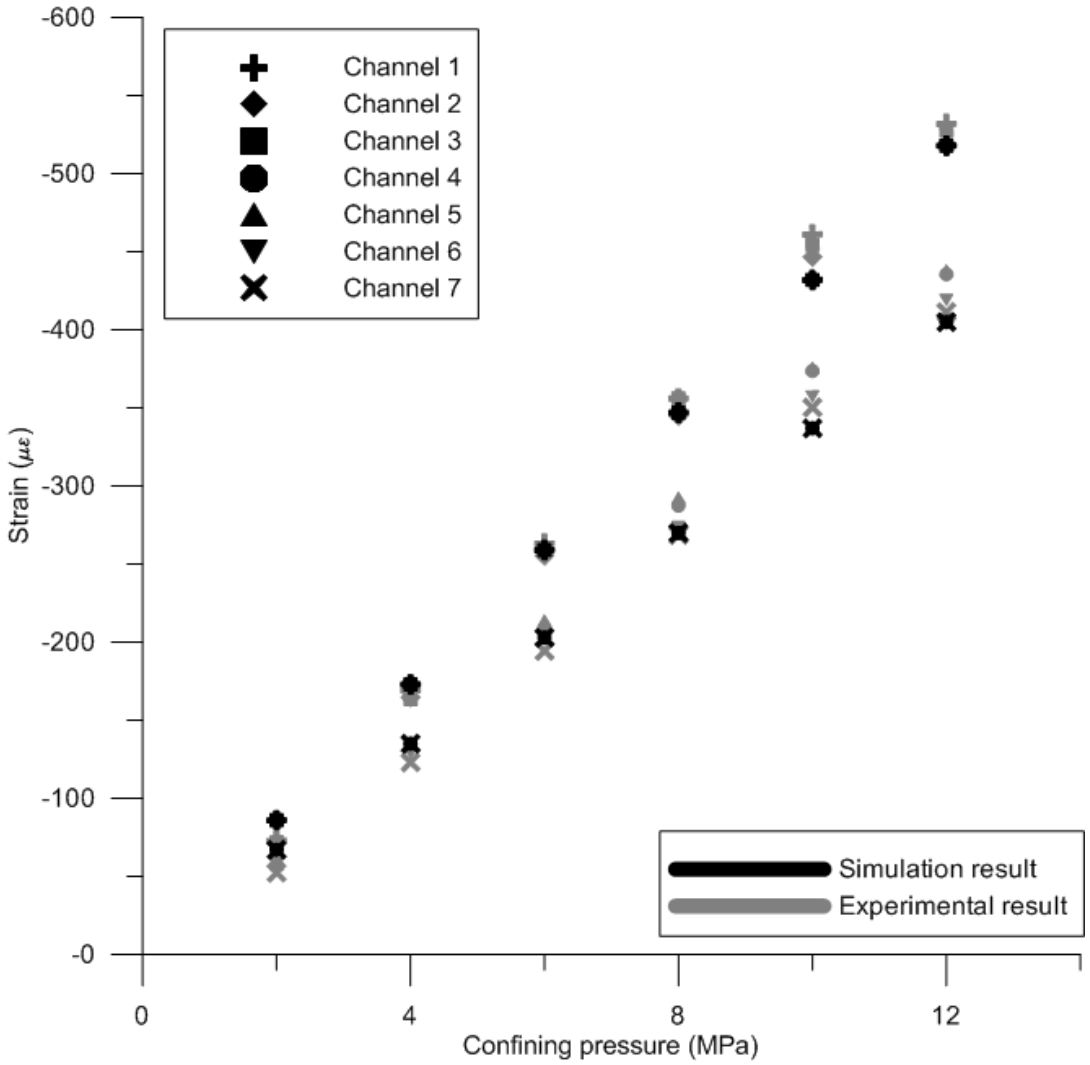


**Figure 7.5 Tako sandstone's deformations in coarse layers of simulation and experimental results of confining pressure change stage**

## 7.5.2 Rock deformation in fine-grain part at confining pressure change stage

At fine-grain part, the deformation (shrinkage) as shown in Figure 7.6 also separated into two groups. The higher shrinkages (Channel no. 11-14) were called fine layer, while the lower

shrinkages (Channel no. 8-10) were called fine-transition layer. The different deformations of both groups in this section also show that the difference was high when confining pressure was increased.

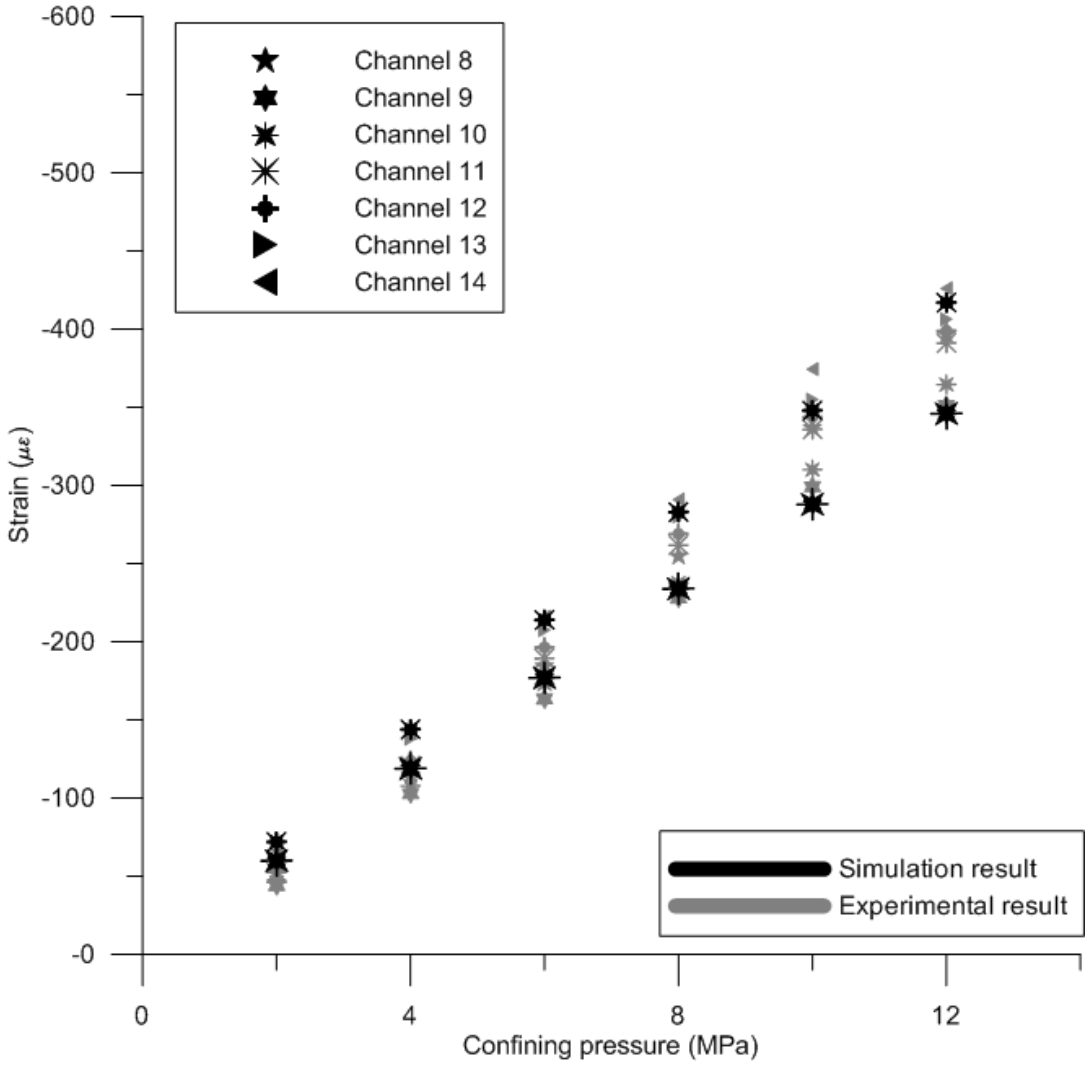


**Figure 7.6 Tako sandstone's deformations in fine layers of simulation and experimental results of confining pressure change stage**

## 7.5.3 Comparison of experimental and simulation results in confining pressure change stage

The strain decreases due to increase in confining pressure (Figure 7.4) in both case of simulation and experiment. This study simulated deformations of rock in this stage using trial and error of dry bulk modulus of rock as input parameters as shown in Table 7.2. In the final, the simulation results seem to be consistent with experimental results and show almost straight line.

As mentioned that the core sample was divided into 4 layers, *i.e.* coarse layer, coarse-transition layer, fine layer and fine-transition layer, and the coarse-grain part was more deformed than fine-grain part (including transition layers). This is because the poorly sorted grains in coarse-grain part are more compressible than the well sorted grains in fine-grain part following compaction concept of Meade (1966) as shown in Figure 7.7. Table 7.2 shows that dry bulk modulus of rock ($K_d$) changed only in fine and fine-transition layer, this means that the effective porosity of rock, might be decreased since the pore space compressibility ($K_\phi$) is smaller than the dry bulk modulus ($K_d$) and caused increase of $K_d$ due to pore connection closing, affected only in fine-grain part. On the other hands, coarse and coarse-transition layers which have more spaces so that the pore connection closing did not influence in coarse-grain part. Consequently, $K_d$ of these layers (coarse and coarse-transition layers) in Table 7.2 shows constant numbers throughout confining pressure changes. The calculations of porosities (Table 7.2) used Eq. 2.15 and Figure 2.16, and the coefficient of pore space stiffness ($k$) was 0.15 in which mineral bulk modulus of quartz ($K_m$= 36 GPa) represented matrix bulk modulus of Tako sandstone. The calculation of average porosity at 2 MPa of confining pressure was very close to initial porosity of Tako sandstone (Table 7.1), and therefore the dry bulk modulus of Tako sandstone at atmosphere condition was concluded that is very close to 13.3 GPa (average $K_d$ of 2 MPa confining pressure in Table 7.2). In addition, Figure 7.4 shows the strain changes are straight line trends and the different deformations in coarse-grain part were more than fine-grain part when confining pressure was increased. Finally, in this stage the rock behaved deformations as a simple contraction in this stage.

With increasing confining pressure, variations of strain measurement at each location become visible in the same with Figure 6.6 in section 6.6. This is also due to inhomogeneous of confining pressure exerted on the sample and the core sample itself.

**Table 7.2: The relationship of dry bulk modulus and porosity of Tako sandstone at each confining pressures**

| $P_c$ (MPa) | Coarse layer | | Coarse-Transition layer | | Fine-Transition layer | | Fine layer | |
|---|---|---|---|---|---|---|---|---|
| | $K_d$ (GPa) | $\phi$ (%) | $K_d$ (GPa) | $\phi$ (%) | $K_d$ (GPa) | $\phi$ (%) | $K_d$ (GPa) | $\phi$ (%) |
| 2 | 10.9 | 27.63 | 13.8 | 25.74 | 15.5 | 26.45 | 13.0 | 27.42 |
| 4 | 10.9 | 27.63 | 13.8 | 25.74 | 15.6 | 26.15 | 13.1 | 27.10 |
| 6 | 10.9 | 27.63 | 13.8 | 25.74 | 15.7 | 25.86 | 13.2 | 26.77 |
| 8 | 10.9 | 27.63 | 13.8 | 25.74 | 15.8 | 25.57 | 13.3 | 26.45 |
| 10 | 10.9 | 27.63 | 13.8 | 25.74 | 15.9 | 25.28 | 13.5 | 25.83 |
| 12 | 10.9 | 27.63 | 13.8 | 25.74 | 15.9 | 25.28 | 13.5 | 25.83 |

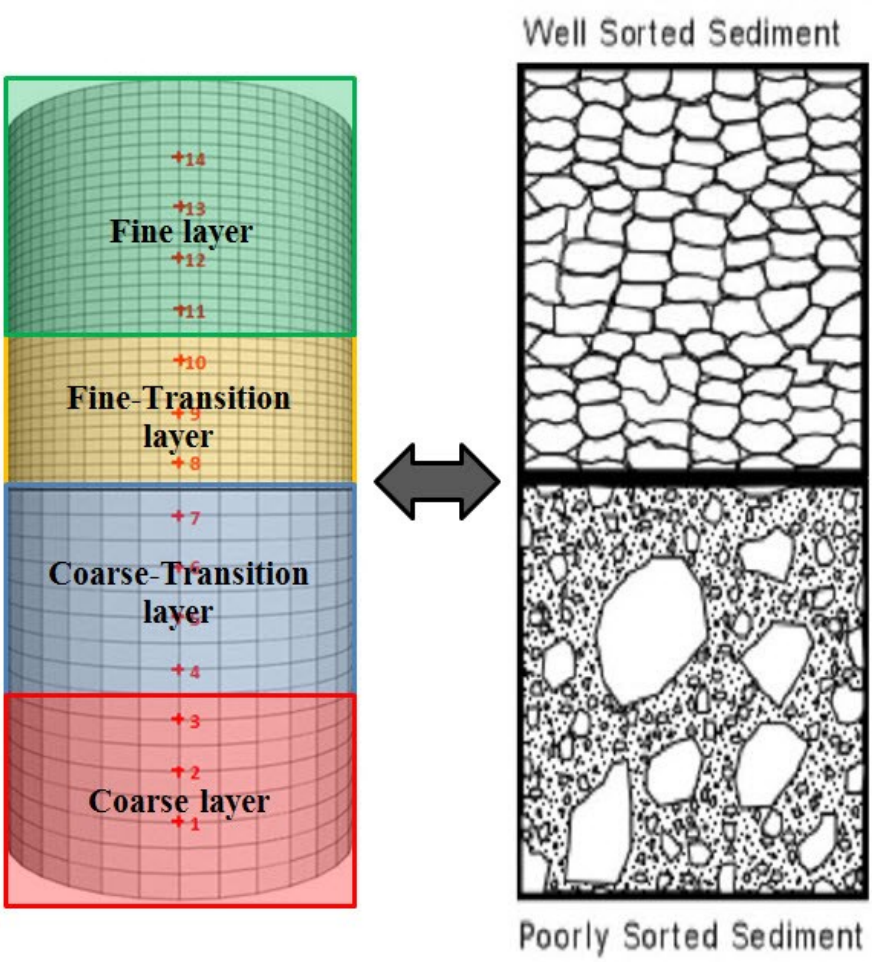


**Figure 7.7 Four layers of Tako core deformation demonstrating sorted sediments at each layer**

## 7.6 Water injection (pore pressure change) stage

After confining pressure change stage, was reached at 12 MPa, the water injection stage were performed continuously. Almost procedures were the same as Berea sandstone's experiment, but, in this stage, the water was injected at the bottom of the sample. Therefore, the valve at the outlet of water (see on Figure 6.3) was closed at the top, and therefore the water did not flow out the core sample and it was not 100% water saturation state. The volume of injection water was measured at each injection pressure, and there were 40.67 ml and 41.56, 42.14, 42.73, 43.36 ml respectively, Strain changes of experimental results are shown in Figure 7.8 at each injection pressures were caused due to increased pore pressures.

The variations of strain measurement at each layer of water injection stage (Figure 7.8) were less than confining pressure change stage (Figure 7.4). This is because fluid was injected to sample directly and, after confining pressure was reached at 12 MPa, all of channels were set at zero microstrain before water injection in order to measure deformations induced by water injection.

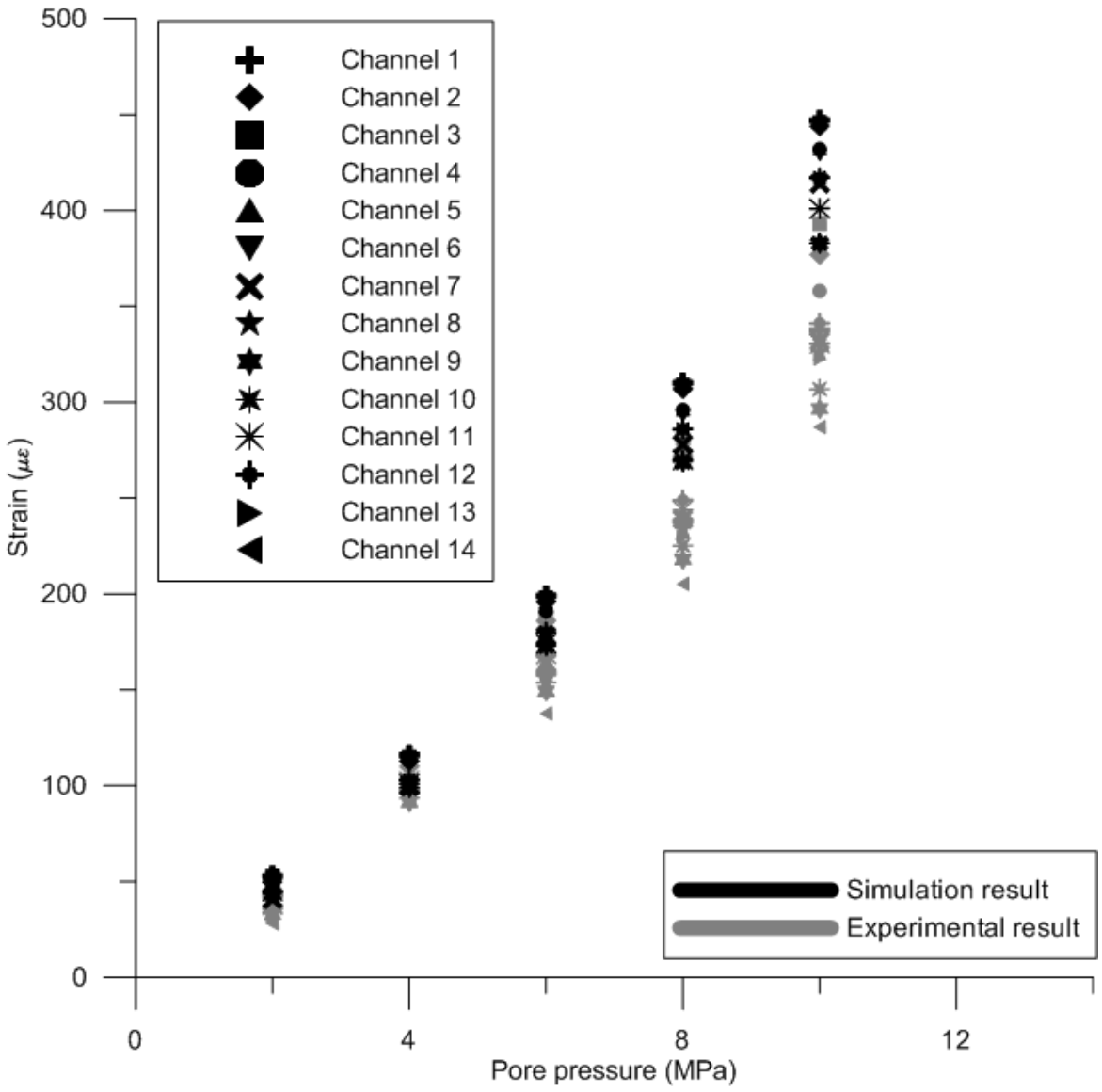


**Figure 7.8 Comparison between simulation and experimental results of water injection stage of Tako sandstone**

## 7.6.1 Simulation of strain change in water injection stage

The coupled fluid flow and mechanical simulations were performed using FLAC3D following Eq. 6.6. Biot's coefficient, $\alpha$, also keep unity for loose sediments during effective stress changes.

The relationship of changes of effective porosity and dry bulk modulus of rock was conducted in this section. As mentioned above, effective porosity changes by pore closing or opening, then this change of effective porosity affects changes of $K_{d\ (new)}$(Figure 2.16 and Eq. 2.15). Furthermore, it needs to evaluate effective bulk modulus of rock, which is saturated with water.

The data of injection volume of water from laboratory testing was shown in Table 7.3. The concept of effective porosity was adopted in order to evaluate bulk modulus of core sample saturated with water. Consequently, the input parameters of modifications of dry bulk modulus and effective bulk modulus of rock substituted with water were also shown in Table 7.3. The $\phi_w$ in the Table 7.3 is the porosity which was occupied by injected water, while $\phi_e$ is the effective porosity which increased with increases of injection pressures. Therefore, the strain changes can be determined by simulations of strain changing at each stage of injection pressure based on concept of effective porosity change.

**Table 7.3: Information of injection volume of water, effective porosity, effective porosity of water and modification of effective bulk modulus of rock**

| $P_p$ (MPa) | $V_{H_2O}$ (ml) | $\phi_w(\%) = \frac{V_{H_2O}}{V^a_{rock}}$ | $\phi_e$ (%) | $K_{H_2O-sat}$ (GPa) |
|---|---|---|---|---|
| 2 | 40.67 | 20.7 | - | 18.04 |
| 4 | 41.56 | 21.2 | 0.5 | 34.95 |
| 6 | 42.14 | 21.5 | 0.3 | 35.31 |
| 8 | 42.73 | 21.8 | 0.3 | 35.30 |
| 10 | 43.36 | 22.1 | 0.3 | 35.25 |

[a] *Rock volume, $V_{rock}$, is 196.35 $cm^3$*

The porosity is change according to effective pressure change can also be explained by Figure 6.9. At this stage also assumed that $K_f$ is the bulk modulus of water ($K_f = 1$ GPa) for a given pressure and temperature in which the effect of air, even the air exists in the pore space, was omitted. Using the relationship of dry bulk modulus and effective porosity, the simulations of the strain behaviors of the rock sample can be simulated by using parameters which show in Table 7.4. The average effective bulk modulus of rock in Table 7.4 is the same as Table 7.3.

**Table 7.4: The effective bulk modulus of rock using for input parameters of simulations of water injection stage**

| $P_p$ (MPa) | Coarse layer | Coarse-Transition layer | Fine-Transition layer | Fine layer | Average |
|---|---|---|---|---|---|
| | $K_{H_2O-sat}$ (GPa) | $K_{H_2O-sat}$ (GPa) | $K_{H_2O-sat}$ (GPa) | $K_{H_2O-sat}$ (GPa) | $K_{H_2O-sat}$ (GPa) |
| 2 | 17.08 | 17.08 | 19.00 | 19.00 | 18.04 |
| 4 | 30.50 | 32.50 | 38.30 | 38.50 | 34.95 |
| 6 | 33.00 | 36.00 | 36.12 | 36.12 | 35.31 |
| 8 | 33.00 | 36.00 | 35.01 | 37.20 | 35.30 |
| 10 | 33.00 | 34.00 | 35.00 | 39.00 | 35.25 |

## 7.6.2 Rock deformation in coarse-grain part at water injection stage

Figure 7.9 shows core sample deformations (expansions) in coarse (Channel no. 1-3) and coarse-transition (Channel no. 4-7) layers of water injection stage. The expansions increase with increases of pore pressures and they were represented by non-linear trend. In addition, they show more variations when pore pressure was increased. The simulation results seem to be overestimations at high pore pressures ($P_p = 8$ and 10 MPa) as same as Berea sandstone's water injection stage (section 6.7). This is because the strain change in water injection stage is controlled by several factors as shown in Eq. 6.6, and therefore the simulation in water injection stage was more complex than the simulation of confining pressure change stage.

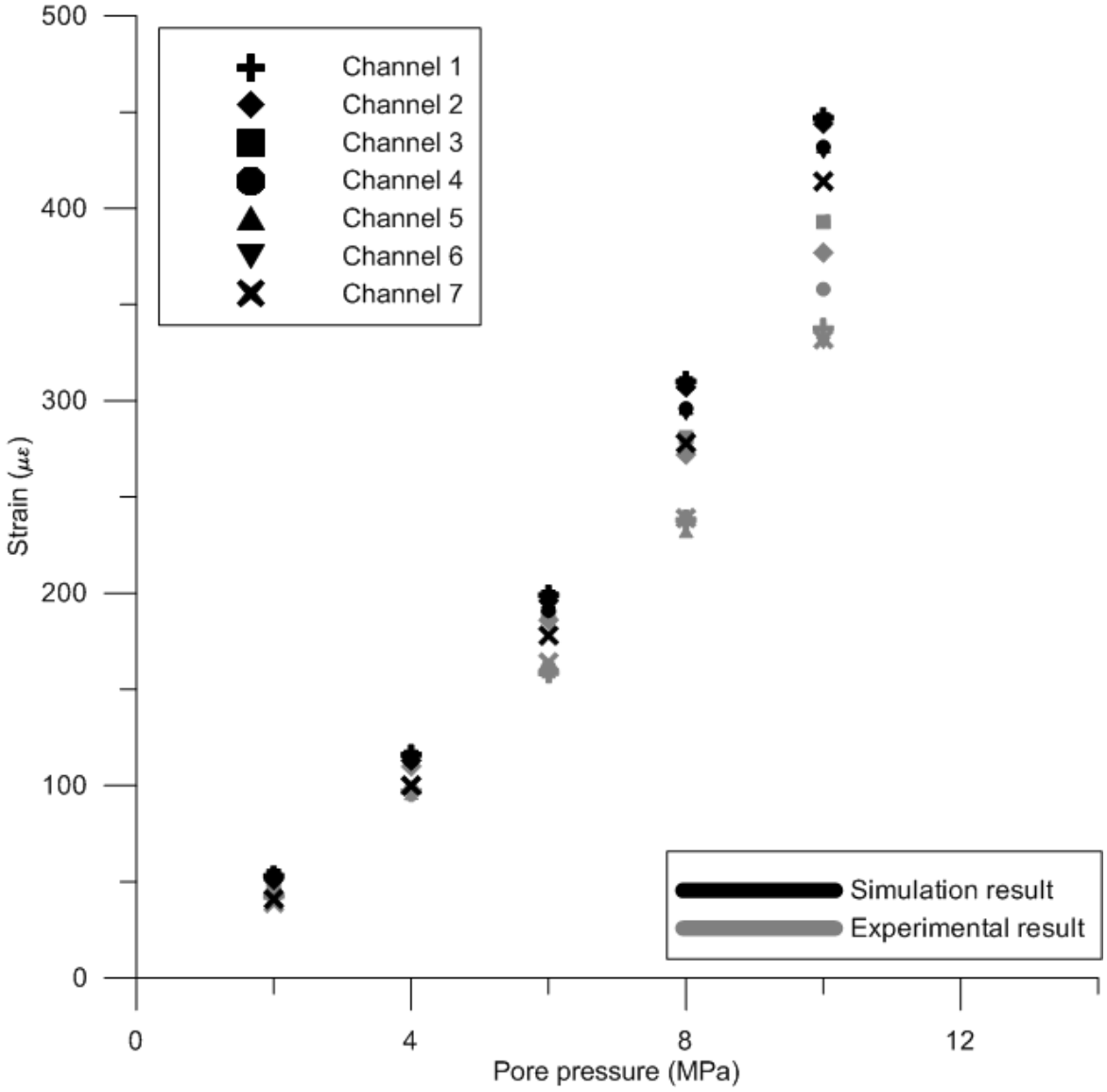


**Figure 7.9 Tako sandstone's deformations in coarse layers of simulation and experimental results of water injection stage**

## 7.6.2 Rock deformation in fine-grain part at water injection stage

The simulation results in fine (Channel no. 11-14) and fine-transition (Channel no. 8-10) layers also show overestimations comparing with experimental results. The fine layer was more deformed than transition layer except the strain of channel no. 14 from experimental results. This might be due to, in real situation, the water could not reach this position where has very low permeability. The expansion trend in this part shows a little curvature comparing with coarse-grain part.

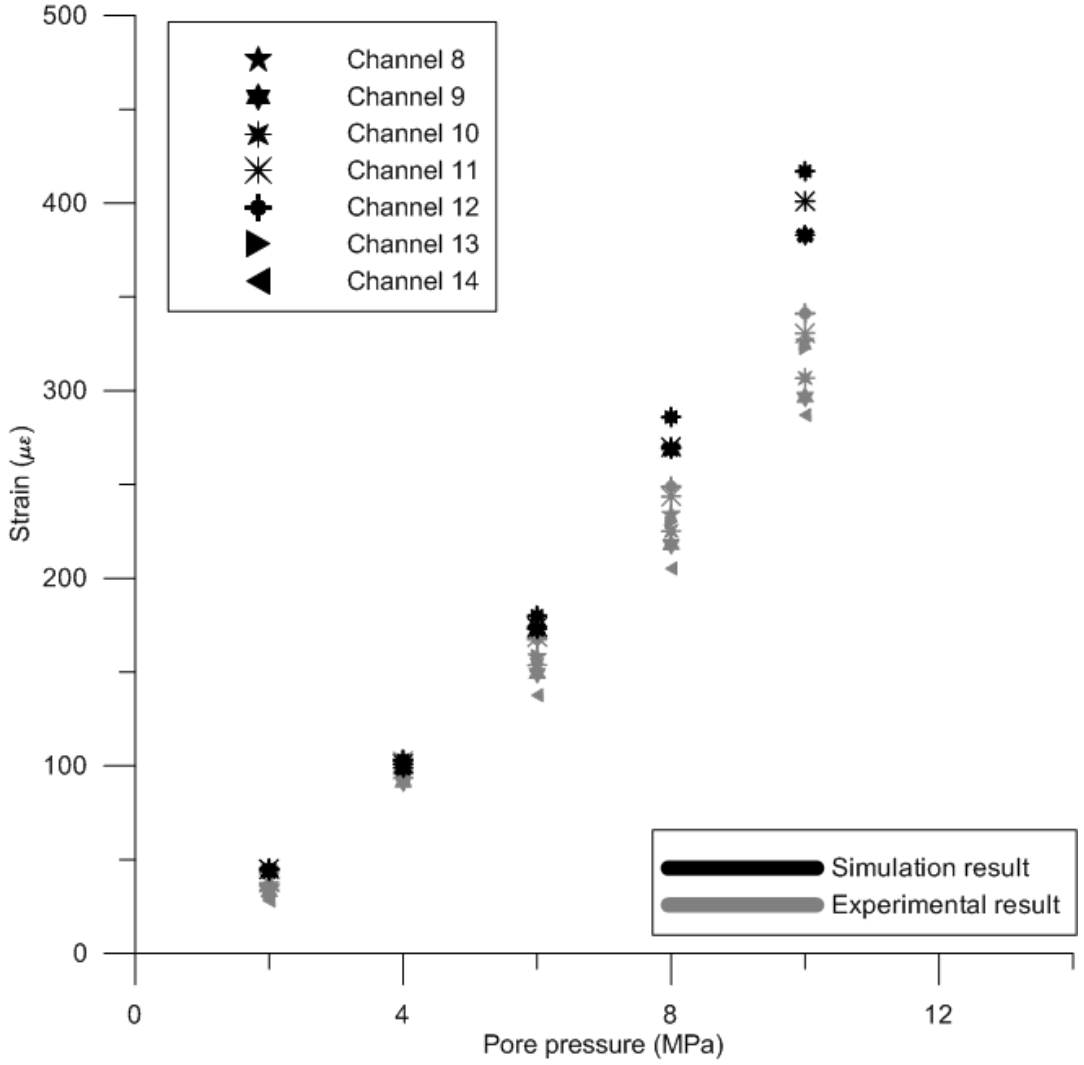


**Figure 7.10 Tako sandstone's deformations in fine layers of simulation and experimental results of water injection stage**

## 7.6.3 Comparison of experimental and simulation results in water injection stage

Figure 7.8 shows that the coarse-grain part was more deformations than the fine-grain part both simulation and experimental results. This might be due to the water can be accumulated more at coarse-grain part, which have higher porosity and permeability, than fine-grain part where have lower porosity and permeability. A trend of simulation results shows non-linear

trend similar to experimental results. The transition layers could be seen clearly at high pore pressures (8 and 10 MPa) comparing at low pore pressure (2, 4 and 6 MPa). The deformations (expansions) in this stage can be explained by changes of effective porosity and effective bulk modulus of rock.

## 7.7 S.C.$CO_2$ injection stage

The injection pressure of S.C.$CO_2$ was 10.5 MPa. This is different from Berea sandstone's experiments (10.05 MPa of S.C.$CO_2$ injection pressure) in S.C.$CO_2$ injection stage because the permeability of Tako sandstone is lower than Berea sandstone. However, the pressure difference between injection pressure and pore pressure was still low (0.5 MPa), it takes very long time to reach the stable state of strain changes than Berea sandstone. In addition, the existing fluid was expelled from the top of the core sample through a water syringe pump as same as Berea sandstone's experiment. Strain was measured corresponding to elapsed time of S.C.$CO_2$ flows inside the core. The experimental results of time variation of strains according to the injection time are shown in Figure 7.11. In this experiment, the low viscosity S.C.$CO_2$ could invade whole pores of the core sample. Likewise, this experiment also confirmed that the change of the pore pressure alone (only 0.5 MPa) could not produce the measured strain in several hundred microstrains (με). The S.C.$CO_2$ properties, specially the low viscosity value of S.C.$CO_2$ compare to water, were one effective factor for deformation induced by S.C.$CO_2$ injection.

The suspicious strain at this stage was determined by simulation. A rate of pore pressure increase with 0.5 MPa is not possible to generate a rate of strain increment in the laboratory testing for S.C.$CO_2$ injection stage. Consequently, the high rate of strain increment, in this stage, is due to S.C.$CO_2$ migration to narrow and small pores where water could not reach these pores during water injection stage because pore connections were closed together during increase of confining pressure. In the experiments, the effective porosity at final stage of water injection, *i.e.* at 10 MPa of pore pressure, the effective porosity is 22.1 % as shown in Table 7.3. The initial porosity of Tako sandstone is average 27.8% (as same as reported by Kitamura and Xue, 2007). Therefore, pores, which will be occupied by S.C.$CO_2$ ($\phi_{CO_2}$), can be determined by a difference of initial porosity and effective porosity at 10 MPa of pore pressure (27.8 – 22.1 = 5.7 %). Afterward, a rock model was created to simulate a rock that has 5.7 % of porosity and effective bulk modulus of rock ($K_{(CO_2)_{sat}}$) which saturated with S.C.$CO_2$, is 26.11 GPa as shown in Table 7.5.

**Table 7.5: Input parameters for simulation of S.C. $CO_2$ injection stage in Tako sandstone**

| $P_{CO_2-inj}$ (MPa) | $\phi_{CO_2}$ (%) | $K_{(CO_2)_{sat}}$ (GPa) |
|---|---|---|
| 10.5 | 5.7 | 26.11 |

**Table 7.6: The effective bulk modulus of Tako sandstone using for input parameters of simulations of S.C.$CO_2$ injection stage**

| $P_{CO_2-ing.}$ (MPa) | Coarse layer | Coarse-Transition layer | Fine-Transition layer | Fine layer | Average |
|---|---|---|---|---|---|
| | $K_{(CO_2)sat}$ (GPa) | $K_{(CO_2)sat}$ (GPa) | $K_{(CO_2)sat}$ (GPa) | $K_{(CO_2)sat}$ (GPa) | $K_{(CO_2)sat}$ (GPa) |
| 10.5 | 30.02 | 25.20 | 27.20 | 22.02 | 26.11 |

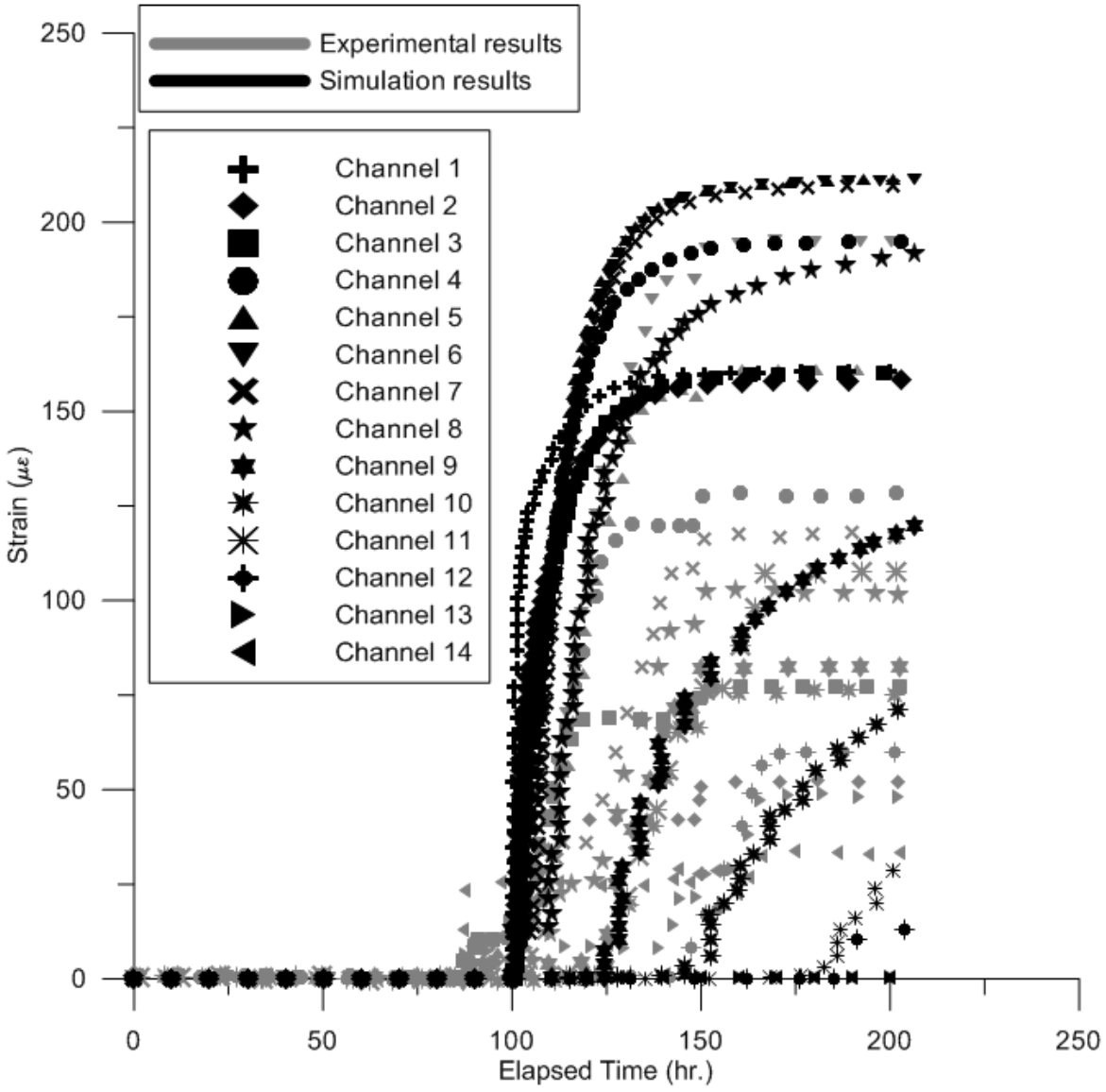


**Figure 7.11 Comparison between simulation and experimental results of S.C.$CO_2$ injection stage of Tako sandstone**

Table 7.6 represents the calculated dry bulk modulus of Tako sandstone at each layer as input parameters using in simulation. Eq. 2.15 and 2.12 were used to determine a dry bulk modulus

of rock due to porosity changes to 5.7 %, and the effective bulk modulus of rock which saturated with S.C.$CO_2$. The fluid bulk modulus of S.C.$CO_2$ is equal to 0.059 GPa, as same as Berea sandstone's S.C.$CO_2$ injection stage. Finally, all input parameters here were used for simulation in this stage, and strain changes were generated from pore pressure change of 10.5 MPa.

### 7.7.1 Comparison of experimental and simulation results in S.C.$CO_2$ injection stage

The strains change corresponding to pore pressure changes are common in mechanical deformation of rock. However, simulation results show that pore pressure change caused by S.C.$CO_2$ injection cannot be only one factor to consider rock deformations, the dry bulk modulus of rock change due to effective porosity change is also a factor which should be paid more attention.

A motion of S.C.$CO_2$ front inside rock, which was represented by channel No. 1-14 of strain increases with elapsed times, can be explained by Figure 7.11. This figure shows that rock deformed due to pore pressure generating from S.C.$CO_2$ front flow. However, in coarse-grain part, both simulation and experimental results show the same results that coarse-transition layer was more expanded than coarse layer, this results was not in consistent with rock deformed corresponding with S.C.$CO_2$ front flow (strain should be increased corresponding with S.C.$CO_2$ flow). It can be explained that when the S.C.$CO_2$ flowed through high porosity and permeability (Coarse-grain part) to low porosity and permeability (Fine-grain part), some S.C.$CO_2$ flowed back and accumulated at coarse-transition layer in a given time. Therefore, coarse-transition layer would deform more than other layers. The coarse-grain part were more deformation than fine-grain part as same as the first and second stages because they have more spaces in cases of accumulations with fluid.

Furthermore, the concept of effective porosity change was used for simulation in this stage, the simulation results showed a good match with experimental results. There were differences on some channels between simulation and experimental results because the pore distributions in the real core sample were not perfectly uniform. Finally, the high rate of rock deformation could be concluded that the S.C.$CO_2$ properties, especially the low viscosity value compare to water, were an important factor to move in the narrow pores and generate pore pressure change of 10.5 MPa influencing rock deformations.

## 7.8 Discussions and conclusions

The complex deformations caused by S.C.$CO_2$ injected into heterogeneous and anisotropic rock, such as Tako sandstone, could be simulated by using FLAC3D simulator coupled with fluid-mechanic interaction feature to explain laboratory experiments. A suspicion of high rate of strain increments in $CO_2$ injection stage also occurred in Tako sandstone as same as Berea sandstone. The changes of the effective porosity and the effective bulk modulus were used to

explain this suspicion. Based on simulations and experiments the Tako sandstone showed transition layers in deformations at both coarse-grain and fine-grain parts, and the transition layers were less deformations than both coarse and fine layers. In addition, this study shows that coarse-grain part, as poorly sorted sediment, has higher porosity and permeability than fine-grain part, which is the well sorted sediment; the coarse-grain part was more deformations than fine-grain part following compaction concept of Meade (1966).

Noticeably, this study confirmed that increase of pore pressure or pressurization cannot be considered to be a main factor for the rock deformation caused by S.C.$CO_2$ injection into sandstone; the effective porosity change relating to change of dry bulk modulus of rock is also an important factor, which should be paid more attention. In addition, the coarse-grain part (high porosity and permeability) is more deformations induced by $CO_2$ injection than the fine-grain part (low porosity and permeability). Because when S.C.$CO_2$ flows through interface from coarse-grain to fine-grain, some $CO_2$ could not flow and it accumulated in area where is near the interface. Hence, that area is more deformation than another area.

Finally, the simulation results studied on the deformations of the double layers of Tako sandstone deformations can help to understand some advantages of deformations of multiple sediments as shale-sandstone sequences. Therefore, this study might give better understanding for topics, *e.g.*, sealing leakage problem, fault reactivation problem and especially $CO_2$ injection in which it can be inferred on surface uplift problem of $CO_2$ storage in abandoned oil and gas fields of CCS project.

# CHAPTER 8

# CONCLUDING REMARK AND FURTHER RECOMMENDATION

## 8.1 Concluding remarks

The aim of this research is to understand more on rock properties and deformation mechanisms of both compaction (shrinkage) and dilation (expansion). The rocks deform based on fluid flow behaviors, *i.e.* the fluids are expelled from rocks influencing compaction mechanism, on the other hands, the fluids are injected into rocks; the rocks perform deformation as dilation mechanism. Mudstones and sandstone were selected corresponding to major types of rocks in petroleum industries (caprock and reservoir rock). Mudstone compactions were focused because it is more complications and has yet to understand. Furthermore, there are still no unique mathematic expression has been setup up to now. Consequently, the studies of the mudstone compactions can give benefits on understanding of caprock properties before $CO_2$ injection. Similarly, sandstones are a main rock type of reservoir formations in order to inject $CO_2$ for CCS projects. Hence, understanding in sandstone deformations caused by $CO_2$ injection can help to better understand on surface uplift problems after $CO_2$ injection. The major findings corresponding to each specific purpose are summarized below:

The Chapter 3 showing variations and scatters of mudstone compaction data from several locations, especially at shallow parts of basins dominated by mechanical compaction, was analyzed based on real and published data. Many factors cause on variations and scatters of mudstone compaction data were classified and analyzed in order to explain and give answers these variations and scatters.

- Firstly, it can conclude that the compaction curves could be represented by exponential function (Eq. 2.1). Likewise, the compaction factors, *i.e.* porosity of mudstone at datum depth ($\phi_0$) and constant value of exponential function ($a$), were determined by fitting curves.

- Mechanical compaction or burial depth is certainly one of the main controlling factors of compaction of mudstones; the thicker strata, the larger compaction factors. However, it cannot be a single factor to explain the compaction curves of mudstones from various basins.

- The variations of compaction curves of mudstones can be due to several factors and the compaction is affected by several factors which control compaction under localized environments. However, Time (or age) is likely to be a major factor that influences variations of compaction processes of mudstones. It is because the coefficients of compactions show an increasing tendency with increasing time.

- A mathematical expression of compaction of mudstones considering both time and depth were setup based on assumptions in theory of consolidation by Terzaghi (1925, 1943) and slow compaction concept of Fowler and Yang (1998). As long as sticking the actual data, the ignorance of mutual dependence of depth and time can be implicitly expressed in analysis of the actual data is cancelled in an evaluation of constants $\phi_0$ and $a$.

- Due to the mathematic equation of shale compaction with consideration of time effect was set up as shown in Chapter 3, and thus it leads to adjust pore pressure prediction using compaction concept method based on time effect.

- Although porosity is a good indicator of mudstone compaction in determining an over-pressured zone of sedimentary basin because it is predictive and economical in practice, in some basins, conditions occur where overpressured zone are characterized, while their porosity are not anomalously high. Consequently, the pore pressure prediction by porosity approach based on adjustment of time effect might be possible to explain this discrepancy between porosity-depth relationship and pressure-depth relationship in some areas.

According to the discrepancy between the mudstone compaction curve considering with Paleozoic time ($t$ = 250 Ma of Figure 3.5) and the Paleozoic mudstone data of Athy (1930), especially at the shallow part. From the knowledge of geologic information reported that the Athy (1930)'s data had been affected by uplift and erosion processes as known as unloading mechanism, and thus the Chapter 4 re-constructed the mudstone compaction curve of Athy (1930) based on a correction of unloading effect. The conclusions in this chapter are presented as follows.

- More curvature of compaction curve of Athy (1930), especially at shallow part, was affected by uplift and erosion. An estimation of eroded thickness in this study showed that there is a sedimentary thickness (overburden loss or unloading effect) was absent during deposition after erosion. This causes the compaction curve of the Athy (1930)'s data shifted to the direction of abnormal high porosity.

- Porosity data were corrected based on depth correction. Therefore, a mudstone compaction curve of Athy (1930) could be re-constructed. Noticeably, the corrected data of the mudstone compaction in this study was in accord with the mudstone compaction curve considering with Paleozoic time ($t$ = 250 Ma of Figure 3.5).

- Consequently, a compaction curve of Paleozoic mudstone could be proposed. This curve is also consistent with porosity data of mudstones within Paleozoic period by Manger (1963). It means that the porosity of mudstone in Paleozoic age should not exceed 20% at any present depth.

Moreover, the standard compaction curve of mudstones was proposed in the Chapter 5 by adding corrections of temperature effect collaboration with time effect. The porosities of the mudstones were corrected based on time effect model (Chapter 3) and model of Keith and Rimstidt (1985) toward a diminution on variations and scatters of compaction data, and thus the standard curve of mudstone compactions was determined after data corrections. The conclusions of the Chapter 5 are listed as shown in below.

- Based on time and temperature effects the compaction data could be divided three group, *i.e.* (1) young and high temperature mudstones, (2) young and low temperature mudstones and (3) old and low temperature mudstones.

- Porosity correction due to time effect was based on an assumption that many clay lattices in old mudstone appear to have been dehydrated completely under normal compaction comparing with young mudstone, which have been occurred incomplete dehydration. Therefore, high porosity reductions of old mudstones were corrected by using the equation that has been applied by time effect model from Chapter 3.

- In case of temperature effect, the porosity correction caused by temperature effect was based on the subsurface temperature tends to expand volume of water as fluid expansion. Hence, the fluid expansion of high geothermal environments lead to the de-watering processes will be slower than the areas having normal geothermal environments. Consequently, low porosity reductions of high temperature mudstones were corrected by fluid expansion concept of Keith and Rimstidt (1985).

- The standard curve of compaction for mudstones will be very useful to apply for basin modeling works. In basin modeling works, reconstruction of basin geometries normally use default compaction curves and default thermal properties, the parameters which influence on compaction curves, *i.e.* time and temperature, are normally not considered in basin analysis. Consequently, the standard curve of compaction will be useful to improve accuracy in basin modeling works.

In cases of rock deformations due to fluid injection, first case is deformation of Berea sandstone caused by S.C.$CO_2$ injection. As surface uplift has been an important problem in $CO_2$ sequestration promising and is lately gaining increasing attention within the reservoir engineer community; therefore the Chapter 6 presents geomechanical simulations of Berea sandstone deformations induced by S.C.$CO_2$ injection constraining with experimental results to emulate surface deformation problem for CCS projects. Berea sandstone was selected to represent a homogenous and an isotropic rock and lead to better understand on simple deformations of ideal rocks. Furthermore, the Berea sandstone could be represented as storage formations as in the case of depleted oil and gas reservoirs because sandstones are a main reservoir for oil and gas fields. The findings are presented as follows.

- Geomechanical simulations could be used to reproduce and explain laboratory experiments for Berea sandstone deformations, especially the deformation induced by $CO_2$ injection.

- Although rock deformed (strain changes) corresponding to pore pressure changes as shown in simulation results, but this study also revealed that only pore pressure cannot be considered for the rock deformations. Properties of fluid are also important and should be paid more attention. Low viscosity and high mobility of $S.C.CO_2$ induced more deformations comparing with deformations by water injection, even at the same pore pressure change.

- Changes of effective porosity could be used to explain mechanisms of Berea sandstone deformations induced by fluid injections. A suspicion of high strain in $S.C.CO_2$ injection was explained by simulation using changes of effective bulk modulus of rock, which were influenced by effective porosity changes.

- In case of $S.C.CO_2$ injection, the rock deformed based on a flow of $S.C.CO_2$ front inside the rock. This was confirmed by changing strains from each channel location (No. 1-11) both simulation and experimental results.

- Using simulations constraining with laboratory experiments in this Chapter can help to understand deformation mechanisms of Berea sandstone, especially, for $CO_2$ injection in which it can be inferred on surface uplift problem of $CO_2$ storage in abandoned oil and gas fields, where are normally clastic sandstone reservoir.

To understand more on complex of rock deformations, Tako sandstone was selected to use in laboratory experiments and simulations because it is a heterogeneous and an anisotropic rock as same as the natural rocks. All procedures of Tako sandstone's experiments were almost the same with Berea sandstone, but a main difference was in $S.C.CO_2$ injection stage in which the injection pressure of $S.C.CO_2$ was increased from 10.05 MPa to 10.5 MPa because Tako sandstone has low permeability and porosity comparing with Berea sandstone. Chapter 7 presents the results of both simulation and experiment, and therefore the conclusions in this chapter are below.

- Two different parts (coarse-grain and fine-grain parts) of Tako sandstone showed different deformations at every stage. Coarse-grain part was more deformations than fine-grain part, these were due to the coarse-grain part has higher porosity and permeability as known poorly sorted sediment than fine-grain part, which were known as well sorted sediment.

- Transition layers could be found on both coarse-grain and fine-grain parts at every stage of experiments. At high confining and injection pressures the transition layers were classified clearly comparing with low confining and injection pressures.

- Strain changes at S.C.$CO_2$ injection stage in this experiment were confirmed that low viscosity and high mobility of S.C.$CO_2$ were the key factors to induce a suspicion of high strain rate. Likewise, fluid properties should be paid attention coupling with pore pressure change in cases of deformation mechanisms.

- Changes of effective porosity were also applied to simulate for Tako sandstone deformations. Dry bulk modulus and effective bulk modulus of rocks could be determined by changes of effective porosity in order to use controlling parameters for simulations at every stage of experiments.

- According to S.C.$CO_2$ flowed from coarse-grain part to fine-grain part, some S.C.$CO_2$ could not flow through fine-grain part because of low permeability and porosity. Therefore, S.C.$CO_2$ was more accumulated in a transition layer of coarse-grain part, this causes the coarse-transition layer was the highest deformation.

- Finally, the simulations and experiments of Tako sandstone can help to understand a mechanism of rock deformations as multiple sediments as seal-storage sequences. Hence, the mechanisms of Tako sandstone deformations can be inferred for surface uplift and sealing leakage problems caused by $CO_2$ injection in CCS projects.

## 8.2 Further recommendations

As engineers and geologists have known that compaction mechanisms of mudstones are more complex than sandstones, and the variations and scatters of compaction data of mudstones are due to several factors under localized environments. Although effect of time was proven and explained as shown in this study, but other factors, *e.g.* temperature and so on, which also influence on mechanical compaction processes of mudstones should be paid further attention in order to have a thorough knowledge on mechanisms of deformations caused by fluid expulsion from mudstones. Furthermore, the models and assumptions that were used to prove time effect are based on simple and ideal rocks, though they were constrained by 3D plots of natural compaction data. Therefore, more complex models of mudstone compactions should be a further research. Also, modern and time variety data of mudstone compactions should be used in the future research coupling with the published data.

According to mechanisms of overpressure have been remained doubts, however compaction disequilibrium relating mechanical compaction accounts for widespread areas of overpressure. Porosity approach is a new and useful tool for pore pressure prediction to identify overpressure zone. Nevertheless, the relationship of porosity and depth is not usually associated with overpressure in some areas, *e.g.* Niger Delta basin, North Sea basin, *etc.* Due to scanty data of overpressured areas in this study, and therefore the next research should supplement that data with an adjustment of pore pressure prediction proposed by this study to

give an answer discrepancy between porosity-depth trend and overpressure in pressure-depth trend.

In cases of sandstone (Berea and Tako sandstones) deformations induced by S.C.$CO_2$ injections, the simulations constrained with laboratory experiments seem to help better understand on mechanisms of rock dilations. Anyway, field data are necessary to use in the further research in order to contribute for simulations of surface uplift in CCS sites. In addition, to achieve completely understands on rock deformations induced by $CO_2$ injection, some parameters, *e.g.* temperature, chemical reactions, buoyancy force, multi-phase flows, *etc.*, which were kept constant and omitted in this study, should be considered and supplemented both simulations and experiments.

Other types of rocks are also interesting to be tested and simulated as same as procedures of Berea and Tako sandstones. Another types of storage formations, *e.g.* carbonate rocks, fractured rocks, *etc.*, should be selected for laboratory experiments and simulations in the further research.

# REFERENCES


Alam, M.M., Borre, M.K., Fabricius, I.L., Hedegaard, K., Rogen, B., Hossain, Z. and Krogsboll, A.S., 2010. Biot's coefficient as an indicator of strength and porosity reduction: Calcareous sediments from Kerguelen Plateau. Journal of Petroleum Science and Engineering, 70, 282-297

Angus, D., Lynch, T. and Lorinczi, P., 2012. Investigating the link between surface - Proceedings of the 3rd EAGE $CO_2$ Geological Storage Workshop Understanding the Behaviour of $CO_2$ in Geologic Storage Reservoirs, March 26-27, 2012, Edinburgh, UK.

Aoyagi, K. and Asakawa, T., 1979. Primary migration theory of petroleum and its application to petroleum exploration. Organic Geochemistry, vol.2, Pergamon Press Ltd, Great Britain: 33-43.

Aoyagi, K., Kazama, T., Sekiguchi, K. and Chilingarian, G.V., 1985. Experimental compaction of Na-montmorillonite clay mixed with crude oil and seawater, Water-rock interaction, 49(1-3), Elsevier, 385-392.

Athy, L.F., 1930. Density, porosity, and compaction of sedimentary rocks. Bull. Am. Assoc. Pet. Geol., 14 (1): 1-24.

Barker, C., 1972. Aquathermal pressuring – the role of temperature in development of abnormal pressure. Bull. Am. Assoc. Pet. Geol., 56, 2068-2071.

Baldwin, B., 1971. Ways of deciphering compacted sediments. Jour. Sedimentary Petology, 41(1), 293-301.

Baldwin, B. and Butler, C.O., 1985. Compaction curves. Bull. Am. Assoc. Pet. Geol., 69: 622-626.

Biot, M.A., 1941. General theory of three dimensional consolidation. J. Appl. Phys., 12(2), 155-164.

Boden, T.A., Marland, G. and Andres, R.J., 2010. Global, regional, and national fossil-fuel $CO_2$ Emissions. Carbon Dioxide Information Analysis Center, Oak Ridge National Labloratory, U.S. Department of Energy, Oak Ridge, Tenn., U.S.A.

Bowers, G.L., 1995. Pore pressure estimation from velocity data; accounting for overpressure mechanisms besides undercompaction. SPE Drilling and Completions, 89-95.

Bradley, J.S., 1975. Abnormal formation pressure. Bull. Am. Assoc. Pet. Geol., 59(6), 957-973.

Burst, J.F., 1969. Diagenesis of gulf coast clayey sediments and its possible relation to petroleum migration. Bull. Am. Assoc. Pet. Geol., 53 (1): 73-93.

Cekerevac, C. and Laloui, L., 2004. Experimental study of thermal effect on the mechanical behavior of a clay. Intl' Jour. Numer. Anal. Meth. Geomech., 28, 209-228.

Chopra, S. and Huffman, A., 2006. Velocity determination for pore pressure prediction. CSEG Recorder, 28-46.

Chowdhury, M.H. and Schmitt, D.R., 2012. Seismic behavior of $CO_2$ saturated Fontainebleau sandstone under in situ conditions. GeoConvention 2012, 1-6.

Clark, G.C. and Cooper, C.L., 1927. Oil and gas in Oklahoma – oil and gas geology of Kay, Grant, Garfield and Noble counties. Oklahoma Geological Survey, 40-H, 48 pp.

Couples, G.D., Lewis, H., Olden, P., Workman, G.H. and Higgs, N.G., 2007. Insights into the faulting process from simulations of rock layer bending. In: The relationship between damage and localization (eds., H. Lewis and G.D. Couples), Geological Society of London, 161-186.

Crook, A.J.L., Willson, S.M., Yu J.G. and Own D.R.J., 2006. Predictive modeling of structure evolution in sandbox experiments. Jour. Structural Geology, 28, 729-744.

Culshaw, B., 2000. Measuring strain using optical fibres. Strain, 36(3), 105-113.

Demenico, P.A. and Palciauskas, V.V., 1979. Thermal expansion of fluids and fracture initiation in compacting sediments, Geol. Soc. Am. Bull., part II, 90, 953-979.

Dickinson, G., 1953. Geological aspects of abnormal reservoir pressures in the Gulf Coast Louisiana. Bull. Am. Assoc. Pet. Geol., 37(2), 410-432.

Dolton, G.L. and Finn, T.M., 1989. Petroleum geology of the Nemaha Uplift, Central Mid-Continent. U.S. Geological Survey Open-File Report, 88-450D, 39 pp.

Durmishyan, A.G., 1974. Compaction of argillaceous rocks. Intl' Geol. Review, 16(6), 650-653.

Dusseault, M.B., 2011. Geomechanical challenges in petroleum reservoir exploitation. KSCE Journal of Civil Engineering 15(4), 669-678.

Dutta, N.C., 2002. Geopressure prediction using seismic data: current status and the road ahead. Geophysics, 67: 2012-2041.

Dzevanshir, R.D., Buryakovskiy, L.A., and Chilingarian, G.V., 1986. Simple quantitative evaluation of porosity of argillaceous sediments at various depths of burial. Sedimentary Geology, 46: 169-175.

Eaton, B.A., 1972. The effect of overburden stress on geopressures prediction from well logs. Paper SPE3719 JPT, 929-934.

Eaton, B.A., 1975. The equation for geopressure prediction from well logs. SPE of AIME, paper SPE 5544.

Engelhardt, W.V. and Gaida, K.H., 1963. Concentration changes of pore solutions during the compaction of clay sediments. Journal of Sedimentary Petrology, 33 (4): 919-930.

Flemings, P.B., Stump, B.B., Finkbeiner, T. and Zoback, M., 2002. Flow focusing in overpressured sandstones: theory, observations, and applications. Am. J. Sci., 302: 827-855.

Fowler, A.C. and Yang, X.S., 1998. Fast and slow compaction in sedimentary basins. Siam J. Appl. Math., 59, (1): 368-385.

Fowler, S.R. White, R.S. and Louden, K.E., 1985. Sediment dewatering in the Makran accretionary prism. Earth and Planetary Science Letters, 75 (4): 427-438.

Gale, J., 2004. Geological storage of $CO_2$: what do we know, where are the gaps, and what more needs to be done?, Energy, 29(9-10), 1329-1338.

Gassmann, F., 1951. Elastic waves through a packing of spheres, Geophysics 16, 673-685.

Goulty, N.R., 1998. Relationships between porosity and effective stress in shales, First Break, 16(12), 413-419.

Ham, H.H., 1966. New charts help estimate formation pressures. Oil and Gas Jour., 65(51), 58-63.

Hamilton, E.L., 1978. Sound velocity-density relations in sea-floor sediments and rocks. J. Acoust. Soc. Am., 63: 366-377.

Han, D.H., Nur, A. and Morgan, D., 1986. Effects of porosity and clay content on wave velocities in sandstone. Geophysics, 51, 2093-2107.

Hansen, S., 1996. A compaction trend for cretaceous and tertiary shales on the Norwegian shelf based on sonic transit times. Petrol. Geosci., 2(2), 159-166.

Hedberg, H.D., 1926. The effect of gravitational compaction on the structure of sedimentary rocks. Bull. Am. Assoc. Petrol. Geol., 10, 1035-1072.

Hedberg, H.D., 1936. Gravitational compaction of clays and shales. American Journal of Science, 31 (184): 241-287.

Heppard, P.D., Cander, H.S. and Eggertson, E.B., 1998. Abnormal pressure and the occurrence of hydrocarbons in offshore eastern Trinidad, West Indies. In: Abnormal pressures in hydrocarbon environments(eds., B.E Law, G.F. Ulmishek and V.I. Slavin), Am. Assoc. Pet. Geol. Memoir, 70, 215-246.

Hepple, R.P. and Benson, S.M., 2005. Geologic storage of carbon dioxide as a climate change mitigation strategy: performance requirements and the implications of surface seepage. Environ. Geol., 47, 576-585.

Holbrook, P.W., Maggiori, D.A. and Hensley, R., 2005. Real-time pore pressure and fracture gradient evaluation in all sedimentary lithologies. SPE Form. Eval., 10(4), 215-222.

Holloway, S., 1996. An overview of the joule II project: the underground disposal of carbon dioxide. Energy Convers Manages, 37(6-8), 1149-1154.

Hottman, C.F. and Johnson, R.K., 1965. Estimation of formation pressures from log-derived shale properties. Jour. Petroleum Technology, 17(6), 717-722.

IPCC, 2001. Climate change 2001: Mitigation, contribution of working group III, Summary for Policy Makers, 20pp.

IPCC, 2005. Special report on carbon dioxide capture and storage: summary for policymakers and technical summary, Cambridge University Press, 429pp.

Issler, D.R., 1992. A new approach to shale compaction and stratigraphic restoration, Beaufort-Mackenzie Basin and Mackenzie Corridor, Northern Canada. American Association of Petroleum Geologists, 76, 1170-1189.

Itasca, 2006a. User's Guide FLAC3D - Fast lagrangian analysis of continua in 3 dimensions. Version 3.10, Itasca Consulting Group, Minneapolis, Minnesota, USA, 248pp.

Itasca, 2006b. Theory and Background FLAC3D - Fast lagrangian analysis of continua in 3 dimensions. Version 3.10, Itasca Consulting Group, Minneapolis, Minnesota, USA, 176pp.

Itasca, 2006c. Fluid-Mechanical Interaction FLAC3D - Fast lagrangian analysis of continua in 3 dimensions. Version 3.10, Itasca Consulting Group, Minneapolis, Minnesota, USA, 142pp.

Johnson, F.W., 1950. Shale density analysis. In: Subsurface geologic methods 2nd ed. (eds., L.W. LeRoy), Colo. School Mines, 329-341.

Keith, L.A. and Rimstidt, J.D., 1985. A numerical compaction model of overpressuring in shales. Mathematical Geology, 17(2), 115-135.

Kitamura, K. and Xue, Z., 2007. Experimental study of residual $CO_2$ saturation in the sandstones with different pore structures. In: 6th annual conference on Carbon Capture & Sequestration, Pittsburgh, Pennsylvania, May 7-10, 2007.

Korvin, G., 1984. Shale compaction and statistical physics. Geophys J.R. astr. Soc., 78: 35-50.

Larsen, G. and Chilingarian, G.V., 1983. Diagenesis in sediments and sedimentary rocks; 2, Introduction, developments in sedimentology 25B. Elsevier Scientific Publishing Co., New York.

Lawrence, C.M., Nelson, D.V., Udd, E. and Bennett, T., 1999. A fiber optic sensor for Transverse strain measurement. Experiment Mechanics, 39 (3), 202-209.

Liu, H.H., Rutqvist, J. and Berryman, J.G., 2009. On the relationship between stress and elastic strain for porous and fractured rock. Intl' Jour. Rock Mechanics and Mining Sciences, 46, 289-296.

Lewis, H., Hall, S.H., Guest, G. and Couples, G.D., 2007. Kinematically-equivalent but geomechanically-different simulations of fault evolution: the role of loading configurations. In: Structurally Complex Reservoirs (eds S.J. Jolley, D. Barr, J.J. Walsh and R. Knipe), Geological Society of London, 159-172.

Magara, K., 1966. Application of sonic logs in exploration, JAPT Jour., 31(2), 51-58.

Magara, K., 1968. Compaction and migration of fluids in Miocene mudstone, Nagaoka plain, Japan. Bull. Am. Assoc. Petrol. Geol., 52(12), 2466-2501.

Magara, K., 1971. Permeability consideratioins in generation of abnormal pressures. Soc. Pet. Eng. J., 11, 236-242.

Magara, K., 1974. Aquathermal fluid migration. Bull. Am. Assoc. Petrol. Geol., 58(12), 2513-2521.

Magara, K., 1978. Compaction and fluid migration practical petroleum geology. Developments in Petroleum Science, Vol. 9. Elsevier, Amsterdam, 343pp.

Manger, G.E., 1963. Porosity and bulk density of sedimentary rocks. U.S. Geol. Survey, 1144-E: 34-40.

Mavko, G. and Nur, A., 1978. The effect of nonellipitcal cracks on the compressibility of rocks. J. Geophys. Res. 83, 4459-4468.

Mavko, G. and Mukerji, T., 1995. Seismic pore space compressibility and Gassman's relation. Geophysics 60 (6), 1743-1749.

Mavko, G., Mulerji, T. and Dvorkin, J., 1998. The rock physics handbook. Cambridge University Press, 35p.

McCoy, A.W. and Keyte, W.R., 1934. Present interpretations of the structural theory for oil and gas migration and accumulatlion. Problem of Petroleum Geology (Sidney Powers Memorial Volume), American Association of Petroleum Geologists, Tulsa, Oklahoma: 279-282.

Meade, R.H., 1963. Relation of the pore volume of silty sediments to overburden load, particle size, and sorting. Art. 210 in U.S. Geol. Survey Prof., paper 450-E, E111-E114.

Meade, R.H., 1966. Factors influencing the early stages of the compaction of clays and sands-review. Journal of Sedimentary Petrology, 36 (4): 1085-1101.

Mese, A. and Tutuncu, A.N., 2000. A novel experimental technique for investigation of pore pressure effect on acoustic and mechanical properties in unconsolidated shaly sands and shales. Pacific Rocks 2000: Rock Around the Rim, proceedings of the 4th North American Rock Mechanics Symposium Seattle, Washington, July 31-August 3, 2000, 173-179.

Minkoff, S.E., Stone, C.M., Bryant, S., Peszynska, M. and Wheeler, M.F., 2003. Coupled fluid flow and geomechanical deformation modeling. Petroleum Science and Engineering 38, 37-56.

Minshull, T.A. and White, R., 1989. Sediment compaction and fluid migration in the Makran accretionary prism. Jour. Geophy. Research, 94(6), 7387-7402.

Miyazaki, H., 1966. Gravitational compaction of the Neogene muddy sediments in Akita oil fields, northeast Japan. J. Geosci., Osaka City Univ., 9: 1-23.

Mondol, N.H., Bjorlykke, K., Jahren, J. and Hoeg, K., 2007. Experimental mechanical compaction of clay mineral aggregates-Changes in physical properties of mudstones during burial. Marine and Petroleum Geology, 24: 289-311.

Murphy, W., Reischer, A. and Hsu, K., 1993. Modulus decomposition of compressional and shear velocities in sandstones. Geophysics 58, 227-239.

Nelson, P.H. and Bird, K.J., 2005. Porosity compaction trends and regional uplift derived from sonic logs, National Petroleum Reserve, Alaska. U.S. Geological Survey Scientific Investigations Report 2005-5051, 24 pp.

NETL, 2013. The national methane hydrates R&D program: The Alaska North slope stratigraphic test well. [online]. Accessed on: http://www.netl.doe.gov/technologies/oil-gas/FutureSupply/MethaneHydrates/rd-program/ANSWell/MDTool.html. (Search date: January 15, 2013)

NFOR, Ndicho, B. and Ikechukwu, O.M., 2011. Porosity as an overpressure zone indicator in an X-field of the Niger Delta Basin, Nigeria. Scholars Research Library: Archives of Applied Science Research, 3(3), 29-36.

Orlic, B., 2008. Some geomechanical aspects of geological $CO_2$ sequestration. In: the 12th International Conference of International Association for Computer Methods and Advances in Geomechanics (IACMAG), Gao, India, 2204-2212.

Oullet, A., Berard, T., Desroches, J., Frykman, P., Welsh, P., Minton, J., Pamukcu, Y., Hurter, S. and Schmidt-Hattenberger, C., 2011. Reservoir geomechanics for assessing containment in $CO_2$ storage; a case study at Ketzin, Germany. Energy Procedia, 4, 3298-3305.

Peng, S. and Zhang, J., 2007. Engineering geology for underground rocks. Springer.

Preisig, M. and Prevost, J.H., 2011. Couple multi-phase thermo-poromechanical effects - Case study: $CO_2$ injection at In Salah, Algeria. Intl' Jour. Greeenhouse Gas Control, 5, 1055-1064.

Proshlyakov, B.K., 1960. Reservoir properties of rocks as a function of their depth and lithology. Geol. Nefti I Gaza, 12, 24-29.

Rubey, W.W., 1927. The effect of gravitational compaction on the structure of sedimentary rocks. Bull. Am. Assoc. Petrol. Geol., 11, 621-33, 1333-6.

Rubey, W.W. and Hubbert, M.K., 1959. Role of fluid pressure in mechanics of overthrust faulting. II. Overthrust belt in geosynclinals area of western Wyoming in light of fluid-pressure hypothesis. Geological Society of America, 70 (2): 167-205.

Russell, B.H. and Smith, T., 2007. The relationship between dry rock bulk modulus and porosity-An empirical study. CREWES Research Report 19, 1-14.

Rutqvist, J., 2012. The geomechanics of $CO_2$ storage in deep sedimentary formations. Geotechnical and Geological Engineering 30(3), 525-551.

Rutqvist, J., 2010. Status of the TOUGH-FLAC simulator and recent applications related to coupled fluid flow and crustal deformations. Computers and Geosciences, 1-12.

Rutqvist, J. and Tsang, C.F., 2003. TOUGH-FLAC: A numerical simulator for analysis of coupled thermal-hydrologic-mechanical processes in fractured and porous geological media under multi-phase flow conditions. In: TOUGH Symposium 2003, Berkeley, California, USA, 1-9.

Rutqvist, J., Tsang,. C.F., 2002. A study of caprock hydromechanical changes associated with $CO_2$-injection into a brine formation. Environmental Geology, 42, 296-305

Rutqvist, J., Vasco, D.W. and Myer, L., 2009. Coupled reservoir-geomechanical analysis of $CO_2$ injection at In Salah, Algeria. Energy Procedia, 1, 1847-1854.

Sayers, C.M., Johnson, G.M. and Denyer, G., 2002. Predrill pore pressure prediction using seismic data. Geophysics, 67, 1286-1292.

Schneider, J., Flemings, P.B., Dugan, B., Long, H. and Germaine, J.T., 2009. Overpressure and consolidation near the seafloor of Brazos-Trinity Basin IV, northwest deepwater Gulf of Mexico. Jour. Geophys. Res., 114, B05102.

Sclater, J.G. and Christie, P.A.F., 1980. Continental stretching; an explanation of the post-Mid-Cretaceous subsidence of the central North Sea basin. Jour. Geophy. Research, 85(B7), 3711-3739.

Settari, A. and Walters, D.A., 2001. Advances in coupled geomechanical and reservoir modeling with application to reservoir compaction. SPE Journal, 334-342.

Shaker, S.S., 2002. Predicted vs. measured pore pressure: Pitfalls and perceptions. Proceedings of Offshore Technology Conference, Houston, Texas, U.S.A., May 6-9, 2002, 1-11.

Shi, J.Q., Xue, Z. and Durucan, S., 2010. Supercritical $CO_2$ core flooding and imbibition in Tako sandstone – Influence of sub-core scale heterogeneity. Intl' Jour. Greenhouse Gas Control, 1-13.

Shukla, R., Ranjith, P.G., Choi, S.K. and Haque, A., 2010. Study of caprock integrity in geosequestration of carbon dioxide. International Journal of Geomechanics, 11(4), 294-301.

Skempton, A.W., 1944. Notes on the compressibility of clays. Q.J.G.S. c: 119-135.

Slotnick, M.M., 1936. On seismic computation with applications. Geophysics, 1, 9-22.

Sorby, H.C., 1908. On the application of quantitative methods to the study of the structure and history of rocks. Quart. Jour. Geol. Soc. London, 64, 171-232.

Soufi, N., 2009. Pressure measurement in shale. NTNU, 148pp.

Spencer, C.W., 1987. Hydrocarbon generation as a mechanism for overpressuring in rocky mountain region. Bull. Am. Assoc. Petrol. Geol., 71, 368-388.

Storer, D., 1959. Compaction of clayey sediments in the Po basin. In: I Giacementi Gassiferi dell'Europa Occidentale, 2 Rome (Accad. Naz. dei Lincei), 519-544.

Terzaghi, K., 1925. Erdbaumechanik. Deuticke, Vienna. (Casagrande, A., translated, 1960; From Theory to Practice in Soil Mechanics; selections from the writings of Karl Terzaghi, with bibliography and contributions on his life and achievents). NY, John Wiley and Sons: 425pp.

Terzaghi, K., 1943. Theoretical of soil mechanics. John Wiley and Sons: 510 pp.

Van Olphen, H., 1963. Compaction of clay sediments in the range of molecular particle distances, in Clays and clay minerals. 11th Natl. Clays and Clay Mineral Conf. Proc., New York, Macmillan Co.: 178-187.

Vasco, D.W., Rucci, A., Ferretti, A., Novali, F., Bissell, R.C., Ringrose, P.S., Mathieson, A.S. and Wright, I.W., 2010. Satellite-based measurements of surface deformation reveal fluid flow associated with the geological storage of carbon dioxide, Geophysical Research Letters, 37, L03303.

Vassoevich, N.B., 1960. Experiment in constructing typical gravitational compaction curve of clayey sediments. Nov. Neft. Tekh. Geol. Ser. (News Pet. Tech. Geol.), 4, 11-15.

Velde, B., 1996. Compaction trends of clay-rich deep sea sediments. Marine Geology, 133 (3-4): 193-201.

Versluys, J., 1927. An hypothesis explaining some characteristics of clay. Proc. Konink. Akad. Van Wetenschappen te Amsterdam, 30: 104-112.

Wallace, W.E., 1965. Logs measure abnormal subsurface pressure. Oil and Gas Jour., 63(27), 102.

Weatherby, B.B. and Faust, L.Y., 1935. Influence of geological factors on longitudinal seismic velocities. Bull. Am. Assoc. Petrol. Geol., 19, 1-8.

Weller, J.M., 1959. Compaction of sediments. Bull. Am. Assoc. Petrol. Geol., 43(2), 273-310.

Wikipedia, 2012. Diagram shows a drill stem test in a borehole. [online]. Accessed on: http://en.wikipedia.org/wiki/File:Drill_Stem_Test.png. (Search date: January 15, 2013)

Winterfeld, P.H. and Wu, Y.S., 2011. Parallel simulation of $CO_2$ sequestration with rock deformation in saline aquifers. In: SPE Reservoir Simulation Symposium, Woodlands, Texas, USA, 1-22.

Zhang, J., 2011. Pore pressure prediction from well logs-Methods, modifications, and new approaches. Earth-Science Reviews, 108: 50-63.